ISSN 2074-272X

науково-практичний журнал 2019/4

Електротехніка і Електромеханіка

Electrical Engineering & Electromechanics

Електротехніка. Визначні події. Славетні імена
Електричні машини та апарати
Електротехнічні комплекси та системи. Силова електроніка
Теоретична електротехніка та електрофізика
Техніка сильних електричних та магнітних полів. Кабельна техніка
Електричні станції, мережі і системи
Ювілеї

З 2015 р. журнал індексується у міжнародній наукометричній базі Web of Science Core Collection: Emerging Sources Citation Index

«ELECTRICAL ENGINEERING & ELECTROMECHANICS»

SCIENTIFIC & PRACTICAL JOURNAL
Journal was founded in 2002
Founders:
National Technical University «Kharkiv Polytechnic Institute» (Kharkiv, Ukraine)
State Institution «Institute of Technical Problems of Magnetism of the NAS of Ukraine» (Kharkiv, Ukraine)

ISSUE 4 / 2019

TABLE OF CONTENTS

Editorial office address: Dept. of Electrical Apparatus, NTU «KhPI», Kyrpychova Str., 2, Kharkiv, 61002, Ukraine
phones: +380 57 7076281, +380 67 3594696, **e-mail:** a.m.grechko@gmail.com (**Grechko O.M.)**

ISSN (print) 2074-272X
ISSN (online) 2309-3404

Printed 15 August 2019. Format 60 x 90 ⅛. Paper – offset. Laser printing. Edition 200 copies.
Printed by Printing house «Madrid Ltd» (11, Maksymilianivska Str., Kharkiv, 61024, Ukraine)

UDC 629.7:930.1 **doi: 10.20998/2074-272X.2019.4.01**

M.I. Baranov

AN ANTHOLOGY OF THE DISTINGUISHED ACHIEVEMENTS IN SCIENCE AND TECHNIQUE. PART 50: ROCKET-SPACE TECHNOLOGY DESIGNER WERNHER VON BRAUN AND HIS ACCOMPLISHMENTS IN MISSILE DESIGN

Purpose. *Preparation of short scientifically-historical essay about one of founders of world rocket production, distinguished German-American designer of modern space-rocket technique Wernher von Braun.* ***Methodology.*** *Known scientific methods of collection, analysis and analytical treatment of scientific and technical information, touching becoming and development in the world of space-rocket technique and resulted in scientific monographs, journals and internet-reports.* ***Results.*** *A short scientifically-historical essay is presented about the distinguished German-American designer of space-rocket technique Wernher von Braun, becoming one of founders of world rocket production. Basic scientific and technical achievements of talented and purposeful scientist Doctor of Physics Wernher von Braun in area of modern rocket production, getting over on persistent initiative of the American special services after the defeat of Germany in World War II in the USA (1945) for continuation of the work in area of missile technology (he was the main designer of the German battle ballistic rocket V-2 of midrange with a liquid rocket engine (LRE), created in 1944), carrying military-strategic character by that time. It is shown that Wernher von Braun is the founder of the space program of the USA and leader of developments of the American pilot-controlled spaceships of series «Apollo» within the framework of the Lunar program of the USA. It is marked that under scientific and technical guidance of Wernher von Braun in the USA powerful launch vehicles were created with LRE of battle series «Redstone» of midrange (1958, military index of PGM-11) and space series «Saturn» (1969), due to which on a circumterrestrial orbit the first artificial satellite of the USA «Explorer-1» launched (31 January, 1958 y.), and the American astronaut Neil Armstrong first in history of humanity stepped on the surface of the Moon (20 July, 1969).* ***Originality.*** *Certain systematization is executed known from mass media of scientific and technical materials, touching becoming and development in 20-th century of world rocket production, at the sources of which the talented scientist Doctor of Physics and distinguished German-American designer of space-rocket technique Wernher von Braun.* ***Practical value.*** *Scientific popularization and deepening for the students of higher school, engineer and technical and scientific workers of physical and technical knowledge in area of world history of becoming and development of modern rocket production, extending their scientific and technical range of interests and further development of scientific and technical progress in society.* References 18, tables 1, figures 10.

Key words: **space-rocket technique, distinguished German-American designer of missile technology Wernher von Braun, his basic achievements in a modern rocket production, scientifically-historical essay.**

Приведений короткий науково-історичний нарис про видатного німецько-американського конструктора ракетно-космічної техніки Вернера фон Брауна, що став одним з основоположників світового ракетобудування. Описані основні науково-технічні досягнення Вернера фон Брауна в галузі сучасного ракетобудування, що перебрався за наполегливою ініціативою американських спецслужб після розгрому Німеччини в Другій світовій війні в США (1945 р.) для продовження роботи в області ракетної техніки, що носить військово-стратегічний характер. Показано, що Вернер фон Браун є засновником космічної програми США і керівником розробок американських космічних кораблів «Аполлон». Під його науково-технічним керівництвом в США були створені потужні ракетоносії серії «Редстоун» і «Сатурн», завдяки яким на навколоземну орбіту був запущений перший штучний супутник США «Експлорер-1» (1958 р.), а американський астронавт вперше в історії людства ступив на поверхню Місяця (1969 р.). Бібл. 18, табл. 1, рис. 10.

Ключові слова: **ракетно-космічна техніка, видатний німецько-американський конструктор ракетної техніки Вернер фон Браун, його основні досягнення у сучасному ракетобудуванні, науково-історичний нарис.**

Приведен краткий научно-исторический очерк о выдающемся немецко-американском конструкторе ракетно-космической техники Вернере фон Брауне, ставшем одним из основоположников мирового ракетостроения. Описаны основные научно-технические достижения Вернера фон Брауна в области современного ракетостроения, перебравшегося по настойчивой инициативе американских спецслужб после разгрома Германии во Второй мировой войне в США (1945 г.) для продолжения работы в области ракетной техники, носящей военно-стратегический характер. Показано, что Вернер фон Браун является основателем космической программы США и руководителем разработок американских космических кораблей «Аполлон». Под его научно-техническим руководством в США были созданы мощные ракетоносители серии «Редстоун» и «Сатурн», благодаря которым на околоземную орбиту был запущен первый искусственный спутник США «Эксплорер-1» (1958 г.), а американский астронавт впервые в истории человечества ступил на поверхность Луны (1969 г.). Библ. 18, табл. 1, рис. 10.

Ключевые слова: **ракетно-космическая техника, выдающийся немецко-американский конструктор ракетной техники Вернер фон Браун, его основные достижения в современном ракетостроении, научно-исторический очерк.**

Introduction. World literature is replete with a huge number of human stories, in the plot of which is human passion. We know how this feeling can lower a person in the «eyes» and consciousness of other people and how can raise him high above the ever-changing «ocean» of events and human emotions on our planet. Akin to human passion and the talent of man – the gift of God! Talent flashing with its «flame» of the knowledge of the world around us the human soul and pushing the chosen person to surrender and realize his planned goal by any means. Here, the direction of the goal (two extreme points of reference for it – for a good cause and the creation of weapons of mass destruction of people) and the problem

of morality for such a person can also be moved, consciously or unconsciously, to the background. By and large, the true vocation of a person is higher and more important than the prevailing political conditions and systems in which such a person has to work and live. Wernher von Braun (his full name in German is Wernher Magnus Maximilian Freiherr von Braun), an outstanding German-American designer of rocket and space technology, turned out to be one of such talented people, to which all of the above can be fully attributed. This scientific and historical essay is devoted to brief description of the life and career of this internationally recognized scientist, Doctor of Physics and design engineer in the field of rocketry (Fig. 1).

The goal of the paper is preparation of a brief scientific and historical essay on one of the founders of world rocket production, an outstanding German-American designer of modern rocket and space technology Wernher von Braun.

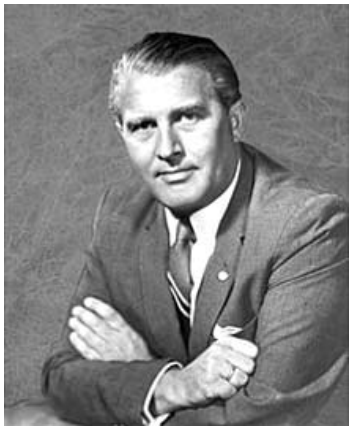

Fig. 1. Distinguished designer of rocket and space technology Wernher von Braun (23.03.1912-16.06.1977) [1]

1. The beginning of the life and career of Wernher von Braun. He was born on March 23, 1912 in the city of Wirsitz (province of Posen, the German Empire, now it is the city of Wyrzysk, Poland) [1]. His parents belonged to the ancient aristocratic families. Therefore, their son Wernher inherited the title «Freiherr», corresponding to the Baronial title. His father, Magnus von Braun (1878-1972), held the high post of Minister of Food and Agriculture in the German government of the Weimar Republic [1].

His mother, Emmy von Quistorp (1886-1959), who had royal «roots» along the line of ancestors, which ascended to Rurik [2], instilled in young Wernher a love of music and art. In the period of training (1925-1930) in a boarding school with strict Prussian orders, located near the city of Weimar, he became interested in the book by Hermann Oberth «*The Rocket into Interplanetary Space*» [2]. This forced him to actively engage in physics and mathematics, which he needed to independently design handicraft rockets at that time. In 1930, Wernher von Braun entered the Berlin Higher Technical School (now this is known in the world the Berlin Technical University), where he joined the research group «*Space Travel Society*» and together with H. Oberth (1894-1989) he participated in testing first liquid rocket engines (LRE) [1]. At this time, he firmly decided to devote his life to penetration into extraterrestrial space [1, 2]. It is believed that it was H. Oberth who had a great influence on the formation of Wernher von Braun as a future rocket maker. Later, Wernher von Braun wrote about this German pioneer of rocket science [1]: «*... Personally, I see in him not only the guiding star of my life, but also I owe him my first contacts with theoretical and practical issues of rocket engineering and space flights*». In 1932, he was admitted to the military missile scientific group of Walter Dornberger (then captain of artillery, who became Major General in 1941), engaged in the development and creation for the Reichswehr (German military) both solid-fuel missiles and missiles with LRE. In April 1934, Wernher von Braun successfully defended at the Friedrich Wilhelm Berlin University his Doctoral Thesis on the topic [1] «*Design, theoretical and experimental approaches to the problem of creating a liquid-fuel rocket*» (at one time this Thesis was classified and its materials were not published until 1960 [2]). For this scientific work (the supervisor of this Thesis was German physicist Erich Schumann [1]), he was awarded the degree of Doctor of Physics (rocket science).

2. The main achievements of Wernher von Braun in the field of rocket science (German period 1934-1945). In 1933, the Nazi regime in Germany prohibited the conduct of civilian experiments in rocket production in the country and all relevant amateur scientific societies were eliminated. Rockets were allowed to build only by the military. For these purposes, in the north of Germany (on the island Usedom in the Baltic Sea with the village of Peenemünde) large German rocket center and a test site were built in 1937, the Military Head of which was W. Dornberger, and the Technical Director was Wernher von Braun [1, 2] . Under these conditions, Wernher von Braun was forced to join the National Socialist Party of Germany (May 1937). In addition, it is believed that from May 1940 to May 1945 he was an SS officer (he began his service from the rank of Untersturmführer – Lieutenant and rose to the rank of Sturmbannführer – Lieutenant Colonel) [1, 2]. The specified period of work and military service of Wernher von Braun in Germany is a «black spot» in his biography (this information was subsequently hidden for a long time by the secret services from the American public). Despite this SS trail in the life of the essay's main person, Wernher von Braun and his team managed to create an A-4 (V-2) combat rocket launcher by the fall of 1944, capable of hitting cities in the UK and other countries of Europe from a long distance. The first combat missile V-2 (Fig. 2) was launched to London on September 7, 1944 (21 months after the official adoption «at the top» of this German project «The Weapon of Retribution») [1, 2]. Note that the first launches of prototypes of the V-2 rocket from the Peenemünde test site began in October 1942 [3]. The cost of one such rocket, despite the use of free labor by prisoners in its production, amounted to 300 thousand Reichsmarks [3]. Table 1 shows the main tactical and technical characteristics of the V-2 rocket [3, 4].

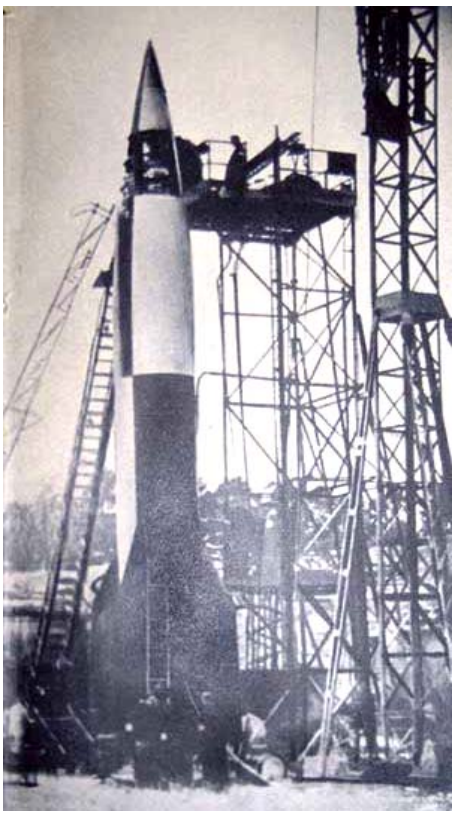

Fig. 2. General view of the single-stage combat missile V-2 with LRE during its preparation on the launch pad for launch (photo of 1944; Peenemünde test site) [3]

Table 1

The main tactical and technical characteristics of a combat German single-stage ballistic missile with LRE V-2 [3, 4]

No.	Characteristic	Value
1	Total length, m	13,9
2	Diameter, м	1,6
3	Weight of the warhead, kg	1000
4	Maximum thrust of the LRE:	
	- near the surface of the Earth, t	26
	- at flight altitude, t	30
5	Starting weight, t	13
6	Maximum range in near-earth space, km	300
7	Type of liquid fuel for LRE	80 % ethanol
8	Mass of liquid fuel, kg	3600
9	Mass of oxidizer (liquid oxygen) for LRE, kg	5000
10	Maximum flight speed in near-earth space, m/s	1500
11	LRE operating time, s	65
12	Maximum flight height above Earth, km	95
13	Speed when meeting with hit target, m/s	800

From the data of Table 1 it can be seen that the V-2 rocket, when flying in near-Earth space, could move at speed of about 5,400 km/h, which significantly exceeded the speed of sound in air, which at normal atmospheric conditions is about 1,194 km/ h (331.8 m/s) [5]. The V-2 missiles were made by foreign workers, prisoners of war and prisoners of concentration camps at the huge underground factory Mittelwerk near the city of Nordhausen in German Thuringia [3]. The design capacity of this plant was up to 30 rockets per day. In 1944, the power of this military plant was brought to release 600 rockets per month [3]. German specialists involved in the V-2 missile solved an important and fundamental task: ensuring its launch from the vertical position on the launch pad [3, 4].

Why is this combat single-stage ballistic missile called the V-2? It is believed that this name comes from the first letter of the German word «Vergelfungswaffee», meaning «Weapon of Retribution» [2]. By the way, the German competitors of Wernher von Braun, engaged in the development and creation of only ballistic missiles in Germany, from the air force set up an industrial production of combat projectiles (cruise missiles), which they called V-1 a little earlier [2, 6]. Note that on June 13, 1944, London was subjected to the first bombardment of V-1 cruise missiles. However, the effect of the combat use of German V-1 missiles with ground targets was extremely weak [2, 3]: such missiles flew at subsonic speeds and could be relatively easily hit by anti-aircraft forces; their accuracy in hitting the target was low; the autonomous mechanism for controlling their flight was poorly protected from external electromagnetic interference (in this connection, due to the directional impact of the English radars on them, they fell off the flight path and often fell into the sea). The V-2 ballistic missiles have no these disadvantages (project scientific manager for its development was Wernher von Braun; military and administrative Head of this project was Wehrmacht Lieutenant General W. Dornberger), including a «mechanical» computer, a turbopump unit, gyros, electromechanical controls of the flight of a rocket, a cooled combustion chamber of liquid fuel in the LRE, and many other devices characteristic of a modern powerful rocket with LRE [7]. Ballistic missiles V-2, made in a total quantity of up to 4300 pcs. (for the period September 1944 – March 1945), inflicted on the British city of London (from the occupied territory of the north of France the said German rocket reached it in just about 6 minutes) and the Dutch city of Antwerp enormous material damage and irreparable human damage (13029 people became their victims) [2, 3]. It should be noted that because of the relatively quick, primarily due to the offensive actions of the USSR and its main allies (USA and Great Britain), approaching the end of the Second World War in Europe and the collapse of Nazi Germany that followed in May 1945, the German strategic project (the Head of works was W. von Braun), associated with the development and creation of an intercontinental two-stage ballistic missile A-9/10 with a range of 5000 km, was unrealized [2, 4].

According to the authoritative opinion of the prominent Soviet specialist in the field of rocket engine technology (the General Designer of the RD-253 type LRE widely known all over the world [6]), twice Hero of Labor, Academician of the Academy of Sciences of the USSR V.P. Glushko [2]: «... *The creation of the V-2*

rocket was a great technical achievement in the field of rocket production».

According to archival data, a prototype of the V-2 rocket launched from the German Peenemünde rocket test site on October 3, 1942 exceeded the speed of sound in the air for the first time in the history of rocketry [7]. It is known that space begins from a height of 70 km above the surface of the Earth [6, 7]. In this regard, it can be argued that the V-2 rocket is the first apparatus of terrestrial origin that has fallen into outer space. The reason for this is that the prototype of the V-2 rocket launched with instruments on February 17, 1943 reached a height above the Earth of 190 km [7]. By the way, Wernher von Braun launched to the same height later in the USA with the help of his new Redstone ballistic missile also the first two American astronauts – A. Shepard (May 5, 1961, 185 km) and V. Grissom (July 21 1961, 190 km) [7].

It is also necessary to point out that military rocket technology in the former USSR and the USA began with the V-2 ballistic missiles, the technical documentation for which, and the very prototypes of which were promptly obtained by the intelligence services of these countries, were carefully studied and used in the respective design offices [4, 7]. Note that the first Soviet ballistic missile P-1 was an exact replica of the German V-2 missile, only manufactured at our factories according to domestic drawings and of domestic materials [4, 7].

Was the relatively young 32-year-old and undoubtedly talented Wernher von Braun the «father» of the V-2 ballistic missile in 1944 (the year when the combat model of the V-2 missile was created)? According to the memoirs of the military and administrative Head of work on the creation of this German rocket W. Dornberger [8]: «*... The V-2 was directly developed by the design bureau led by Walter Riedel. Successes in designing the engine for this rocket were mainly due to the works of Walter Thiel. Although von Braun and Riedel also contributed many ideas to the design of the engine. Riedel, with his calm nature, deep thinking and extensive knowledge, was a good counterbalance to the overly temperamental von Braun. Von Braun's main concern was the elimination of the difficulties encountered in the work. Von Braun's talent as a leader was not without flaws. His undoubted leadership qualities were not always accomplished. However, Wernher von Braun's personal contribution to all areas of the development of the V-2 rocket was decisive, guiding, and truly invaluable*». Summarizing the scientific and technical history of the creation of the V-2 rocket, the former German Wehrmacht Lieutenant General Walter Dornberger (Head of the German Peenemünde test site) in his memoirs came to the deeply thoughtful conclusion that its creation cannot be associated with one person [8]: «*... Days of lonely creative geniuses are over. Such achievements can only be the fruit of the work of a team of unknown researchers and experts who can work side by side without self-indulgence*».

On May 2, 1945, in the Bavarian Alps (southern Germany), Wernher von Braun, along with the V-2 rocket documentation and most of the specialists (first out of 115, and later out of 650 people) from the German rocket group, surrendered to the troops of the advancing American the army (specifically the militants of the 44th US Infantry Division), whose intelligence services already had instructions for a targeted «hunt» for them [3, 7]. In the course of secretly planned US operations, codenamed «Paperclip», they were all taken out of defeated Germany to America and were placed first in Fort Bliss, Texas, which became a major base of the US Army [3]. The US Department of State, through the Joint Intelligence Objectives Agency, developed fictitious biographies for all 765 German experts in rocket technology and removed information about their connection with the Nazi regime in Germany [1, 2]. In this way, the American government provided the German rocket scientists, who had become «state scientists», with the necessary security guarantees for their work in the United States. To this we should add the fact that in 1945, 350 railway cars with valuable technical equipment and nodes for V-2 missiles were delivered by sea to the USA [9].

3. The main achievements of Wernher von Braun in the field of rocket science (the American period 1945-1975). According to the available historical materials typical for Wernher von Braun was that if he set himself a goal, he always achieved it [9]. Largely due to his will and purposefulness, and not only to his talent, he, as a born scientific leader and design engineer, has reached unattainable for many super-high scientific and technical «peaks» in the field of rocket production. Once, on the slope of his long years, an outstanding Soviet aircraft designer, Colonel-General-Engineer, three times Hero of Labor, Academician of the Academy of Sciences of the USSR S.V. Ilyushin [10], personally and well acquainted with many outstanding designers of the USSR in the field of aviation and rocket technology, in an interview with students-graduates of the N.E. Zhukovsky Air Force Academy about the main personal qualities of the Chief Designer said that for such a person [7]: «*... The main quality is the great, all-consuming desire to become the Chief and not stop at nothing on the way to his goal*». The author thinks that in relation to the outstanding designer of rocket and space technology, Wernher von Braun, our patriarch of aircraft construction, as we say, got into the bull's eye. It is this personal quality that was central and characteristic of the leader we are considering in the field of world rocket production.

From September 1945, Wernher von Braun headed the US Army Design and Development Service at the designated Fort Bliss, located near the White Sands Proving Ground, New Mexico [1]. It was from this military test side that Wernher von Braun launched his ballistic missiles. Apparently, these places should be considered the «cradle» of American rocket production. From 1950, together with his German fellow rocket

engineers (Fig. 3), he began working at the Redstone Arsenal (Huntsville, Alabama) [3].

Paying tribute shown in Fig. 3 rocket engineers, we indicate their positions in the Redstone Arsenal of the United States [3]: E. Stuhlinger – Director of the Office of Scientific Research; H. Hoelzer – Director of the Computing Center; K. Heimburg – Director of the Testing Laboratory; E. Geissler – Director of the Aeroballistic Laboratory; E. Neubert – Director of the Laboratory of Reliability and Systems Analysis; W. Haeussermarn – Director of the laboratory of Guidance and Control; Wernher von Braun – Chief Designer and Director of Development Division; W. Mrazek – Director of the Laboratory of Design and Mechanics; H. Hueter – Director of the Laboratory of Ground Systems; E. Rees – Deputy Director of the Development Division; K. Debus – Director of the Missile Launch Laboratory; H. Maus – Director of the Laboratory for the Production and Assembly of Missiles.

Fig. 3. Twelve main German rocket engineers, who replaced the Peenemünde Rocket Center (Germany) with the Redstone Arsenal of the USA (rare NASA photo; from left to right: Ernst Stuhlinger; Helmut Hoelzer; Karl L. Heimburg; Ernst Geissler; Erich W. Neubert; Walter Haeussermarn; Wernher von Braun; William A. Mrazek; Hans Hueter; Eberhard Rees; Kurt Debus; Hans H. Maus; 1959, Redstone Arsenal, USA) [3]

Already, only by the names of the services headed by these rocket men can one indirectly judge the complexity of the scientific and technical tasks facing these developers of US military ballistic missiles, who soon became the first German-American explorers of near-Earth space. In 1951, by the German rocket men shown in Fig. 3, the first American Viking ballistic missile was created, which developed a speed of up to 1.8 km/s (6480 km/h) [6]. Of course, this speed was significantly lower than the first cosmic speed, which is about 7.9 km/s (28440 km/h) [5]. In 1952, under the leadership of Wernher von Braun, a Redstone combat ballistic missile (PGM-11 military index) was created in the United States (Fig. 4) [11], which was used by the US Army in the period 1958-1964 and used at the launch on January 31, 1958 of the first American artificial satellite of the Earth «Explorer 1» (weight –14 kg) [6, 12, 13]. The US launch of this artificial satellite was the American response for the USSR, which launched on October 4, 1957 with the help of an intercontinental ballistic missile P-7 the world's first artificial satellite of 83.6 kg weight [6, 7].

We point out that Redstone combat ballistic missiles (PGM-11) with a thermonuclear warhead W-39 aboard with a power of 4 Mt of TNT were deployed in West Germany [11]. The range of these medium-range missiles was up to 350 km, and their accuracy at hitting the target was up to 300 m (at that time, this accuracy was impressive) [11].

The launch of the first US cigar-shaped artificial satellite Explorer-1 (Fig. 5), which had 8.3 kg of scientific instruments on board, marked the beginning of space flights in the United States, as well as scientific research of space by scientists (for example, the study of the atmosphere, ionosphere and magnetosphere of Earth, energy particles, meteorites and monitoring of solar radiation) [13]. By the way, with the help of the «Explorer 1» artificial satellite which flew around the Earth in 114 minutes on an elliptical orbit at altitudes of 362 – 2565 km, the Van Allen radiation belt was first discovered [14].

Fig. 4. The start of the Redstone medium-range ballistic missile (length – 21.1 m; diameter – 1.78 m) with a detachable warhead created in the USA under the scientific and technical guidance of Wernher von Braun [11]

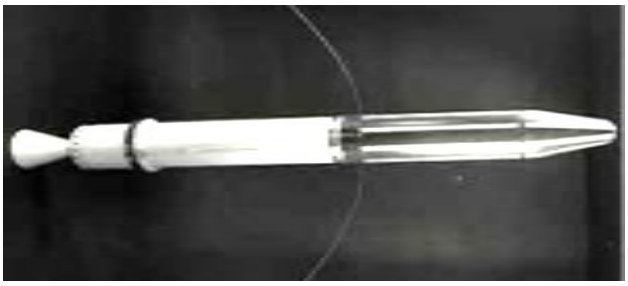

Fig. 5. External view of the first American artificial satellites Explorer-1 (1958, gross weight – 14 kg, USA) [14]

Note that since 1955, Wernher von Braun is a US citizen, the mention of whose name in the press was prohibited by special services [3]. In 1960, the rocket

men, led by Dr. Wernher von Braun, were transferred to the National Aeronautics and Space Administration (NASA) of the United States [15]. So the rocket genius (German Baron by birth), who has now officially become the American designer of rocket and space technology, began to serve NASA, a prestigious US government agency, with full scientific and engineering efficiency. During this period, NASA created the Marshall Space Flight Center, Huntsville, Alabama, as the first Director of which Wernher von Braun was appointed [15]. Now, under his leadership, about 2 thousand people worked, and the leaders of all 30 Departments of this US Space Center were his German colleagues, who, like him in 1955, received American citizenship. At this time, another Soviet call came in the US in the space race: in the USSR on April 12, 1961, into a near-earth orbit using a three-stage ballistic missile P-7 and the Vostok-1 spacecraft (their chief designer was an outstanding Soviet designer of rocket and space technology, twice Hero of Labor, Academician of the Academy of Sciences of the USSR S.P. Korolev), the first Soviet cosmonaut (astronaut in «American») in the history of mankind Yu.A. Gagarin was launched [6, 7]. After the shock from such a course of international events in the field of space exploration in the United States (and throughout the world), Wernher von Braun suggested to the US leadership to carry out several suborbital space flights for the US astronauts with the help of the Redstone launch vehicle. These flights under the direction of Wernher von Braun were performed on May 5, 1961 (A. Shepard traveled in space at an altitude of 185 km) and on July 21, 1961 (V. Grissom traveled in space at an altitude of 190 km) [7]. But this was not enough for ambitious America. In the conquest of space by mankind by such the richest country on our planet as the USA, it was necessary to surprise the world with some kind of a grand event. And such a planned event was found, discussed by experts and voiced in the keynote speech of US President John F. Kennedy [1]: «*... For the prestige of the nation, it is necessary to ensure the landing of the American astronaut on the Moon until 1970*». For the practical implementation of this great goal, the US Lunar Program was prepared, Wernher von Braun was appointed the Head of which [1].

Huge financial resources were allocated for the implementation of the US Lunar program by the US government in the 1960s – about USD 20 billion USA (for comparison, we point out that for the creation in US of the first plutonium and uranium atomic bombs in the United States under the secret Manhattan Project about USD 2 billion budget allocations were allocated [16, 17]) [15]. In order for the United States to fulfill this national space program, a new powerful launch vehicle was needd, called Saturn-V Wernher von Braun was appointed the chief designer of this launch vehicle intended for manned flights to the Moon with the help of Apollo spacecrafts. US President John F. Kennedy (Fig. 6) paid close attention to the development work carried out by NASA in the framework of the Lunar Program [8, 18].

Fig. 6. US President John F. Kennedy (center), Chief Designer of the American Saturn-V launcher Wernher von Braun (left) and US Vice President Lyndon Johnson (right) in the assembly and test building with a prototype of this launch vehicle (1962, the spaceport at Cape Canaveral, Florida, USA) [8]

Everything in our world is relative. So, the German rocket V-2 with the LRE height in a 6-storey house (chief designer - Wernher von Braun; year of creation – 1944) was able to «throw» at a speed of about 5,4 thousand km/h (1.5 km/s) in the Earth's atmosphere 1 ton of payload for a distance of about 300 km (see Table 1). Created in the USA the Saturn-V launch vehicle with LRE of height of 33-storey building (chief designer - Wernher von Braun; year of creation 1969) was able to deliver 50 tons of payload at a speed of about 40,4 thousand km/h (11.2 km/s, corresponding to the second space speed [5]) in space at a distance of about 384 thousand km, equal to the average distance of the Moon from the planet Earth [8]. It is clear that in 25 years (for the period 1944-1969) of active scientific and technical work in the field of rocket technology, Wernher von Braun achieved incredible results: to ensure the increase in the velocity of movement of a multi-ton rocket more than 7 times (from 1.5 to 11.2 km/s); increase the mass of payload delivered by a rocket by 50 times (from 1 to 50 tons); to increase the range of delivery of a payload by a rocket by 1,280 times (from 0.3 to 384 thousand km). Just a gigantic evolution of integral indicators in the field of modern rocket and space technology!

Now it becomes clear the answer to the question of why the United States ahead of the USSR in landing on the surface of the Moon a representative (resident) of our planet. They were ahead due to the superiority in the operational creation by the American specialists of a powerful launch vehicle. The organizational and scientific and technical talent of designer Wernher von Braun in this advance is paramount. As a result, on July 20, 1969, the American Apollo-11 spacecraft with three astronauts on board (Neil Armstrong, Michael Collins and Buzz Aldrin), driven by the energy of the Saturn-V launch vehicle in outer space, carried out with the help of a descending lunar module Eagle with two astronauts on board (N. Armstrong and B. Aldrin) landing on the lunar surface [6, 15]. In Fig. 7 the moment of N. Armstrong walking on the Noon is captured [9].

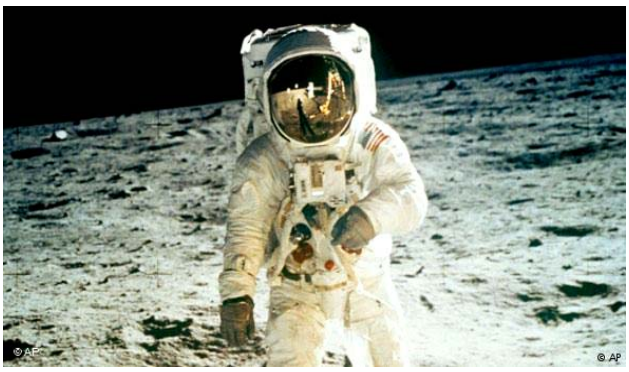

Fig. 7. Historical moment: for the first time in the history of mankind, the American astronaut Neil Armstrong was on the lunar surface (a photo of July 20, 1969, Moon)

It is interesting for the reader to quote the remarkable, inspired and truly pathetic words of the American astronaut Neil Armstrong (August 5, 1930 – August 25, 2012), the first earthman to enter the lunar soil, after his walk for 2 hours 41 minutes in a spacesuit on the surface of the Moon [6]: «*... It was a small human step. But it was a great leap for humanity*».

For this flight of the American Apollo-11 spacecraft, Wernher von Braun in 1969 was awarded the NASA medal «For Distinguished Service» [1]. From January 1970, he becomes the NASA Deputy Assistant Administrator for planning. Wernher von Braun reached the top of his career in 1972 (Fig. 8) when he became the NASA Deputy Director and at the same time the Head of the US space center at Cape Canaveral, Florida [2]. However, in the same 1972, in the conditions of the economic crisis, he was offered to cancel expensive flights to the Moon with the aim of studying it and to engage in more economically advantageous launches of reconnaissance and scientific-technical satellites of the Earth [2, 9].

Fig. 8. The finest hour of the twentieth-century rocket and space technology designer Wernher von Braun during the leadership of the spaceport at Cape Canaveral, on the launch pad of which, at the time of the photo, its launch vehicle Saturn-V was preparing to launch.(1972, USA) [2]

The «father» of the US space program apparently did not agree with such a commercial statement of the issue in the field of space exploration and was soon dismissed by the NASA leadership [2]. He did not remain without work: representatives of the American business, who knew his business skills well, immediately offered him the position of Vice-President of Fairchild Space Industries, Germantown, Maryland engaged in the production of aerospace equipment [15]. Then the «black» life strip came: he was diagnosed with a serious illness - pancreatic cancer. Virtually the entire 1973 went to Wernher von Braun for surgery and intensive treatment of this disease. In 1974, despite the weakened health, he continued to work on the project of a new satellite, and gave all his free time to flying on his own glider [2].

In Fig. 9 space dreamer and a true fan of space exploration Wernher von Braun is depicted against the backdrop of the impressive design of the Saturn-V heavy American launch vehicle, for the development and creation of which he, as its chief designer, gave so much strength and health.

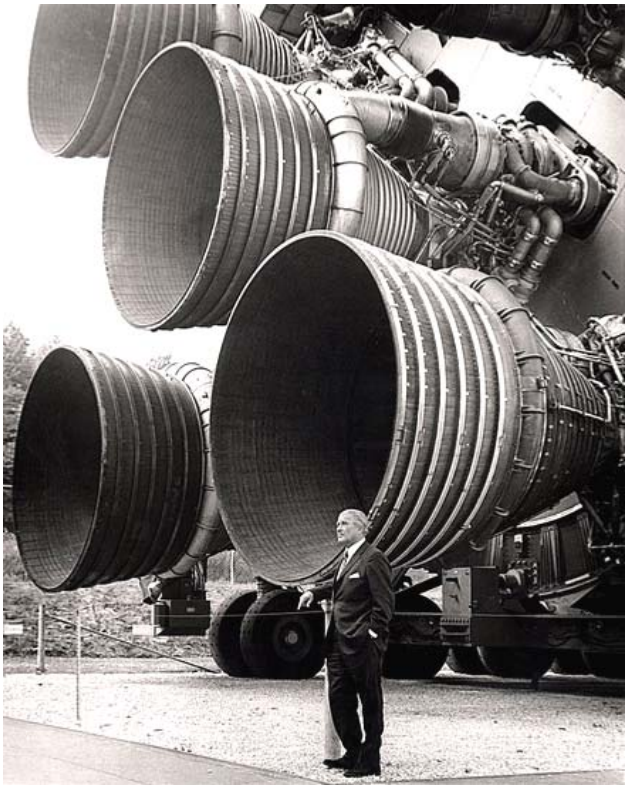

Fig. 9. Outstanding designer of rocket and space technology Wernher von Braun near with his main space «brainchild» in the United States – the museum exhibit of the powerful launch vehicle Saturn-V (in the foreground – nozzles of combustion chambers of LRE fuel of its first stage) [1]

4. Awards and honors of Wernher von Braun. He didn't have many of them, he had only the awards and badges of the Federal Republic of Germany and the United States [1]:

- The Grand Cross of the Order of Merit for the Federal Republic of Germany (1951);
- Order «For Services to the Federal Republic of Germany» (1951);
- NASA Medal «For Distinguished Service» (1969);

- Elliott Cresson Medal (1962);
- Langley Gold Medal (1967);
- Wilhelm Exner Medal (1969);
- National Science Medal of the United States (1975);
- Werner von Siemens Ring (1975).

On June 16, 1977, after a long struggle with serious illness, Wernher von Braun died. He was buried with honors at the Ivy Hill Cemetery, Fig. 10 in Alexandria, Virginia, USA [1]. On the NASA website, this great rocket technology designer is given the following characteristic [15]: «*... Without any doubt, Wernher von Braun was the greatest scientist in the field of rocket physics in history*».

Fig. 10. A modest gravestone on the grave of Wernher von Braun, an outstanding designer of the 20th century in the field of rocket and space technology (1977, Ivy Hill Cemetery, Alexandria, Virginia, USA) [1]

In 1977, US President Jimmy Carter responded on the death of Wernher von Braun as follows [8]: «*... For millions of Americans, the name of Wernher von Braun was inextricably linked with the exploration of space by the American nation and the creative use of technology. He was not only a skilled engineer, but also a man with a bold vision. His inspirational leadership style helped us to mobilize and preserve the efforts that made us reach the Moon and move on. Not only the representatives of our nation, but also the people of the whole Earth, benefited from the fruits of his work. His legacy will continue to benefit us*».

The famous American science fiction writer Arthur Clark wrote about the hero of our essay [8]: «*... There are only a few people in the entire history of our civilization who have left behind such a set of achievements as Wernher von Braun, or who could themselves see such a complete triumph of their ideas and the realization of their dreams. His example will inspire future generations of people. The fact that I happened to call him my friend, I consider one of the greatest successes in my life*».

The current generations of earthlings will remember Wernher von Braun as a great man who helped people pave the «road» into space and get them to often seen by us on the night sky the satellite of our planet Earth – the Moon. They will remember him as a person who has managed in his life, in spite of everything, to realize not only his own, but also the dream of all mankind – to penetrate into other worlds of the Universe. He managed to bring a bright «flame» from the torch of his scientific and technical knowledge to the consciousness of all earthlings.

Conclusions. Wernher von Braun, a talented scientist and Doctor of Physics, as a German designer of rocket technology (chief designer of a single-stage ballistic V-2 missile with LRE created in Germany in 1944) and as an American (from 1955) designer of rocket-space technology (chief designer of the three-stage, high-power Saturn-5 launch vehicle with LRE, created in the USA in 1969, and the US manned space spacecraft Apollo), which provided for the first time in the history of mankind the landing of the planet Earth's resident Neil Armstrong on the ground of the Moon, became one of the founders of modern world rocketry. The outstanding results of his fruitful work on American soil became the worldwide scientific and technical foundation for the further conquest and study of the near and far space of our Universe by other scientists and designers of rocket and space technology.

REFERENCES

1. Available at: https https://en.wikipedia.org/wiki/Wernher_von_Braun (accessed 16 May 2018).

2. Available at: http://historius.narod.ru/spravka/braun/index.htm (accessed 22 February 2018). (Rus).

3. Available at: http://osiktakan.ru/1-isz3_1.html (accessed 10 March 2018). (Rus).

4. Chertok B.E. *Rakety i liudi. V 4-kh tomakh. Tom 1* [Rockets and people. In 4-th volumes. Vol. 1]. Moscow, Mashinostroenie Publ., 1999. 416 p. (Rus).

5. Kuhling H. *Spravochnik po fizike. Per. s nem*. [Dictonary on Physics. Translated from German]. Moscow, Mir Publ., 1982. 520 p. (Rus).

6. Baranov M.I. *Antologiia vydaiushchikhsia dostizhenii v nauke i tekhnike: Monografiia v 2-kh tomakh. Tom 2.* [An anthology of outstanding achievements in science and technology: Monographs in 2 vols. Vol.2]. Kharkov, NTMT Publ., 2013. 333 p. (Rus).

7. Available at: https://zn.ua/SOCIETY/samaya_bolshaya_tayna_sovetskoy_raketnoy_tehniki.html (accessed 21 April 2018). (Rus).

8. Available at: https://www.golos-ameriki.ru/a/von-braun-annivesary-2012-03-24-144087166/666031.html (accessed 06 March 2018). (Rus).

9. Available at: https://www.dw.com/ru/вернер_фон_браун_от_фау-2_до_полетов_на_луну/a-4752846 (accessed 11 May 2018). (Rus).

10. Available at: http://www.ilyushin.org/about/history/biography (accessed 28 January 2018). (Rus).

11. Available at: https://en.wikipedia.org/wiki/PGM-11_Redstone (accessed 15 February 2018).

12. Available at: https://history.wikireading.ru/80560 (accessed 14 March 2018). (Rus).

13. Available at: https://www.gazeta.ru/science/2018/01/31_a_11631439.shtml (accessed 02 May 2019). (Rus).
14. Available at: https://ecoruspace.me/Эксплорер-1.html (accessed 28 September 2018). (Rus).
15. Available at: https://topwar.ru/11774-verner-fon-braun-raketnyy-baron-na-sluzhbe-nasa.html (accessed 11 August 2018). (Rus).
16. Baranov M.I. An anthology of outstanding achievements in science and technology. Part 7: Nuclear and thermonuclear weapon creation. *Electrical engineering & electromechanics*, 2012, no.2, pp. 3-15. (Rus). **doi: 10.20998/2074-272X.2012.2.01.**
17. Baranov M.I. An anthology of the distinguished achievements in science and technique. Part 40: The scientific opening of the method of explosive implosion for the obtaining above critical mass of nuclear charge and Ukrainian «track» in the «Manhattan» American atomic project. *Electrical engineering & electromechanics*, 2017, no.5, pp. 3-13. **doi: 10.20998/2074-272X.2017.5.01.**
18. Pishkevich D. *Verner fon Braun. Chelovek, kotoryi prodal Lunu* [Vernher von Braun. Man which sold the Moon]. Moscow, Popurri Publ., 2011. 360 p. (Rus).

Received 08.04.2019

M.I. Baranov, *Doctor of Technical Science, Professor,*
Scientific-&-Research Planning-&-Design Institute «Molniya»,
National Technical University «Kharkiv Polytechnic Institute»,
47, Shevchenko Str., Kharkiv, 61013, Ukraine,
phone +380 57 7076841,
e-mail: baranovmi@kpi.kharkov.ua

How to cite this article:
Baranov M.I. An anthology of the distinguished achievements in science and technique. Part 50: Rocket-space technology designer Wernher von Braun and his accomplishments in missile design. *Electrical engineering & electromechanics*, 2019, no.4, pp. 3-11. **doi: 10.20998/2074-272X.2019.4.01.**

UDC 621.313 **doi: 10.20998/2074-272X.2019.4.02**

O.V. Bibik, L.I. Mazurenko, M.O. Shykhnenko

FORMATION OF CHARACTERISTICS OF OPERATING MODES OF SWITCHED RELUCTANCE MOTORS WITH PERIODIC LOAD

Purpose. ***The purpose of the article is to create dependencies of efficiency on effective power when changing the supply voltage and switching angles, pulsation speeds of the rotor from the moment of inertia of the drive and mechanical characteristics of switched-reluctance motors with a periodic load, developing recommendations to ensure their effective and reliable operating modes in single-cylinder piston compressors.*** ***Methodology.*** ***To carry out research simulation mathematic modeling was used, to calculate the nonlinear inductance dependence on current and rotor angle, the finite element method.*** ***Results.*** ***The measures of improve the efficiency and reliability of drives single-cylinder piston compressors on the basis of the SRM has been proposed.*** ***Originality.*** ***Approaches that provide maximum efficiency values and a regulated level of ripple speeds of rotors SRM of single-cylinder reciprocating compressors in the operating frequency control range, with periodic load have been developed.*** ***Practical value.*** ***Algorithm for changing the supply voltage and switching angles of the SRM of single-cylinder compressors, which provides maximum efficiency values SRM when the rotational speed changes within the 1:6 range, has been developed.*** ***The minimum values of the moments of inertia of the drive of single-cylinder compressors, providing a regulated level of pulsations of the rotational speed of the rotor SRM with its regulation, were determined.*** References 10, figures 5.

Key words: **switched reluctance motor, periodic load, characteristics, efficiency, rotation frequency ripples.**

Мета. ***Метою статті є формування залежностей ККД від корисної потужності за зміни напруги живлення і кутів комутації, пульсацій частоти обертання ротора від моменту інерції приводу та механічних характеристик вентильно-індукторних двигунів з періодичним навантаженням, розроблення рекомендацій щодо забезпечення їх ефективних і надійних робочих режимів у складі одноциліндрових поршневих компресорів.*** ***Методика.*** ***Для проведення досліджень використано імітаційне математичне моделювання, для розрахунку нелінійної залежності індуктивності від струму і кута повороту ротора – метод скінченних елементів.*** ***Результати.*** ***Запропоновано заходи по підвищенню ефективності і надійності приводів одноциліндрових поршневих компресорів та основі ВІД.*** ***Наукова новизна.*** ***Розроблено підходи, що забезпечують максимальні значення ККД і регламентований рівень пульсацій частоти обертання роторів ВІД одноциліндрових поршневих компресорів у робочому діапазоні регулювання частоти обертання з врахуванням періодичного навантаження.*** ***Практичне значення.*** ***Розроблено алгоритм зміни напруги живлення і кутів комутації ВІД одноциліндрових компресорів одинарної дії, що забезпечують максимальні значення ККД при регулюванні частоти обертання в межах діапазону 1:6. Визначено мінімальні значення моментів інерції приводу одноциліндрових компресорів з ВІД потужністю 100 Вт, що забезпечують регламентований рівень пульсацій частоти обертання ротора ВІД при її регулюванні.*** Бібл. 10, рис. 5.

Ключові слова: **вентильно-індукторний двигун, періодичне навантаження, характеристики, коефіцієнт корисної дії, пульсації частоти обертання.**

Цель. ***Целью статьи является формирование зависимостей КПД от полезной мощности при изменении напряжения питания и углов коммутации, пульсаций частоты вращения ротора от момента инерции привода и механических характеристик вентильно-индукторных двигателей с периодической нагрузкой, разработка рекомендаций по обеспечению их эффективных и надежных рабочих режимов в составе одноцилиндровых поршневых компрессоров.*** ***Методика.*** ***Для проведения исследований использовано имитационное математическое моделирование, для расчета нелинейной зависимости индуктивности от тока и угла поворота ротора – метод конечных элементов.*** ***Результаты.*** ***Предложены меры по повышению эффективности и надежности приводов одноцилиндровых поршневых компрессоров и основе ВИД.*** ***Научная новизна.*** ***Разработаны подходы, которые обеспечивают максимальные значения КПД и регламентированный уровень пульсаций частоты вращения роторов ВИД одноцилиндровых поршневых компрессоров в рабочем диапазоне регулирования частоты вращения с учетом периодической нагрузки.*** ***Практическое значение.*** ***Разработан алгоритм изменения напряжения питания и углов коммутации ВИД одноцилиндровых компрессоров, который обеспечивает максимальные значения КПД при регулировании частоты вращения в пределах диапазона 1:6. Определены минимальные значения моментов инерции привода одноцилиндровых компрессоров с ВИД мощностью 100 Вт, обеспечивающие регламентированный уровень пульсаций частоты вращения ротора ВИД при ее регулировании.*** Библ. 10, рис. 5.

Ключевые слова: **вентильно-индукторный двигатель, периодическая нагрузка, характеристики, коэффициент полезного действия, пульсации частоты вращения.**

Problem definition. Features of operation of compressor plants require the use of a regulated electric drive, which provides energy-efficient operating modes [1-4]. Promising are induction motors with short-circuited rotors and frequency converters, which carry out a smooth adjustment of the rotational speed. Alternatives for them are controlled synchronous motors with electromagnetic excitation or with excitation from permanent magnets, as well as switched reluctance motors with reactive rotor [5]. The use of regulated switched reluctance motors due to their high energy performance, starting and adjusting properties provides solution of the problem of increasing the efficiency and reliability of electromechanical equipment operating under variable load conditions.

In order to create a competitive switched reluctance motors drive of hermetic piston compressors (HPCs), usually of single-cylinder compressors with power up to

500 W, with a significant reloading capacity (up to 3.0), it is necessary to provide efficient modes of their operation with the maximum values of efficiency in the range of 1:6 with the permissible level of the ripples of the rotor rotational speed and to reduce the weight and size indicators as well as costs of the main units of the machine.

Analysis of recent research and publications. The power indicators of electric drives with periodic loads are estimated using cyclic efficiency, which is determined in the period of one cycle of load variation. The long period of operation of the induction electric drive with periodic load with significant values of maximum and starting torques, in the mode of underloading leads to a decrease in energy efficiency and non-optimal energy use [6].

The level of the ripples of the rotation speed of motor rotors, traditionally induction, hermetically sealed piston compressors, is strictly regulated by standards and can not exceed 20 %. To reduce the amplitude of these ripples, on the motor rotor an additional inertial mass is mounted – the flywheel [7]. An important step to increase the reliability of the HPC drive is to reduce the ripples of rotational speed of the rotor to a predetermined level when it is adjusted in the required range. Analysis of the research of the switched reluctance drive [8] shows that in steady-state modes, its efficiency decreases by 4 % with a double load reduction, which is confirmed by the results [9]. In this paper [9] the authors give the characteristics of the SRM with switch with C-reset and vibrational energy return for change in supply voltage and switching angles at a constant load. The switch and its control circuit are simple enough, which is important for the mass production of compressors, pumps, etc.

Studies in this direction need to be continued for the purpose of evaluating the efficiency and ripples of the rotational speed of the SRM rotor at the change in the angles of switching, voltage and moment of inertia of the drive, taking into account the periodic load. This will allow the development of measures for adjusting the SRM rotor speed of rotation in the composition of compressor equipment and to reduce the costs of motor development.

The goal of the work is to form the dependencies of the efficiency on the power output at the changes in the supply voltage and switching angles, the ripples of the rotor rotation speed on the moment of inertia of the drive and the mechanical characteristics of the switched reluctance motors with periodic load, the development of recommendations for the provision of their efficient and reliable operating modes in the single-cylinder piston compressors.

Mathematical model of the switched reluctance drive. The object of the study is a SRM, which is developed on the basis of an induction motor 4AA56A4У3 (nominal power of 120 W and rotational speed of 3000 rpm) with a number of poles of 6/4 and of phases m=3 phases with a switch with C-reset and a vibrational energy return [9]. A mathematical model [9] is used to study the modes of operation, the adequacy of which is confirmed by comparing the results of numerical and experimental studies. Its equations describe the structural elements of the motor and take into account their mutual influence.

For the phase of the switched reluctance machine, the following equation holds true

$$\frac{d\psi_{ph}}{dt} = u_{ph} - i_{ph} \cdot R_{ph},$$

where u_{ph}, R_{ph}, i_{ph}, ψ_{ph} are the voltage at the output of the switch; resistance, current and flux linkage of the stator phase, respectively.

Phase current is determined as

$$\frac{di_{ph}}{dt} = \frac{1}{L_{ph}}\left(\frac{d\psi_{ph}}{dt} - i_{ph}\omega\frac{\partial L_{ph}}{\partial \theta_{ph}}\right),$$

where L_{ph} is the inductance of the stator phase, which is calculated by the finite element method [9] and is represented as a function of the current and the rotation angle of the rotor relative to the stator phase $L_{ph} = f(\theta_{ph}, i_{ph})$; $\frac{\partial L_{ph}}{\partial \theta_{ph}}$ is the partial derivative of the tabular function L_{ph} by the angle θ_{ph}; ω is the angular rotor rotation speed; θ_{ph} is the rotation angle relative to the stator phase.

Electromagnetic moment formed by a single phase of the SRM

$$M_{ph} = \frac{1}{2} i_{ph}^2 \frac{\partial L_{ph}}{\partial \theta_{ph}},$$

and the total torque M of the switched reluctance motor from the action of m phases

$$M = \sum_{k=1}^{m} M_{ph(k)}.$$

Differential equations of motion

$$\frac{d\omega}{dt} = \frac{1}{J}(M - M_c),$$

where J is the compressor moment of inertia; M_c is the load torque.

The angle of rotation of the rotor is obtained from the equation

$$\frac{d\theta}{dt} = \omega.$$

This angle relative to the stator phase

$$\theta_{ph} = \mathrm{mod}(\theta; \frac{2\pi}{Z_R}),$$

where Z_R is the number of rotor teeth

Mathematical modelling of the SRM is carried out in MATLAB – Simulink environment using the SymPowerSystems library. As the input parameters of the mathematical model, the angles θ_{on} of switching on and θ_{off} of switching off, the voltage of the DC link U_d and the phase inductance dependencies on the angle of rotation of the rotor and the phase current are used.

The mathematical model takes into account the dependence of the load torque of the single-cylinder HPC of single action on the rotation angle of the motor rotor $M_c = f(\theta)$ applied in the range $7\pi/9$ on the period 2π, the temporal dependence of which is shown in Fig. 1. To compare the calculations of operating modes with constant and periodic load, the average value $M_{c(mean)}$ of

the last one during the load period is used. For Fig. 1 – 0.33 N·m.

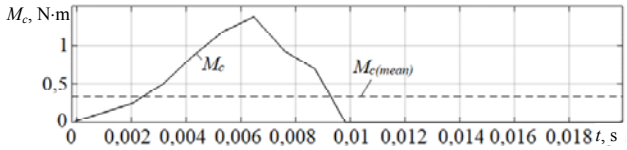

Fig. 1. Temporal dependence of the load torque of the single-cylinder compressor

Numerical experiment. With the help of the mathematical model of the SRM, its efficiency is calculated taking into account losses in copper, magnetic and mechanical losses in operating modes at periodic loading. The calculation of the magnetic losses consisting of losses on hysteresis and eddy currents is based on the approach [10]. Mechanical losses are determined taking into account the change in rotor rotation speed and torque due to friction in bearings [9]. A method for controlling the SRM based on the change of the angle of switching on ($\theta_{on} = var$) in the range θ_{on} = 36°…51° at a constant clock angle (θ_k = 30°) and symmetric switching is used.

Dependencies of efficiency on the useful power P_2 at changes in the supply voltage and switching angles at steady and periodic load, when $M_{c(mean)}$ = 0.33 N·m, are shown in Fig. 2. Each dependence is obtained at steady angles of switching on and switching off and change of voltage. The power of 103 W corresponds to the rotation speed of 3000 rpm, 52 W – 1500 rpm. The obtained dependencies of the efficiency with periodic loading with the moment of inertia $J = 0.5 \cdot 10^{-3}$ kg·m^2 practically do not differ from the efficiency of the motor with a constant load at $J = 1 \cdot 10^{-4}$ kg·m^2 (the constant torque equals the average value of the periodic load).

Shift of the switching zone towards the lowering of the angles of switching on and switching off leads to an increase in the motor efficiency, but the increase in efficiency is not observed throughout the entire range of loads. This allows to formulate an algorithm for changing the angles of commutation, which provides the maximum values of the efficiency of the switched reluctance motors of single-cylinder compressors on single action for the entire range of rotor rotation frequency control:

- in the range 3000…1500 rpm the SRMs should operate with commutation angles θ_{on} = 36°, θ_{off} = 66° and the voltage U_d = 133…77 V;
- from 1500 to 1000 rpm – with angles θ_{on} = 39°, θ_{off} = 69°, U_d = 185…137 V;
- from 1000 to 500 rpm – with θ_{on} = 42°, θ_{off} = 72°, U_d = 149…88 V.

The influence of the moment of inertia of the drive of a hermetic piston single-cylinder compressor on the ripples of the rotation speed of the SRM rotor for the range of regulation of the rotation speed of 1:6 at constant angles of commutation is investigated. It is shown that the regulated level of ripple (δn = 20 %) with frequency regulation in the range of 1:3 (3000...1000 rpm) can be provided at the moment of inertia of the drive $5 \cdot 10^{-4}$ kg·m^2, in the range of 1:4 (3000...750 rpm) – $1 \cdot 10^{-3}$ kg·m^2 (Fig. 3). Increasing the moment of inertia leads to a reduction of ripples and expansion of the range of regulation.

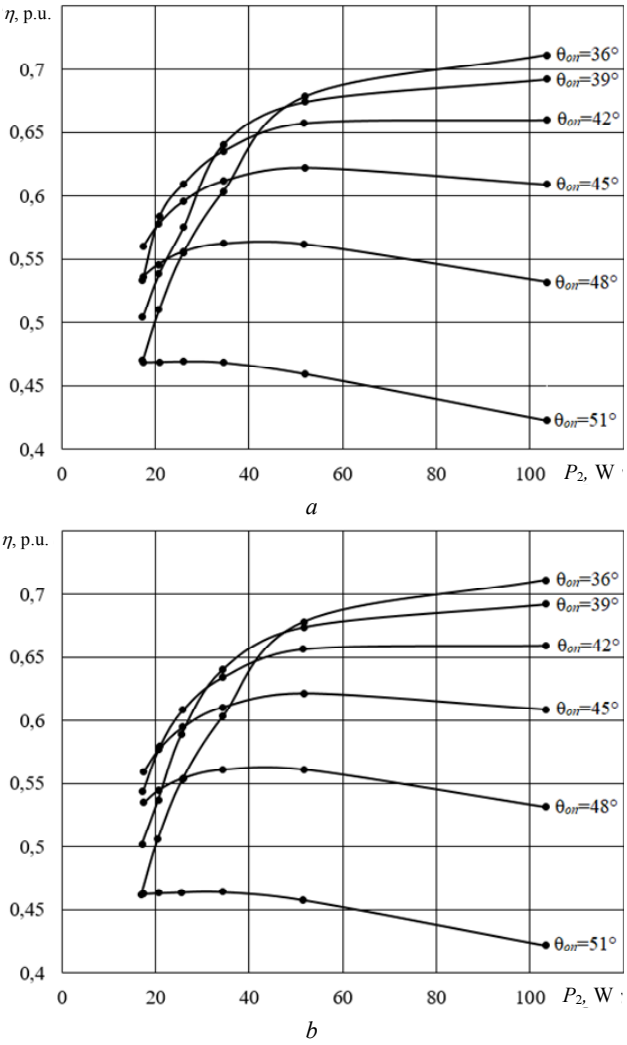

Fig. 2. Dependencies of efficiency on the useful power at changing the supply voltage for different switching angles at steady state M_c=const (*a*) and periodic M_c=*f*(θ) (*b*) load for moments of inertia J=1·10^{-4} kg·m^2 and J=1·10^{-3} kg·m^2, respectively

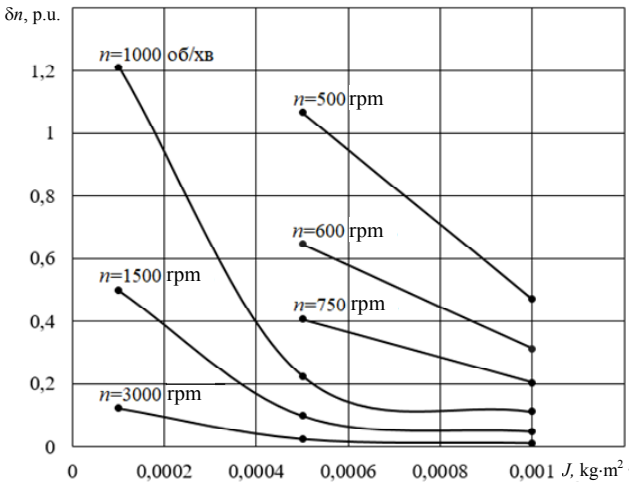

Fig. 3. Dependence of the ripples of the SRM rotor rotational speed on the moment of inertia of the drive of a single-cylinder HPC at steady angles θ_{on} = 42°, θ_{off} = 72°.

Extension of the range (up to 1:6) under this condition can be implemented:

- for pulsating load of a two-cylinder compressor ($M_{c(mean)}$ = 0.33 N·m, moment of inertia of the drive $1 \cdot 10^{-3}$ kg·m^2), which provides ripples of frequency in the range of 0.3...12.8 %
- for less than twice the load at steady angles of switching due to a change in supply voltage.

Figure 4 shows the mechanical characteristics of the SRM at constant switching angles (θ_{on} = 42°, θ_{off} = 72°) at changing the supply voltage in the range 31...121 V, which makes it possible to regulate the frequency of rotor rotation in the range of 1:6 with periodic load $M_{c(mean)}$ = 0.165 N·m.

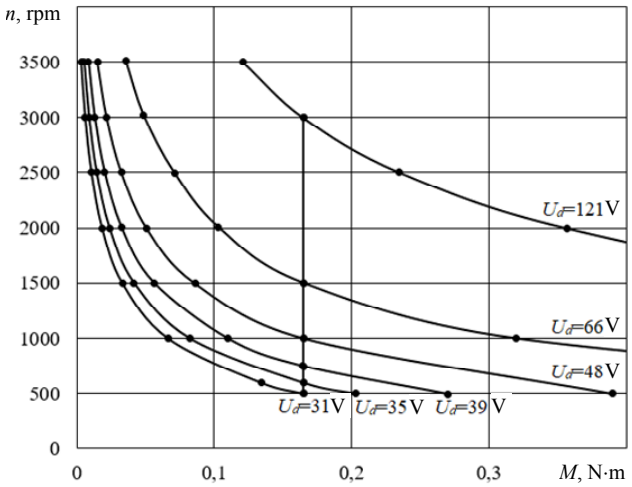

Fig. 4. Mechanical characteristics of the SRM at different values of supply voltage (θ_{on} = 42°, θ_{off} = 72°).

The study of the effect of reducing the loading torque twice on the motor efficiency at changes in the angles of commutation (Fig. 5) is carried out. It is shown that when the rotation speed of the motor is reduced from 3000 to 500 rpm for angles θ_{on} = 36° and θ_{off} = 66° and $M_{c(mean)}$ = 0.165 N·m its efficiency decreases by 1 ... 5 % in comparison with $M_{c(mean)}$ = 0.33 N·n.

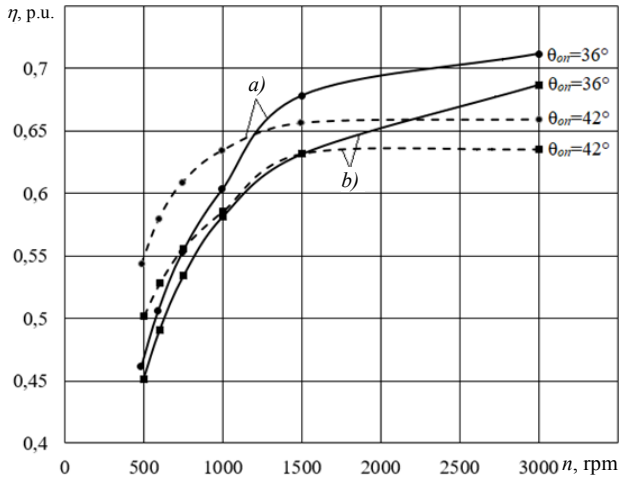

Fig. 5. Dependencies of efficiency on the rotational speed of the SRM rotor at regulating the rotor rotation speed by changing the supply voltage and constant angles:
a) $M_{c(mean)}$ = 0.33 N·m; *b*) $M_{c(mean)}$ = 0.165 N·m

It is found that at the nominal rotational speed at $M_{c(mean)}$ = 0.165 N·m, the highest efficiency is provided by switching angles θ_{on} = 36°, θ_{off} = 66°, at rotation frequencies in the range of 750...500 rpm – by angles θ_{on} = 42°, θ_{off} = 72°, which allow to increase the efficiency by 2…5 % in comparison with the angles θ_{on} = 36° and θ_{off} = 66°.

Conclusions.

1. Using the mathematical model, the operating modes of the switched reluctance motors with a switch and C-reset and a oscillatory return of energy of single-cylinder piston compressors at the changes in the supply voltage, switching angles and moment of inertia, taking into account the periodic load are investigated, which allowed to form the characteristics of the motors that provide an increase their energy efficiency and reliability.
2. The algorithm for changing the supply voltage and switching angles of the SRM is proposed, which provides the maximum values of efficiency at change in the frequency of rotation in the range of 1:6.
3. The values of moments of inertia of SRM of hermetic piston compressors are determined, which provide the recommended level of ripples of the rotational speed of the rotor of 20 % in the ranges: 1:4 – for single-cylinder compressors, 1:6 – for double-cylinder ones.
4. The results of the research can be used for the creation of SRMs that operate in compressors and pumps in the areas of municipal and industrial use.

REFERENCES

1. Zhivitsa V.I., Onischenko O.A., Radimov I.N., Shevchenko V.B. Modern electric drive of refrigeration units. *Refrigeration Engineering and Technology*, 1999, iss.64, pp. 112-116. (Rus).

2. Andersen H.R. *Motor drives for variable speed compressors: Introduction and state of the art analysis. PhD Thesis*. Aalborg University Publ., 1996, vol.1, 62 p.

3. Jakobsen A., Rasmussen B. Energy optimization of domestic refrigerators Major energy saving by use of variable speed compressors and evaporator fans. *International Appliance Manufacturing*, 1998, pp. 105-109.

4. Monasry J.F., Hirayama T., Aoki T., Shida S., Hatayama M., Okada M. Development of large capacity and high efficiency rotary compressor. *24th International Compressor Engineering Conference at Purdue*, July 9-12, 2018, paper 2576.

5. Bibik O.V. Analysis and main trends of electromechanical energy converters for systems with periodic load. *Works of the Institute of Electrodynamics of the National Academy of Sciences of Ukraine,* 2016, no.43, pp. 37-43. (Ukr).

6. Bibik O.V. Rationale approaches to designing asynchronous motors with variable load. *Bulletin of the National Technical University «KhPI». Series: Electrical Machines and Electromechanical Energy Conversion*, 2019, no.4(1329), pp. 94-98. (Ukr). **doi: 10.20998/2409-9295.2019.4.14.**

7. Morozyuk L.I., Morozyuk T.V., Iastrebova L.V. *Proektirovanie porshnevogo kompressora holodilnyih mashin i teplovyih nasosov* [Designing a piston compressor for refrigerating machines and heat pumps]. Odessa, OGAH Publ., 2003. 75 p. (Rus).

8. Andrada P., Blanque B., Perat J.I., Torrent M., Martinez E., Sanchez J.A. Comparative efficiency of switched reluctance and induction motor drives for slowly varying loads. *International*

Conference on Renewable Energies and Power Quality (ICREPQ'06), 2007.
9. Mazurenko L.I., Bibik O.V., Bilyk O.A., Shihnenko M.O. Simulation mode and speed control of switched reluctance motor using a converter with the C-dump and the oscillation return of energy at changing switching angles. *Bulletin of the National Technical University «KhPI». Series: Electrical Machines and Electromechanical Energy Conversion*, 2016, no.11(1183), p. 64-69. (Ukr).
10. Kostenko M.P. Piotrovsky L.M. *Elektricheskie mashinyi. V 2-h. ch. Ch.1. – Mashinyi postoyannogo toka. Transformatoryi. Uchebnik dlya studentov vyisshih tehnicheskih uchebnyih zavedeniy* [Electric machines. In 2 parts. Part 1. – DC machines. Transformers. Textbook for students of higher technical educational institutions]. Leningrad, Energy Publ., 1972. 544 p. (Rus).

Received 11.06.2019

O.V. Bibik[1], *Candidate of Technical Science, Associate Professor,*
L.I. Mazurenko[1], *Doctor of Technical Science, Professor,*
M.O. Shykhnenko[1], *Research Associate,*
[1] The Institute of Electrodynamics of the NAS of Ukraine,
56, prospekt Peremogy, Kiev, 03057, Ukraine,
phone +380 44 3662491,
e-mail: bibik@ied.org.ua; mlins@ied.org.ua

How to cite this article:
Bibik O.V., Mazurenko L.I., Shykhnenko M.O. Formation of characteristics of operating modes of switched reluctance motors with periodic load. *Electrical engineering & electromechanics*, 2019, no.4, pp. 12-16. **doi: 10.20998/2074-272X.2019.4.02.**

UDC 621.3.01 **doi: 10.20998/2074-272X.2019.4.03**

B.I. Kuznetsov, T.B. Nikitina, I.V. Bovdui

HIGH VOLTAGE POWER LINES MAGNETIC FIELD SYSTEM OF ACTIVE SHIELDING WITH COMPENSATION COIL DIFFERENT SPATIAL ARRANGEMENT

Aim. The synthesis of single-circuit system of active shielding of magnetic field, generated by group of high voltage power lines, with different spatial arrangement of shielding coil. Methodology. The synthesis is based on the decision of a multi-criteria stochastic game, in which the vector payoff is calculated on the basis of the Maxwell equations solutions in the quasi-stationary approximation. The game decision is based on the stochastic multiagent optimization algorithms by multiswarm particles. The initial parameters for the synthesis of active shielding system are the location of the high voltage power lines with respect to the shielding space, geometry and number of shielding coils, operating currents, as well as the size of the shielding space and normative value magnetic flux density, which should be achieved as a result of shielding. The objective of the synthesis of the active shielding system is to determine their number, configuration, spatial arrangement, wiring diagrams and shielding coils currents, setting algorithm of the control systems as well as the resulting of the magnetic flux density value at the points of the shielding space. Results. Three variant of single-circuit robust system of active shielding with different spatial arrangement of shielding coil synthesis results for reduction of a magnetic field generated by group of high voltage power lines is given. The possibility of a significant reduction in the level of magnetic flux density of the magnetic field source within and reducing the sensitivity of the system to uncertainty of the plant parameters is given. Originality. For the first time carried out the synthesis, theoretical and experimental research of the robust system of active shielding of magnetic field generated by group of high voltage power lines with different spatial arrangement of compensation coil. Practical value. Practical recommendations from the point of view of the practical implementation on reasonable choice of the spatial arrangement of shielding coil of robust single-circuit system of active shielding of the magnetic field generated by the group of high voltage power lines is given. References 49, figures 9.

Key words: **high voltage power lines, power frequency magnetic field, robust system of active shielding, multi-criteria stochastic game.**

Цель. Синтез одноконтурной робастной системы активного экранирования магнитного поля, создаваемого группой высоковольтных линий электропередачи, с различным пространственным расположением экранирующей обмотки. Методология. Синтез основан на решении многокритериальной стохастической игры, в которой векторный выигрыш вычисляется на основании решений уравнений Максвелла в квазистационарном приближении. Решение игры находится на основе алгоритмов стохастической мультиагентной оптимизации мультироем частиц. Исходными параметрами для синтеза системы активного экранирования являются расположение высоковольтных линий электропередачи по отношению к защищаемому пространству, геометрические размеры, количество проводов и рабочие токи линии электропередачи, а также размеры экранируемого пространства и нормативное значение индукции магнитного поля, которое должно быть достигнуто в результате экранирования. Целью синтеза системы активного экранирования является определение количества, конфигурации, пространственного расположения, схем электропитания и токов экранирующей обмоток, алгоритма работы системы управления, а также результирующего значения индукционного магнитного поля в точках экранируемого пространства. Результаты. Приводятся результаты трех вариантов синтеза одноконтурной робастной системы активного экранирования с различным пространственным расположением экранирующей обмотки для уменьшения магнитного поля, создаваемого группой высоковольтных линий электропередачи. Показана возможность существенного снижения уровня индукции исходного магнитного поля внутри экранируемого пространства и снижения чувствительности системы к неопределенности параметров системы. Оригинальность. Впервые проведены синтез, теоретические и экспериментальные исследования одноконтурной робастной системы активного экранирования магнитного поля, создаваемых группой высоковольтными линиями электропередач в области экранируемого пространства, с различным пространственным расположением экранирующей обмотки. Практическая ценность. Приводятся практические рекомендации по обоснованному выбору с точки зрения практической реализации пространственного расположения экранирующей обмотки одноконтурной робастной системы активного экранирования магнитного поля, создаваемого группой высоковольтных линий электропередач. Библ. 49, рис. 9.

Ключевые слова: **высоковольтные линии электропередачи, магнитное поле промышленной частоты, робастная система активного экранирования, многокритериальная стохастическая игра.**

Introduction. Active contour shielding of power frequency magnetic field (MF) generated by high voltage power lines (HVPL) [1-10] is the most acceptable and economically feasible for ensuring the sanitary norms of Ukraine in the power frequency MF [11, 12].Ukraine's electricity networks are characterized by high density, and especially near high-voltage power substations. There is usually a group of overhead HVPL, in the immediate vicinity of which can be located residential buildings. In this case, the main uncertainty in the synthesis of systems of active shielding (SAS) is the variation of the currents of different power lines, which leads not only to a change in the level of magnetic flux density, but also to a change in the position of the space-time characteristics (STC) of the MF in the shielding zone.

Most of the double-circuit HVPL, and groups of HVPL generate MF, which has a slight polarization. The STC of such MF has the form of a strongly elongated ellipse [5] and, therefore, active shielding of such MF is possible with the use of only single shielding coil (SC). Such single-circuit SAS with single SC are most widely used in world practice [2-6]. Naturally, that the realization of SC can be performed by various ways.

The methods of synthesis of SAS for MF, generate by HVPL, was developed in [13-24]. The initial data for the synthesis of the system is the parameters of the transmission lines (working currents, geometry and number of wires, location of the transmission lines relative to the protected space) and the dimensions of the protected space and the standard value of the magnetic flux density, which should be achieved as a result of shielding. In the process of synthesis, it is necessary to determine the parameters of the SC (their number, configuration, spatial arrangement, connection diagram), currents and the resulting magnetic flux density.

The goal of this work is the synthesis of single-circuit systems of active shielding of power frequency magnetic field generated by group of high voltage power lines with different spatial arrangement of the single shielding coil.

Problem statement. In the synthesis of the ASS, the mathematical model of the original MF is known inaccurately [25]. In particular, currents in conductors that have daily, weekly, seasonal variations are approximately known which leads to a change of the STC position of the original MF, generated by the power lines. The geometric dimensions of the SC, the parameters of the regulators, etc. are not accurately realized. Therefore, we introduce a vector of uncertainty of the system parameters from their nominal values δ used in the synthesis of the system. The problem of synthesizing a robust SAS is reduced to the determination of such a vector of spatial arrangement and geometric sizes of compensated windings, as well as parameters of the regulator X and the uncertainty parameters vector δ, at which the maximum value of the magnetic flux density at selected points P_j of the considered space P assumes a minimum value for thevector of spatial arrangement and geometric sizes of compensated windings, as well as parameters of the regulator X but the maximum value for the uncertainty parameters vector δ, so that

$$X^* = \arg \min_{X \in \boldsymbol{X}} \max_{\delta \in \Delta} \max_{P_j \in \boldsymbol{P}} B\left(X, \delta, P_j\right). \quad (1)$$

This technique corresponds to the standard approach to the synthesis of robust systems for the worst-case [25], when the uncertainty parameters vector δ lead to the greatest deterioration in the compensation of the initial MF created by HVPL. The problem (1) can be formulated in the form of the following multi-criteria game [16] with vector payoff

$$B\left(X, \delta\right) = \left[B\left(X, \delta, P_1\right), B\left(X, \delta, P_2\right) ... B\left(X, \delta, P_m\right)\right]^T, \quad (2)$$

the components of which $B(X,\delta,P_i)$ are the magnetic flux density in the m points P_i of the space under consideration. In this case, of course, it is necessary to take into account the constraints on the control vector and the state variables of the system, the uncertainty parameters vector in the form of a vector inequality

$$G\left(X, \delta\right) \le G_{\max}. \quad (3)$$

In the multi-criteria game (2), the first player is the vector of spatial arrangement and geometric sizes of SC, as well as parameters of the regulator X and its strategy is the minimization of the vector payoff (2), and the second player is a uncertainty parameters vector δ and the strategy of this player is maximization of the same vector payoff [25-27].

Note that the components of the vector payoff (2) are nonlinear functions of the vector of spatial arrangement and geometric sizes of SC, as well as parameters of the regulator X and uncertainty parameters vector δ are calculated on the basis of the Maxwell equations solutions in the quasi-stationary approximation [28-36].

Solution algorithm. Consider the algorithm for finding the solution of the game. To find the solution of the multi-criterion game (9) from Pareto-optimal solutions taking into account the binary preference relations [37], we used an particle multi swarm optimization (PSO) algorithm [38, 39], in which the number of swarms are equal the number of components m of the vector payoff (2).

In the standard particles swarm optimization algorithm the particle velocities change is carried out according to linear laws [37-47]. To increase the speed of finding a global solution, special nonlinear algorithms of stochastic multi-agent optimization recently proposed in [48], in which the motion of i particle of j swarm is described by the following expressions

$$\begin{aligned} v_{ij}(t+1) &= w_{1j} v_{ij}(t) + c_{1j} r_{1j}(t) * \dots \\ &\dots * H\left(p_{1ij}(\mathrm{t}) - \varepsilon_{1ij}(t)\right)\left[y_{ij}(t) - \dots\right. \\ &\left.\dots - x_{ij}(t)\right] + c_{2j} r_{2j}(t) H\left(p_{2ij}(t) - \dots\right. \\ &\left.\dots - \varepsilon_{2ij}(t)\right)\left[y_j^*(t) - x_{ij}(t)\right], \end{aligned} \quad (4)$$

$$\begin{aligned} u_{ij}(t+1) &= w_{2j} u_{ij}(t) + c_{3j} r_{3j}(t) H * \dots \\ &\dots * \left(p_{3ij}(t) - \varepsilon_{3ij}(t)\right)\left[z_{ij}(t) - \delta_{ij}(t)\right] + \dots \\ &\dots + c_{4j} r_{4j}(t) H\left(p_{4ij}(t) - \varepsilon_{4ij}(t)\right) * \dots \\ &\dots * \left[z_j^*(t) - \delta_{ij}(t)\right], \end{aligned} \quad (5)$$

$$\begin{aligned} x_{ij}(t+1) &= x_{ij}(t) + v_{ij}(t+1); \\ \delta_{ij}(t+1) &= \delta_{ij}(t) + u_{ij}(t+1), \end{aligned} \quad (6)$$

where $x_{ij}(t)$, $\delta_{ij}(t)$, and $v_{ij}(t)$, $u_{ij}(t)$ are the position and velocity of i particle of j swarm.

Note that in connection with the fact that the vector game solutions (9) is represented in the form of strategies of two players X – the vector of the parameters of the regulators and the δ – the uncertainty parameters vector, where it is necessary to minimize the vector payoff (9) along the regulators parameter vector X and maximize the same vector payoff (9) with respect to the uncertainty parameters vector δ. Therefore, each i particles of j swarm has two components of position $x_{ij}(t)$, $\delta_{ij}(t)$ and two components of velocity $v_{ij}(t)$, $u_{ij}(t)$ to find the two desired components of the regulators parameters vector X and uncertainty parameters vector δ.

In (4)–(6) $y_{ij}(t)$, $z_{ij}(t)$ and $y_j^*(t)$, $z_j^*(t)$ – the best local and global positions of the i-th particle, found respectively by only one i-th particle and all the particles of j swarm.

Moreover, the best local position $y_{ij}(t)$ and the global position $y_j^*(t)$ of the i particle of j swarm are understood in the sense of the first player strategy $x_{ij}(t)$ for minimum of component $B(X,\delta,P_i)$ of the vector payoff (9). However, the best local position $z_{ij}(t)$ and the global

position z_j^* of the i particle of j swarm are understood in the sense of the second player strategy $\delta_{ij}(t)$ for maximum of the same component $B(X,\delta,P_i)$ of the vector payoff (2). This approach corresponds to the movement of particles along the gradient and antigradient when using deterministic game-solving algorithms.

Four independent random numbers $r_{1j}(t)$, $r_{2j}(t)$, $r_{3j}(t)$, $r_{4j}(t)$are in the range of [0, 1], which determine the stochastic particle velocity components.

Positive constants c_1, c_2 determine the cognitive and social weights of the particle velocity components.

Note that this PSO algorithm is a fairly simple optimization algorithm. This algorithm does not require finding partial derivatives – a gradient vector, second order partial derivatives – a Hess matrix, a gradient projection matrix for constraints –Rosen matrix, an inversion of the Hess matrix, and so on. However, despite its simplicity, with the help of this algorithm it is possible to solve quite complex optimization problems in various fields. The success of the use of this algorithm, to a large extent, is determined by the justified choice of the tuning parameters of this algorithm. Let us consider in more detail the informed choice of the tuning parameters of this algorithm for solving the considered problem.

The peculiarity of the solution of this game is that the first player vector strategy components $x_{ij}(t)$ are the SC geometric dimensions, which measured in meters, and the open loop control regulators parameters – the phases of SC currents i, which measured in radians, SC ampere turns, which measured in ampere turns , and closed-loop control regulators gains, which measured in dimensionless quantities. Therefore, the values of these constants c_{1j}, c_{2j} and c_{3j}, c_{4j} are chosen taking into account the range of possible players strategies X and δ.

The peculiarity of the solution of this problem also is the presence of «ravines» and «edges» in the vector payoff (9). This is due, firstly, to the fact that the values of the components of the players' strategies X and δ differ by more than an order of magnitude. Second, the change of some components of the players' strategies, in particular, the closed loops control regulators gains, leads to insignificant changes in the vector game payoff (2). Therefore, to improved the global solution finding speed with small increments changes in the payoff (2) for players' strategies $x_{ij}(t)$, $\delta_{ij}(t)$ a nonlinear Cuckoo search algorithm of stochastic multi-agent optimization [48] used in (4) – (6).

The Heaviside function H is used as a switching function of the motion of a particle, respectively, to the local $y_{ij}(t)$, $z_{ij}(t)$ and global $y_j^*(t)$, $z_j^*(t)$ optimum.

Switching parameters of the cognitive p_{1ij}, p_{3ij} and social p_{2ij}, p_{4ij} components of the particle velocity to the local and global optimum taken in the form of increments changes in the payoff (9) for players' strategies $x_{ij}(t)$, $\delta_{ij}(t)$ when moving to local and global optimum respectively.

Random numbers $\varepsilon_{1ij}(t)$, $\varepsilon_{2ij}(t)$, $\varepsilon_{3ij}(t)$ and $\varepsilon_{4ij}(t)$ determine the switching parameters of the particle motion, respectively, to local and global optima. If $p_{1ij} < \varepsilon_{1ij}(t)$ and $p_{2ij} < \varepsilon_{2ij}(t)$, then the movement speed component $v_{ij}(t)$ of this i particle of j the swarm at the step t does not change and the particle moves in the same direction as at the previous optimization step.

Similarly if $p_{3ij} < \varepsilon_{3ij}(t)$ and $p_{4ij} < \varepsilon_{4ij}(t)$, then the movement speed component $u_{ij}(t)$ of i particle of j the swarm at the step t also does not change.

To improve the quality of the solution finding process, the inertia coefficients w_{1j}, w_{2j} are used in the range of (0.5 – 0.9).

As constraints (3) in this problem, first of all, we took into account the constraints on the SC spatial arrangement, which are first player vector strategy components $x_{ij}(t)$. These limitations are due to the technical possibilities of the SC implementation. In addition, the closed loops control regulators gains, which are also first player vector strategy components $x_{ij}(t)$. In addition, restrictions were set on the maximum particle velocities $v_{ij}(t)$, $u_{ij}(t)$ based on the desired accuracy of obtaining the corresponding components of the vector game solution (2) as well as to improve the game solution convergence.

To find a global solution of the original multiobjective game (2) in the search for optimal solutions to local games, individual swarms exchange information among themselves. In this case, to calculate the velocity of the particles in one swarm, information on the global optimum obtained by the particles of the other swarm is used, which makes it possible to isolate all potential Pareto optimal solutions.

For this purpose, at each step t of the movement of particle i, of swarm j uses the binary preferences functions of local solutions obtained by all swarms. The solution $X_j^*(t)$ obtained in the course of solving the game $B(X(t),\delta(t),P_j)$ with the help of swarm j is preferable to the solution $X_k^*(t)$ obtained during optimization of the game $B(X(t),P_k)$ with the help of swarm k if the condition

$$\max_{i=1,m} B\left(P_i, X_j^*(t), \delta(t)\right) < \max_{i=1,m} B\left(P_i, \dots X_k^*(t), \delta(t)\right) \quad (7)$$

is satisfied.

In this case, as the global optimal solution $X_k^*(t)$ of swarm k, the global solution $X_j^*(t)$ obtained by the swarm j is used, which is more preferable with respect to the global solution $X_k^*(t)$ obtained by swarm k on the basis of the preference relation (7).

In fact with this approach the basic idea of the method of successive narrowing of the field of compromise problems is realized: from the initial set of possible solutions, based on information about the relative importance of local solutions, all Pareto-optimal solutions that can not be selected according to the available information on the relation pre-reverence. Removal is carried out until a globally optimal solution is obtained. As a result of applying this approach, no potentially optimal solution will be removed at each step of the contraction.

In conclusion, we note that the original multiobjective game (2) – (3), taking into account the algorithm for its solution (4) – (6), is a multi-criteria stochastic dynamic game, since it clearly has time and random search [27].

Computer simulation results. Consider the result of synthesis of robust SAS of MF generated by group of

HVPL. This situation is typical for the outskirts of cities, where several power lines are suitable, as well as near power line substations. Figure 1 shows the location of a group of HVPL generating MF, the magnetic flux density of which must be reduced in the shielding zone. In the immediate vicinity of the shielding zone there are two double-circuit 110 k*V* HVPL, a double-circuit 330 kV HVPL and a single-circuit 330 k*V* HVPL.

Fig. 1. Location of a group of high voltage power lines

For the synthesis of SAS, in addition to the geometric dimensions of the transmission lines and the shielding zone, the values of the currents in the bus of the all HVPL are necessary. To this, first, experimental studies of the level of the magnetic field both in the shielding zone and near the transmission lines were carried out. Based on the obtained experimental data, the problem of current identification in current conductors of the power line is solved, under which the sum of the squares of the errors of the measured and model – them magnetic flux density values at given points is minimized.

First, we will look the results of the SAS initial MF in a two-story cottage located at 20 m distance from the HVPL. On the basis of experimental research, it was found that in the shielding zone, the MF generated by group of HVPL has the STC of such MF is a strongly elongated ellipse and, consequently, the initial MF has a negligible polarization. Active screening of such MF is possible with the use of single SC. It should be noted that such systems have become most widespread in the world practice [2]. Based on the model of MF created by group of HVPL, the problem of synthesis of a robust SAS was solved. The SAS contains single SC which is square shape. The upper branch of SC is coordinates (1.0, 10.0), and the lower branch is coordinates (10.0, 1.3).

In Fig. 2,*a* shows the isolines of the resultant magnetic flux density with the SAS is on. As can be seen from Fig. 2,*a*, the minimum magnetic flux density value in the shielding zone is 0.2 μT. The initial MF generated by the HVPL group in the shielding zone exceeds the level of 2.0 μT and, therefore, the maximum shielding factor of the SAS is more than 10. When the active shielding system is on, as can be seen from Fig. 2,*a*, the magnetic flux density level in the residential space under consideration does not exceed 0.5 μT.

Figure 2,*b* shows the STC of MF, created by: group of HVPL (1); SC (2) and total MF with the SAS is on (3).

The STC of the initial MF is ellipse, which confirms the weak polarization of the initial MF. MF STC of SC is a straight line and, consequently, the SC generates unpolarized MF. Naturally, the initial MF with such STC can be effectively compensated for using a single-loop ASS with single SC. Wherein the big axis of the STS ellipse of the initial MF is compensated, so that the STS of the total MF with the SAS is on is an ellipse with an ellipse coefficient 0.8. The STC of the resultant MF is an ellipses of a significantly smaller area compared to the ellipse of the STC of the initial MF, which is due to the initial MF compensation with the help of the SAS.

When implementing the SAS, for mounting such a SC at a height of 10 meters, appropriate supports are necessary, which requires fairly large material costs.

Let us now consider the results of the synthesis of a MF SAS in a single-story building located at a distance of 7 m from HVPL. During SAS synthesis of different variants of the SC spatial arrangement were considered. Three variants of SC spatial arrangement were chosen which are the greatest interest from the point of view of the practical implementation of SC. Let us consider in more detail these three variants. In all these three variants SC are square shape. In the variant a) the upper branch of SC is coordinates (4.9, 4.2), and the lower branch is coordinates (4.9, 3.0).

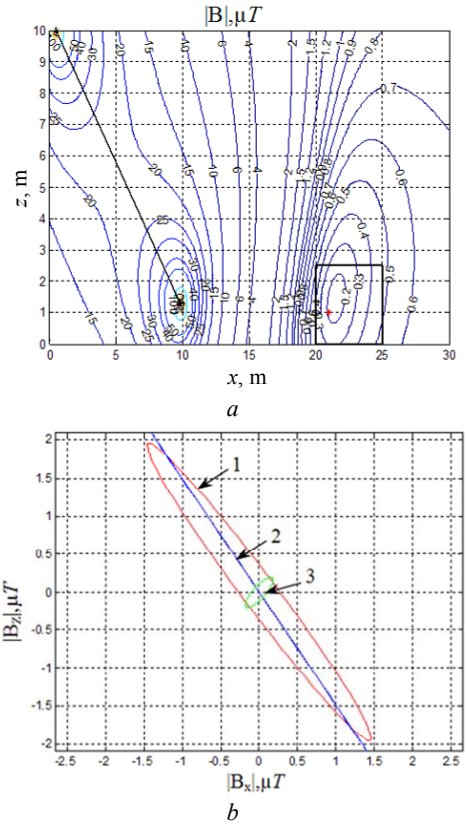

Fig. 2. Isolines of resultant magnetic flux density with the active screening system is on (*a*) and space-time characteristics of magnetic field: initial (1), shielding coil (2) and resultant magnetic field with the system of active shielding is on (3) (*b*) in a two-story cottage

Fig. 3,*a* shows the isolines of the resultant magnetic flux density with the SAS is on in the variant (*a*). As can be seen from Fig. 3,*a*, the minimum magnetic flux density value in the screening zone is 0.2 μT. The initial MF generated by the HVPL group in the shielding zone exceeds the level of 1 μT and, therefore, the maximum shielding factor of the ASS equals 5.

In Fig. 3,*b* shows STC of MF, generated by: 1 – group of overhead HVPL (1); SC (2) and total MF with the SAS is on (3) at the point with the coordinates (8.0, 1.0).

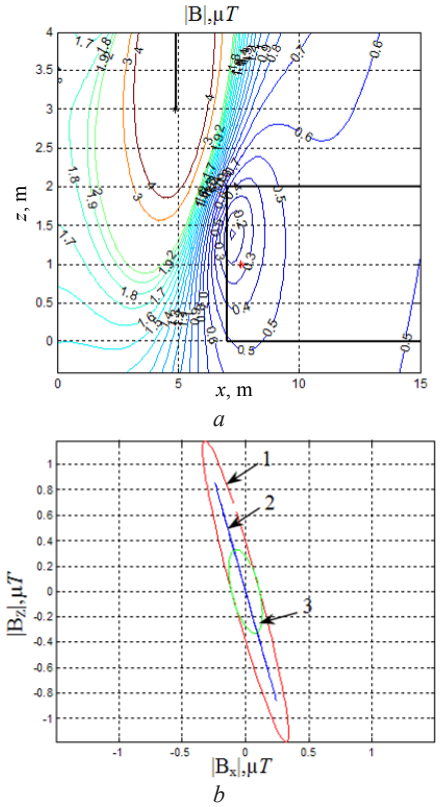

Fig. 3. Isolines of resultant magnetic flux density with the system of active screening is on (*a*) and space-time characteristics of magnetic field: initial (1), shielding coil (2) and resultant magnetic field with the system of active shielding is on (3) (*b*) in a single-story cottage

Let us consider the results of the synthesis of a MF SAS in a single-story building located at a same distance of 7 m from HVPL for the variant (*b*). The upper branch of SC is coordinates (5.0, 0.6), and the lower branch is coordinates (2.0, 0.0).

Fig. 4,*a* shows the isolines of the resultant magnetic flux density with the SAS is on in the variant (*b*). As can be seen from Fig. 4,*a*, the minimum magnetic flux density value in the screening zone also as for variant (*a*) is 0.2 μT and, therefore, the maximum shielding factor of the ASS also as for variant (*a*) is 5.

In Fig. 4,*b* shows STC of MF, generated by: 1 – group of overhead HVPL (1); SC (2) and total MF with the SAS is on (3) at the point with the coordinates (8.0, 1.0) also as for variant (*a*).

Let us consider the results of the synthesis of a MF SAS for the variant (*c*). The upper branch of SC is coordinates (1.0, 3.0), and the lower branch is coordinates (4.0, 1.5). Fig. 5,*a* shows the isolines of the resultant magnetic flux density with the SAS is on in the variant (*c*). As can be seen from Fig. 5,*a*, the minimum magnetic flux density value in the screening zone also as for variant (*a*) and variant (*b*) is 0.2 μT and, therefore, the shielding factor maximum of the SAS also as for variant (*a*) and variant (*b*) is 5. In Fig. 4,*b* shows STC of MF, created by: 1 – group of overhead HVPL (1); SC (2) and total MF with the SAS is on (3) at the point with the coordinates (8.0, 1.0) also as for variant (*a*) and variant (*b*).

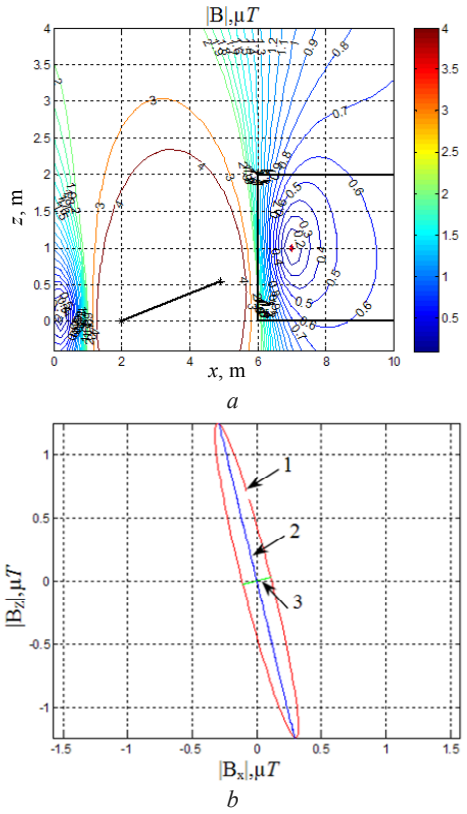

Fig. 4. Isolines of resultant magnetic flux density with the active shielding system is on (*a*) and space-time characteristics of magnetic field: initial (1), shielding coil (2) and resultant magnetic flux density with the systems of active shielding is on (3) (*b*) in a single-story cottage

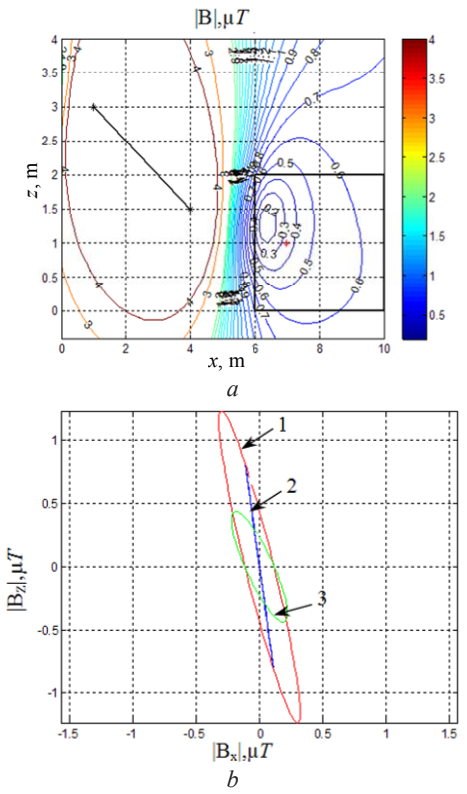

Fig. 5. Isolines of resultant magnetic flux density with the active shielding system is on (*a*) and space-time characteristics of magnetic flux density: initial (1), shielding coil (2) and resultant magnetic flux density with the systems of active shielding is on (3) (*b*) in a single-story cottage

Despite the fact that in all three variants the minimum magnetic flux density value in the screening zone also is 0.2 μT, however, in variant (*a*), the magnetic flux density does not exceed the level of sanitary norms of 0.5 μT in a zone of 6 m up to 15 m., and in the variant (*b*) and (*c*), this shielding zone decreases to 8–9 m. Thus, from the point of view of providing the greatest shielding zone of the MF, the most preferable is variant (*a*). And from the point of view of the simplicity of SC implementing, the most preferable, apparently, is variant (*b*).

Naturally, the STC of the initial MF at this point has the same form (curve 1). However, the position of the STC MF of SC and the resultant MF for the three options considered are somewhat different. In particular, the initial MF at the point under consideration is most strongly shielded in variant (*a*).

Experimental research. Consider the field experimental research of the full scale SAS layout with three variants of SC spatial arrangement. All SC of the full scale SAS layout is a square shape, contains 20 winds and is powered by amplifier type TDA7294. The SAS contains an external Magnetic Flux Density controller and an internal current controller. An inductive sensor is used as an Magnetic Flux Density sensor, and the MF measurement is performed by EMF-828 type magnetometer of the Lutron firm [49]. The SAS is powered by an autonomous source.

Figure 6,*a* shows a picture of the position of SC of SAS for the variant (*a*). The upper branch of SC is located at a height of 4.0 m from the ground, and the lower branch is located at a height of 2.6 m from the ground. Fig. 6,*a* shows the experimental isolines of the resultant magnetic flux density with the SAS is on in the variant (*a*). As can be seen from Fig. 6,*a*, the minimum magnetic flux density experimental value in the screening zone is 0.2 μT. The initial MF generated by the HVPL group in the shielding zone exceeds the level of 1 μT and, therefore, the maximum experimental shielding factor of the SAS is 5.

Figure 7,*a* shows a picture of the spatial arrangement of SC of SAS for the variant (*b*). The upper branch of SC is located at a height of 0.5 m from the ground, and the lower branch is located at and the lower branch is located on the ground.

Figure 7,*b* shows the experimental isolines of the resultant magnetic flux density with the SAS is on in the variant (*a*). As can be seen from Fig. 7,*b*, the minimum magnetic flux density experimental value in the screening zone also as for variant (*a*) is 0.2 μT, and, therefore, the maximum experimental shielding factor of the SAS for the variant (*b*) also as for variant (*a*) equals 5.

Figure 8,*a* shows a picture of the spatial arrangement of SC of SAS for the variant (*c*). The upper branch of SC is located at a height of 3.0 m from the ground, and the lower branch is located at a height of 1.5 m from the ground. Fig. 8,*b* shows the experimental isolines of the resultant magnetic flux density with the ASS is on in the variant (*c*). As can be seen from Fig. 8,*b*, the minimum magnetic flux density experimental value in the screening zone also as for variant (*a*) and for variant (*b*) is 0.2 μT, and, therefore, the maximum experimental efficiency of the SAS for the variant (*c*) also as for variant (*a*) and for variant (*b*) is 5.

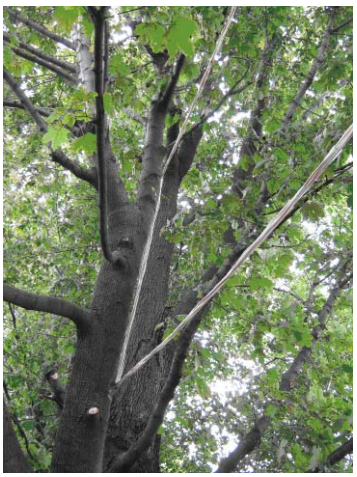

a

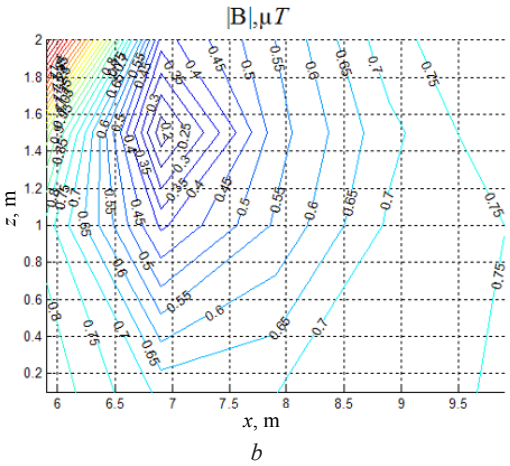

b

Fig. 6. Picture of the shielding coil (*a*) and the experimental isolines of the resultant magnetic flux density with the systems of active shielding is on (*b*)

a

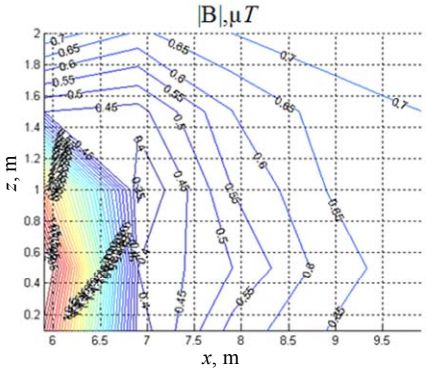

b

Fig. 7. Picture of the shielding coil (*a*) and the experimental isolines of the resultant magnetic flux density with the systems of active shielding is on (*b*)

a

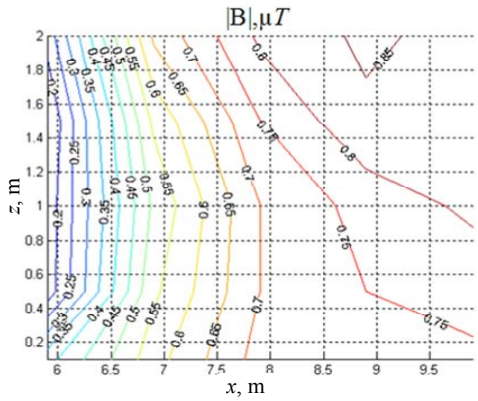

b

Fig. 8. Picture of the shielding coil (*a*) and the experimental isolines of the resultant magnetic flux density with the systems of active shielding is on (*b*)

A comparison of the results of the MF distribution of the synthesized ASS which shown in Fig. 3,*a*, Fig. 5,*a* with the experimental distributions of the SAS, which shown in Fig. 6,*b*, showed that they differ by not more than 20 %.

In conclusion, we note that, of course, it would be tempting not to solve the rather difficult task of synthesizing the SAS in the form of a multi-criteria game (2), but to immediately place the SC in a convenient place, in terms of simplicity of practical implementation, and experimentally adjust the SAS controls. The authors have tried to implement this option SAS, whose spatial location of SC was intuitively chosen. The upper branch of SC has coordinates (4.9, 4.2), and the lower branch has coordinates (6.9, 0.0). A spatial arrangement of such SC is shown in Fig. 9. The upper branch SC is located at a height of 4.2 m from the ground, and the lower branch is located at ground level.

Fig. 9. Picture of the shielding coil, the spatial arrangement of which were chosen without system synthesis

However, with this SC, it was not possible to adjust the SAS regulators with the desired efficiency. Then they changed the position of the lower branch of the SC, so that the coordinates of which were equal (4.9, 0.0), (2.9, 0.0) and (4.9, 1.0). However, it is also not possible to obtain a demand for efficiency with such a spatial arrangement of SC. Then the SAS was synthesized, the spatial position of the SC was determined, and the upper branch of the SC was set at a height of 3 m, which corresponds to variant (*a*). The spatial arrangement of such a SC is shown in Fig. 6,*a*. With this SC it was possible to get the shielding factor of the SAS more than five units.

In conclusion, we note that using single-circuit SAS containing single SC can effectively screen a MF with a small polarization. The STC of such MF is a very elongated ellipse whose ellipse coefficient (ratio of the smaller semiaxis to the larger half-axis) is seeks to zero. SC of single-circuit SAS generates MF, whose STC is a straight line. With such a single-circuit SAS with single SC, the major axis of the STS ellipse of the initial MF is compensated, so that the STS of the total MF with ASS is on is significantly smaller than the STS of the initial MF, which determines the high efficiency of such single-circuit SAS. Single-circuit power lines with horizontal and vertical bus arrangement, double-circuit power lines such as «barrel», «tree» and «inverted tree» generate a MF with a weak polarization. Exactly for such power lines, single-circuit SAS with single SC is most widely used in world practice [2].

The most polarized MF generated by a single-circuit power line with «triangle» type current conductors arrangement. The STC of such a MF is practically a circle. Therefore, for effective screening of such MF it is necessary to have two SC at least [5].

Conclusions.

1. For the first time the synthesis of robust single-circuit systems of active shielding of magnetic field, generated by group of high voltage power lines, with different spatial arrangement of the single shielding coil carried out.

2. The synthesis of robust systems of active shielding is based on multi-criteria game decision, which is based on multiswarm stochastic multi-agent optimization from Pareto-optimal solutions.

3. As a result of the synthesis of a single-circuit systems of active shielding, three variants of the spatial arrangement of the shielding coil were selected, which are of the greatest interest from the point of view of the practical implementation.

4. Field experimental research of the effectiveness of single-circuit systems of active shielding of magnetic field generated by group of overhead high voltage power lines for three variants of the spatial arrangement of the shielding coil carried out. The shielding factor of system of active shielding equals more than 4 units. Comparison of the results of experimental and calculated values of magnetic flux density in the shielding zone shows that their spread does not exceed 20 %.

5. System reduce the level of the initial magnetic flux density throughout the considered residential area up to the Ukraine sanitary norms level and has less sensitivity to plant parameters variations in comparison with the known systems.

REFERENCES

1. Rozov V.Yu., Reutskyi S.Yu., Pelevin D.Ye., Pyliugina O.Yu. The magnetic field of transmission lines and the methods of its mitigation to a safe level. *Technical Electrodynamics*, 2013, no. 2, pp. 3-9. (Rus).

2. Active Magnetic Shielding (Field Cancellation). Available at: http://www.emfservices.com/afcs.html (accessed 10 September 2012).

3. Ter Brake H.J.M., Huonker R., Rogalla H. New results in active noise compensation for magnetically shielded rooms. *Measurement Science and Technology*, 1993, Vol. 4, Issue 12, pp. 1370-1375. **doi: 10.1088/0957-0233/4/12/010.**

4. Celozzi S., Garzia F. Active shielding for power-frequency magnetic field reduction using genetic algorithms optimization. *IEE Proceedings – Science, Measurement and Technology*, 2004, Vol.151, no.1, pp. 2-7. **doi: 10.1049/ip-smt:20040002**.

5. Shenkman A., Sonkin N., Kamensky V. Active protection from electromagnetic field hazards of a high voltage power line. *HAIT Journal of Science and Engineering. Series B: Applied Sciences and Engineering*, Vol. 2, Issues 1-2, pp. 254-265.

6. Beltran H., Fuster V., García M. Magnetic field reduction screening system for a magnetic field source used in industrial applications. *9 Congreso Hispano Luso de Ingeniería Eléctrica (9 CHLIE)*, Marbella (Málaga, Spain), 2005, pp. 84-99.

7. Rozov V.Yu., Grinchenko V.S., Pelevin D.Ye., Chunikhin K.V. Simulation of electromagnetic field in residential buildings located near overhead lines. *Technical electrodynamics*, 2016, no.3, pp. 6-8. (Rus).

8. Bravo-Rodríguez J., Del-Pino-López J., Cruz-Romero P. A Survey on Optimization Techniques Applied to Magnetic Field Mitigation in Power Systems. *Energies*, 2019, vol.12, no.7, p. 1332. **doi: 10.3390/en12071332**.

9. Celozzi S. Active compensation and partial shields for the power-frequency magnetic field reduction. *IEEE International Symposium on Electromagnetic Compatibility*. Minneapolis, USA, 2002, pp. 222-226. **doi: 10.1109/isemc.2002.1032478**.

10. Celozzi S., Garzia F. Magnetic field reduction by means of active shielding techniques. *Environmental Health Risk II*, 8 September, 2003, pp. 64-73. **doi: 10.2495/ehr030091**.

11. The World Health Organization. The International EMF Project. [Online]. Available at: http://www.who.int/peh-emf/project/en/. (accessed 17 February 2017).

12. *Electrical installation regulations*. *5th ed*. The Ministry of Energy and Coal Mining of Ukraine, 2014. 277 p. (Ukr).

13. Cruz Romero P., Izquierdo Mitchell C., Burgos Payan, M. Optimal split-phase configurations*. In Proceedings of the 2001 IEEE Porto Power Tech Proceedings* (Cat. No.01EX502), Porto, Portugal, 10-13 September 2001, vol.3, p. 5.

14. Cruz Romero P., Izquierdo C., Burgos M., Ferrer L.F., Soto F., Llanos C., Pacheco J.D. Magnetic field mitigation in power lines with passive and active loops. *In Proceedings of the CIGRE Session*, Paris, France, 25-30 August 2002.

15. Barsali S., Giglioli R., Poli D. Active shielding of overhead line magnetic field: Design and applications. *Electric Power Systems Research*, 2014, vol.110, pp. 55-63. **doi: 10.1016/j.epsr.2014.01.005.**

16. Del Pino Lopez J.C., Romero P.C. Influence of Different Types of Magnetic Shields on the Thermal Behavior and Ampacity of Underground Power Cables. *IEEE Transactions on Power Delivery*, 2011, vol.26, no.4, pp. 2659-2667. **doi: 10.1109/tpwrd.2011.2158593**.

17. Del Pino-Lopez J.C., Cruz-Romero P., Serrano-Iribarnegaray L. Impact of electromagnetic losses in closed two-component magnetic shields on the ampacity of underground power cables. *Progress in electromagnetics research*, 2013, vol.135, pp. 601-625. **doi: 10.2528/pier12112303**.

18. del-Pino-López J.C., Giaccone L., Canova A., Cruz-Romero P. Design of active loops for magnetic field mitigation in MV/LV substation surroundings. *Electric Power Systems Research*, 2015, vol.119, pp. 337-344. **doi: 10.1016/j.epsr.2014.10.019**.

19. del Pino Lopez J.C., Giaccone L., Canova A., Cruz Romero P. Ga-based active loop optimization for magnetic field mitigation of MV/LV substations. *IEEE Latin America Transactions*, 2014, vol.12, no.6, pp. 1055-1061. **doi: 10.1109/tla.2014.6894000**.

20. Canova A., Giaccone L. Real-time optimization of active loops for the magnetic field minimization. *International Journal of Applied Electromagnetics and Mechanics*, 2018, vol.56, pp. 97-106. **doi: 10.3233/jae-172286**.

21. Canova A., del-Pino-Lopez J.C., Giaccone L., Manca M. Active Shielding System for ELF Magnetic Fields. *IEEE Transactions on Magnetics*, 2015, vol.51, no.3, pp. 1-4. **doi: 10.1109/tmag.2014.2354515**.

22. Femia N., Petrone G., Spagnuolo G., Vitelli M. Optimization of Perturb and Observe Maximum Power Point Tracking Method. *IEEE Transactions on Power Electronics*, 2005, vol.20, no.4, pp. 963-973. **doi: 10.1109/tpel.2005.850975**.

23. Kuznetsov B.I., Turenko A.N., Nikitina T.B., Voloshko A.V., Kolomiets V.V. Method of synthesis of closed-loop systems of active shielding magnetic field of power transmission lines. *Technical electrodynamics*, 2016, no.4, pp. 8-10. (Rus).

24. Kuznetsov B.I., Nikitina T.B., Voloshko A.V., Bovdyj I.V., Vinichenko E.V., Kobilyanskiy B.B.. Synthesis of an active shielding system of the magnetic field of power lines based on multiobjective optimization. *Electrical engineering & electromechanics*, 2016, no.6, pp. 26-30. (Rus). **doi: 10.20998/2074-272X.2016.6.05.**

25. Ren Z., Pham M.-T., Koh C.S. Robust Global Optimization of Electromagnetic Devices With Uncertain Design Parameters: Comparison of the Worst Case Optimization Methods and Multiobjective Optimization Approach Using Gradient Index. *IEEE Transactions on Magnetics*, 2013, vol.49, no.2, pp. 851-859. **doi: 10.1109/tmag.2012.2212713**.

26. Ranković A. Novel multi-objective optimization method of electric and magnetic field emissions from double-circuit overhead power line. *International Transactions on Electrical Energy Systems*, 2016, vol.27, no.2, p. e2243 **doi: 10.1002/etep.2243**.

27. Ummels M. *Stochastic Multiplayer Games Theory and Algorithms*. Amsterdam University Press, 2010. 174 p.

28. Rozov V.Yu., Reutskyi S.Yu. Pyliugina O.Yu. The method of calculation of the magnetic field of three-phase power lines. *Technical electrodynamics*, 2014, no.5, pp. 11-13. (Rus).

29. Panchenko V.V., Maslii A.S., Pomazan D.P., Buriakovskyi S.G. Determination of pulsation factors of the system of suppression of interfering harmonics of a semiconductor converter. *Electrical engineering & electromechanics*, 2018, no.4, pp. 24-28. **doi: 10.20998/2074-272X.2018.4.04.**

30. Buriakovskyi S., Maslii A., Maslii A. Determining parameters of electric drive of a sleeper-type turnout based on electromagnet and linear inductor electric motor. *Eastern-European Journal of Enterprise Technologies*, 2016, vol.4, no.1(82), pp. 32-41. (Rus). **doi: 10.15587/1729-4061.2016.75860**.

31. Zagirnyak M., Chornyi O., Nykyforov V., Sakun O., Panchenko K. Experimental research of electromechanical and biological systems compatibility. *Przegląd Elektrotechniczny*, 2016, vol.1, no.1, pp. 130-133. **doi: 10.15199/48.2016.01.31**.

32. Buriakovskyi S.G., Maslii A.S., Panchenko V.V., Pomazan D.P., Denis I.V. The research of the operation modes of the diesel locomotive CHME3 on the imitation model. *Electrical engineering & electromechanics*, 2018, no.2, pp. 59-62. **doi: 10.20998/2074-272X.2018.2.10.**

33. Rozov V., Grinchenko V. Simulation and analysis of power frequency electromagnetic field in buildings closed to overhead lines. *2017 IEEE First Ukraine Conference on Electrical and*

Computer Engineering (UKRCON). Kyiv, Ukraine, pp. 500-503. **doi: 10.1109/UKRCON.2017.8100538**.

34. Zagirnyak M., Serhiienko S., Chornyi O. Innovative technologies in laboratory workshop for students of technical specialties. *2017 IEEE First Ukraine Conference on Electrical and Computer Engineering (UKRCON)*, May 2017. **doi: 10.1109/ukrcon.2017.8100446**.

35. Chystiakov P., Chornyi O., Zhautikov B., Sivyakova G. Remote control of electromechanical systems based on computer simulators. *2017 International Conference on Modern Electrical and Energy Systems (MEES)*, Nov. 2017. **doi: 10.1109/mees.2017.8248934.**

36. Korol S., Buryan S., Pushkar M., Ostroverkhov M. Investigation the maximal values of flux and stator current of autonomous induction generator. *2017 IEEE First Ukraine Conference on Electrical and Computer Engineering (UKRCON)*, May 2017. **doi: 10.1109/ukrcon.2017.8100302**.

37. Galchenko V.Y., Yakimov A.N. A turmitobionic method for the solution of magnetic defectometry problems in structural-parametric optimization formulation. *Russian Journal of Nondestructive Testing*, 2014, vol.50, no.2, pp. 59-71. **doi: 10.1134/s106183091402003x.**

38. Clerc M. *Particle Swarm Optimization*. London, ISTE Ltd., 2006. 244 p. **doi: 10.1002/9780470612163**.

39. Shoham Y., Leyton-Brown K. *Multiagent Systems: Algorithmic, Game-Theoretic, and Logical Foundations*. Cambridge University Press, 2009. 504 p.

40. Xiaohui Hu, Eberhart R.C., Yuhui Shi. Particle swarm with extended memory for multiobjective optimization. *Proceedings of the 2003 IEEE Swarm Intelligence Symposium. SIS'03* (Cat. No.03EX706). **doi: 10.1109/sis.2003.1202267**.

41. Michalewicz Z., Schoenauer M. Evolutionary Algorithms for Constrained Parameter Optimization Problems. *Evolutionary Computation*, 1996, vol.4, no.1, pp. 1-32. **doi: 10.1162/evco.1996.4.1.1.**

42. Parsopoulos K.E., Vrahatis, M.N. Particle Swarm Optimization Method for Constrained Optimization Problems. *In Proceedings of the Euro-International Symposium on Computational Intelligence*, 2002, pp. 174-181.

43. Pulido G.T., Coello C.A.C. A constraint-handling mechanism for particle swarm optimization. *Proceedings of the 2004 Congress on Evolutionary Computation* (IEEE Cat. No.04TH8753). **doi: 10.1109/cec.2004.1331060**.

44. Ray T., Liew K.M. A Swarm Metaphor for Multiobjective Design Optimization. *Engineering Optimization*, 2002, vol.34, no.2, pp. 141-153. **doi: 10.1080/03052150210915**.

45. . Coello Coello C.A, Reyes-Sierra M. Multi-Objective Particle Swarm Optimizers: A Survey of the State-of-the-Art. *International Journal of Computational Intelligence Research*, 2006, vol.2, no.3, pp. 287-308. **doi: 10.5019/j.ijcir.2006.68**.

46. De Freitas Vaz A.I., Da G. Pinto Fernandes E.M. Optimization of nonlinear constrained particle swarm. *Technological and Economic Development of Economy*, 2006, vol.12, no.1, pp. 30-36. **doi: 10.3846/13928619.2006.9637719**.

47. Zilzter Eckart. *Evolutionary algorithms for multiobjective optimizations: methods and applications*. Ph. D. Thesis Swiss Federal Institute of Technology. Zurich, 1999. 114 p.

48. Xin-She Yang, Zhihua Cui, Renbin Xiao, Amir Hossein Gandomi, Mehmet Karamanoglu. *Swarm Intelligence and Bio-Inspired Computation: Theory and Applications*, Elsevier Inc., 2013. 450 p

49. Kuznetsov B.I., Nikitina T.B., Voloshko A.V., Bovdyj I.V., Vinichenko E.V., Kobilyanskiy B.B. Experimental research of magnetic field sensors spatial arrangement influence on efficiency of closed loop of active screening system of magnetic field of power line. *Electrical engineering & electromechanics*, 2017, no.1, pp. 16-20. **doi: 10.20998/2074-272X.2017.1.03.**

Received 23.04.2019

B.I. Kuznetsov[1], *Doctor of Technical Science, Professor,*
T.B. Nikitina[2], *Doctor of Technical Science, Professor,*
I.V. Bovdui[1], *Candidate of Technical Science,*
[1] State Institution «Institute of Technical Problems of Magnetism of the NAS of Ukraine»,
19, Industrialna Str., Kharkiv, 61106, Ukraine,
phone +380 50 5766900,
e-mail: kuznetsov.boris.i@gmail.com
[2] Kharkov National Automobile and Highway University,
25, Yaroslava Mudroho Str., Kharkov, 61002, Ukraine,
e-mail: tatjana55555@gmail.com

How to cite this article:
Kuznetsov B.I., Nikitina T.B., Bovdui I.V. High voltage power lines magnetic field system of active shielding with compensation coil different spatial arrangement. *Electrical engineering & electromechanics*, 2019, no.4, pp. 17-25. **doi: 10.20998/2074-272X.2019.4.03.**

UDC 681.513 + 621.365, 62-83-52 **doi: 10.20998/2074-272X.2019.4.04**

O.Y. Lozynskyi, A.O. Lozynskyi, Y.S. Paranchuk, R.Y. Paranchuk

SYNTHESIS AND ANALYSIS OF ARC FURNACE ELECTRICAL MODE CONTROL SYSTEM ON THE BASIS OF THREE-DIMENSIONAL PHASE CURRENTS VECTOR DISTRIBUTION

Goal. The purpose of the article is to create the method for the operative synthesis of an arc steel-melting furnace (ASF) electric mode (EM) control signal on the basis of a three-dimensional arc currents vector, which takes into account the stochastic nature of the processes in the melting space and power circuit and has low sensitivity to the control object parameters changes, as well as development of the control system structure for its implementation. Method. The basis of the created control method is formed on the statistical theory of dynamical systems, as well as the provisions of the statistical theory of optimal control based on the Fokker-Planck-Kolmogorov equation, which enables to synthesize operational control by the criterion of approaching the regulated coordinate distribution density to the δ-function, that is to minimize the dispersion of the three-dimensional furnace phases arc currents vector. Results. The system of equations for operational real-time calculation of control influences of the thyristor switch of phase inductors, included in the power supply circuits of three-phase arcs, and the structural scheme of the adaptive contour for the formation of three-dimensional phase currents vector dispersion for the implementation of adaptive optimal control were obtained. Scientific novelty. For the first time, based on the Fokker-Planck-Kolmogorov equation, we obtain a system of equations representing a mathematical model of a stochastic adaptive optimal control of the arc furnace electric mode by the criterion of a minimum dispersion of three-dimensional phase (arcs) currents vector, which enables, in comparison with known methods, to increase dynamic precision of the arc currents stabilization at the level set by the criteria of energy efficiency and electromagnetic compatibility values. Practical value. The use of the proposed adaptive optimal control model and structural system scheme for its implementation allows, in comparison with the serial arc power regulators, to improve the dynamic accuracy of the arc current currents stabilization at the level of given optimal settings and, based on this, to improve the energy efficiency and electromagnetic compatibility indices of the arc furnace and power supply network. References 18, figures 5.
Key words: **arc furnace, electric mode, three-dimensional vector of phase currents, stochastic control, dispersion, optimization, adaptation, arc current control circuit.**

Мета. Метою статті є створення методу оперативного синтезу сигналу керування електричним режимом (ЕР) дугової сталеплавильної печі (ДСП) на основі тривимірного вектора струмів фаз, що враховує стохастичну природу процесів у плавильному просторі, силовому електричному колі печі, має низьку чутливість до зміни параметрів об'єкта керування та розроблення структури системи керування для його реалізації. Методика. В основу створеного методу керування покладено положення статистичної теорії динамічних систем, а також положення статистичної теорії оптимального керування на основі рівняння Фоккера-Планка-Колмогорова, що дає змогу синтезувати оперативне керування за критерієм наближенням густини розподілу регульованої координати до δ-функції, тобто мінімізувати дисперсію тривимірного вектора струмів фаз (дуг) дугової печі. Результати. Отримано систему рівнянь для оперативного в режимі on-line розрахунку керуючих впливів тиристорного комутатора фазних дроселів, що включені у силове коло живлення трифазних дуг, та структурну схему адаптивного контура формування дисперсії тривимірного вектора струмів дуг дугової печі для реалізації адаптивного оптимального керування. Наукова новизна. Вперше на основі рівняння Фоккера-Планка-Колмогорова отримано систему рівнянь, що подають математичну модель стохастичного адаптивного оптимального керування електричним режимом дугової сталеплавильної печі за критерієм мінімуму дисперсії тривимірного вектора струмів дуг, що дає змогу у порівнянні з відомими методами підвищити динамічну точність стабілізації струмів дуг на рівні заданих за критеріями енергоефективності та електромагнітної сумісності значень. Практична цінність. Реалізація запропонованої моделі адаптивного оптимального керування та структурної схеми системи для її реалізації дасть змогу у порівнянні з серійними регуляторами потужності дуг поліпшити динамічну точність стабілізації струмів дуг на рівні заданих оптимальних уставок і на основі цього комплексно поліпшити показники енергоефективності та електромагнітної сумісності режимів дугової печі та електромережі. Бібл. 18, рис. 5.
Ключові слова: **дугова сталеплавильна піч, електричний режим, тривимірний вектор струмів фаз, стохастичне керування, дисперсія, оптимізація, адаптація, контур регулювання струмів дуг.**

Цель. Целью статьи является создание метода оперативного синтеза сигнала управления электрическим режимом (ЕР) дуговой сталеплавильной печи (ДСП) на основе трехмерного вектора токов фаз, который учитывает стохастическую природу процессов в плавильном пространстве, силовой электрической цепи печи, имеет низкую чувствительность к изменению параметров объекта управления и разработка структуры системы управления для его реализации. Методика. В основе созданного метода управления использованы положения статистической теории динамических систем, а также положение статистической теории оптимального управления на основе уравнения Фоккера-Планка-Колмогорова, что позволяет синтезировать оперативное управление по критерию приближения плотности распределения регулируемой координаты к δ-функции, то есть минимизировать дисперсию трехмерного вектора токов дуг дуговой печи. Результаты. Получена система уравнений для оперативного в режиме on-line расчета управляющих воздействий тиристорного коммутатора фазных дросселей, включенных в силовую цепь питания трехфазных дуг, и структурную схему адаптивного контура формирования дисперсии трехмерного вектора токов фаз дуговой печи для реализации адаптивного оптимального управления. Научная новизна. Впервые на основе уравнения Фоккера-Планка-Колмогорова получена система уравнений, представляющих математическую модель стохастического адаптивного оптимального управления электрическим режимом дуговой сталеплавильной печи по

критерию минимума дисперсии трехмерного вектора токов дуг, что позволяет по сравнению с известными методами повысить динамическую точность стабилизации токов дуг на уровне заданных по критериям энергоэффективности и электромагнитной совместимости значений. Практическая ценность. Реализация предложенной модели адаптивного оптимального управления и структурной схемы системы для ее реализации позволяет по сравнению с серийными регуляторами мощности дуг улучшить динамическую точность стабилизации токов дуг на уровне заданных оптимальных уставок и на основе этого комплексно улучшить показатели энергоэффективности и электромагнитной совместимости режимов дуговой печи и электросети. Библ. 18, рис. 5.
Ключевые слова: **дуговая сталеплавильная печь, электрический режим, трехмерный вектор токов фаз, стохастическое управление, дисперсия, оптимизация, адаптация, контур регулирования токов дуг.**

Introduction. Arc furnaces are powerful electrical technological installations that belong to a class of complex systems and are characterized by extremely incident, dynamic, nonlinear, phase by phase non-symmetric nature of loading and continuous action of intense coordinate and parametric disturbances in arc gaps and power supply circuit of three-phase arcs. The specified loading characteristics complicate the control process of such objects and impose appropriate limitations on the system engineering – models, methods and approaches for improving existing systems of control modes and regulation of electric coordinates.

The problem of integrated improvement of energy efficiency and electromagnetic compatibility indices of arc steel-melting furnaces (ASFs) is dictated by the necessity of increasing the competitiveness of electric steels and high alloys on the domestic and foreign markets of metal products. Its state is largely determined by the level of excellence of automatic control systems (ACS) of electrical modes (EM) of arc furnaces, characterized by the speed and dynamic accuracy of coordinate (first of all, arc currents) regulation, the efficiency of electric modes control models, state identification and prediction of the process of electric steelmaking.

It is obvious that for such electrical technological nonlinear stochastic control objects with a range of installed power of power electric equipment of 1...175 MVA, it is most appropriate to use models based on probabilistic characteristics of control processes and that most fully correspond to the nature of the processes which occur in them. Efficiency and completeness of solution of control problems in general and adaptive optimal, in particular, of electrical modes of electric steelmaking are determined, first of all, by the speed and dynamic accuracy of the regulation of the coordinates of the electric mode and, the most important, by currents of arcs.

Problem definition. The complexity of the tasks of the modern theory of adaptive optimal control of stochastic dynamic objects and processes requires the improvement of the mathematical apparatus for their description, identification and control synthesis models, and also requires significant computing power of digital means (microcontrollers, microprocessor devices) for implementation of identification and real-time control.

Unfortunately, the control of modes in the vast majority of arc furnaces is realized on the basis of classical deterministic models of identification of states, parameters, phase by phase regulation of coordinates and control of modes that do not correspond to the stochastic phase by phase interconnected nature of the processes underlying them functioning.

Therefore, in our opinion, the most appropriate approach to solving the above problem is to improve the existing and create new effective methods and approaches for the tasks of controlling modes and coordinate regulation, in particular, the operational formation of control effects based on the three-dimensional vector of phase currents and its probabilistic characteristics.

Review of recent publications. For the first time, the theoretical principles of stochastic models for the formation of control effects for the electromechanical system of displacement of electrodes of three-phase ASFs have been published in [1]. The coefficients of the relationship between the average rectified currents of arcs included in the created model of the ASF are proposed to be determined on the basis of probabilistic analysis and taking into account the correlation interconnections of phase processes in the furnace space of the three-phase arc furnace. The model of electric mode control of the ASF obtained in this work allows to adjust the control signals of typical regulators of the electric mode by current and, thus, to avoid false operations of the regulator of the *i*-th phase (to eliminate false electrodes displacement) by perturbations in adjacent phases. Under this control model, the phase by phase autonomy of electric mode control is improved, which, in turn, increases the efficiency of the electrometallurgical plant. But with the help of such a model, it is impossible to implement the above-stated approach of control of three-phase ASF modes.

Similarly, the problems of the phase by phase autonomy of electric mode control by arc furnace phases on the basis of the account of stochastic parameters of perturbations of adjacent phases are considered in the work [2]. According to this work, the signal formed by the displacement of the electrodes in each phase is formed additively from the signals of the dissonance of all three phases, which are normalized by the weight factors. To find the values of these coefficients, the authors obtained a mathematical model that describes the reactions of such a complex object as the ASF on the pre-synthesized control influences and perturbation processes that convert the electric mode of the furnace to a particular state. In the final case, these coefficients are also some averaged over a certain time interval the coefficients of the weight of the signals of discrepancies of phase modes. Nevertheless, it should be noted here that in this paper for the first time it was noted that optimization of the system of controlling the electric mode of the ASF should be carried out with an orientation to such an integral characteristic of the mode as the variance of the three-dimensional vector of arc currents, but specific solutions in this direction in this work are not offered.

In the paper [3] for the analysis and synthesis of control systems of electric drives, which are under the influence of random perturbations, the expediency of using the probabilistic approach is substantiated. This approach ensures an adequate response of the ACS to the processes and perturbations that take place in the control object. In this paper, the method of formation of the variance of the regulated coordinate, that is, the method of stochastic dynamic stabilization for application in the problems of stabilization of coordinates of electromechanical systems with random perturbations is worked out. In its implementation, it is possible to control the dispersion of the output coordinate of the dynamic system in accordance with the current requirements and conditions of operation of the control object, in particular such as an arc furnace.

In work [4] a mathematical description of the electromechanical control system of electrodes position was worked out, on the basis of which «on-line» synthesis of the desired dynamic characteristics of the state change process on the basis of integral quality criteria is carried out. The proposed approach is based on the account of the phase by phase interconnection of electric modes caused by the peculiarities of the parametric non-symmetric power supply circuit of the three-phase arcs and the impedance or differential law of the formation of a control signal on the displacement of the electrodes. But this work, like the previous one, is far from the idea of applying the control of processes in arc furnaces and the idea of forming a three-dimensional vector of arc currents and its stochastic characteristics.

The mathematical and computer models of control of electrical modes of the three-phase arc furnaces proposed in the papers [5-9] have certain advantages and disadvantages among themselves in terms of the completeness and accuracy of the description of modes, identification of states, conveniences in use and readjustment, but they do not meet the above requirements for energy efficiency and electromagnetic compatibility modes in full, primarily due to the inadequacy of the control models to the nature of the real processes of changing the coordinates of the EM, also because of the high sensitivity of the obtained dynamics to changing parameters of the control object, which is highly undesirable in terms of continuous action of stochastic parametric disturbances in the power circuit of the furnace and in phase arc gaps.

The goal of the work is the development of system and structural solutions for the operative synthesis of the control signal of an arc furnace electric mode on the basis of a three-dimensional vector of arc currents, taking into account the stochastic nature of the processes in the melting space and the power supply circuit of the three-phase arcs and has a low sensitivity to the change of the control object parameters, the use of which in comparison with known solutions allows to increase the dynamic accuracy of the stabilization of arc currents at the level specified by the criteria of energy efficiency and electromagnetic compatibility.

The scientific task is to create the method of adaptive optimal control of the electric mode of an arc furnace according to the criterion of the minimum distribution density of a three-dimensional vector of phase currents and the structural scheme of the control system for its realization, which, in comparison with known control methods, enables to increase the dynamic accuracy of the stabilization of arc currents at the given (in particular, optimal) values and thereby improve the energy efficiency and electromagnetic compatibility indicators of arc furnace and power supply network.

Identification of previously unsolved parts of the general problem. The dynamics of the regulation of the EM coordinates of the ASF, in particular the arc currents, in the overwhelming majority of the existing (serial, typical) control systems of the process of electrical steel molding (by using arc power) does not fully meet the high modern requirements for energy efficiency and electromagnetic compatibility indicators of arc furnace modes and power supply network. Therefore, the problem of creating effective system, circuit and algorithmic solutions, which are based on increasing the speed of processes of regulation of phase (arcs) currents and complex improvement on the basis of indicators of energy efficiency and electromagnetic compatibility of modes for today for the electro-metallurgical industry is important and relevant.

Content of research material. In this paper, the term «optimality» is used in the narrow sense, in which the system of automatic control is evaluated only by the indicators of the quality of dynamic processes, and one of the criteria of this quality is the integral quality index – the generalized dispersion of the regulated coordinate. Such a description of the quality criteria makes it possible to use modern well-developed mathematical optimization apparatus to find optimal control.

Under the action of the flows of random perturbations and control influences, the electric mode (which is estimated by the stochastic characteristics of arc currents) of a three-phase arc furnace can be in different states.

Define these states by a three-dimensional vector of phase currents, which characterizes the electric mode of the arc furnace during the melting company as:

1 – a state characterized by the given (required) values of the coordinates of the electric mode, in particular by the set values of arc currents;

2 – a state characterized by deviations of arc currents in the domain of admissible directive deviations;

3 – a state characterized by deviations of the arc currents into the region of large, in particular extreme, deviations – short circuits, breaks of arcs and close to them.

It is clear that the concept of being in one or another state is associated with some definite time interval T_0. The graph of the states of the three-dimensional vector of states of the electric mode of an arc furnace is shown in Fig. 1.

Each of these states is proposed to be identified by means of the integral parameter (indicator) value, which is the generalized variance of the three-dimensional vector of the ASF arc currents. In turn, this integral indicator is defined as the determinant of the matrix of second order moments, or the correlation matrix [10], and it characterizes the value of the deviation of the vector of

arc currents of the three-phase arc furnace from the desired state.

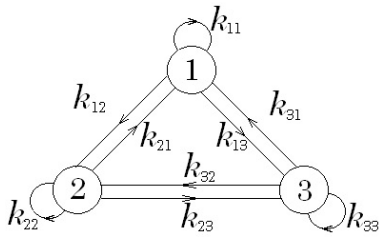

Fig. 1. A graph of states of the electric mode of an arc furnace – $k_{1,1}(t)$, $k_{1,2}(t)$, $k_{2,1}(t)$, $k_{2,2}(t)$, $k_{1,3}(t)$, $k_{2,3}(t)$, $k_{3,3}(t)$, $k_{3,1}(t)$, $k_{3,2}(t)$ – the intensities of the transition from state to state

So, having adopted the designation of a three-dimensional vector of regulated coordinates (for the considered problem of arc currents) as

$$\boldsymbol{I}_a = \boldsymbol{y} = \left| y_1 \;\; y_2 \;\; y_3 \right|,$$

we obtain an expression for the dispersion of the three-dimensional vector in the form:

$$D_{I_a} = D_y = \det \boldsymbol{\Lambda}_y,$$

where $\boldsymbol{\Lambda}_y$ is the correlation matrix, or matrix of moments of the second order of the form:

$$\boldsymbol{\Lambda}_y = \begin{vmatrix} \lambda_{11} & \lambda_{12} & \lambda_{13} \\ \lambda_{21} & \lambda_{22} & \lambda_{23} \\ \lambda_{31} & \lambda_{32} & \lambda 33 \end{vmatrix}.$$

The criterion for the functioning of such a dynamic system is the desired level of probability of being the system in state **1** during the time of the melting of charge. In view of the above, we write the expression for the density of the three-dimensional vector of the regulated coordinate as:

$$p(y_1, y_2, y_3) = \frac{1}{(2/\pi)^{3/2}\sqrt{\det \Lambda_y}} \times \\ \times \exp\left[-\frac{1}{2} \sum_{i,j=1}^{3} \Lambda_{y_{i,j}}^{-1} \cdot \left| y_i - \bar{y}_i \right| \cdot \left| y_j - \bar{y}_j \right| \right], \quad (1)$$

where $\Lambda_{y_{i,j}}^{-1} = \frac{1}{\det \Lambda_y} \cdot A_{i,j}$ are the elements of the inverse matrix $\boldsymbol{\Lambda}_y^{-1}$; $\boldsymbol{A}_{i,j}$ are the corresponding elements of the attached matrix, and the probability of being of the electric mode of an arc furnace in a given state is found as an integral of density (1):

$$P(y_1, y_2, y_3) = \int_0^{y_1^*} \int_0^{y_2^*} \int_0^{y_3^*} p(y_1, y_2, y_3) dy_1 \, dy_2 \, dy_3,$$

where y_1^*, y_2^*, y_3^* are the maximum values of the change of the coordinates of the electric mode, for example, the value of the circuits of the short circuit in the ASF phases.

It is clear that the smaller the variance of the three-dimensional vector of the regulated coordinate (the arc currents of the arc furnace), the greater the probability of a state that is identified by such a variance value, i.e., state **1**. Taking into account that in a real object we have a flow of disturbances and a flow of control influences that change the state of the system (the state of the electric mode), we write the model of state dynamics in the form of the Kolmogorov-Chapman equation [11]:

$$\frac{dP_i(t)}{dt} = \sum_{j=1}^{3} P_{j,i} \cdot k_{j,i}(t) - \sum_{j=1}^{3} P_i \cdot k_{i,j}(t),$$

and the system of equations for determining the probabilities of individual states is written as:

$$\begin{aligned} \frac{dP_1(t)}{dt} &= -P_1(t) \cdot \left[k_{12}(t) + k_{13}(t) \right] + k_{21}(t) \cdot P_2(t) + \\ &\quad + k_{31}(t) \cdot P_3(t); \\ \frac{dP_2(t)}{dt} &= -P_2(t) \cdot \left[k_{21}(t) + k_{23}(t) \right] + k_{12}(t) \cdot P_1(t); \quad (2) \\ \frac{dP_3(t)}{dt} &= -P_3(t) \cdot \left[k_{31}(t) + k_{32}(t) \right] + k_{13}(t) \cdot P_1(t). \end{aligned}$$

From the presented system of equations (2) and graph in Fig. 1 it can be concluded that the intensities of transitions $k_{21}(t)$; $k_{31}(t)$; $k_{32}(t)$ are formed by controlling effects of the control system, which bring the electric mode of the arc furnace from the unwanted states **2** and **3**, and especially from the state **3** to state **1**. At the same time, the intensities of transitions $k_{12}(t)$; $k_{13}(t)$; $k_{23}(t)$ are determined by the disturbances that act in the melting space and power circuit of the ASF.

The method of formation of effective control influences was developed in works [12-15], namely, the method of forming a vector of control effects of the so-called second (high-speed electric) circuit of regulating arc currents included in the structure of existing (serial) one-contour electric control systems of electric mode of an arc furnace. The main feature of such a two-contour structure of the electric mode control system of the arc furnace is the high speed of the arc currents regulation (the current regulation time is 0.03-0.04 s), which allows to significantly improve the control dynamics, that is, to obtain a high dynamic accuracy of the arc currents stabilization, and thus, with high accuracy to control the dynamics of the state graph, in particular, to transfer the electrical mode of the arc furnace to states **1** or **2**.

The functional scheme of such a two-circuit control system of the EM of the arc furnace is shown in Fig. 2. This system contains the traditional electromechanical (or electrohydraulic) contour for regulating the lengths of the arcs EMCRLA (it is traditionally called the regulator of the arcs power), which has a relatively high inertia, which results in the operation of such a regulator of arcs power is accompanied by a significant dispersion of the coordinates of the EM – lengths, voltages, currents and powers of arcs.

Each phase channel of this circuit includes the arcs voltage sensor (VS) and current sensors (CS), the control signal formation unit (CSFU), the electrode displacement electric drive (EDED) and the electrode displacement mechanism (EDM), and also contains a voltage level switch (VLS) of the furnace transformer FT. Most often,

in such EMCRLAs, the control signal on the displacement of the electrode in each phase is formed according to the differential law.

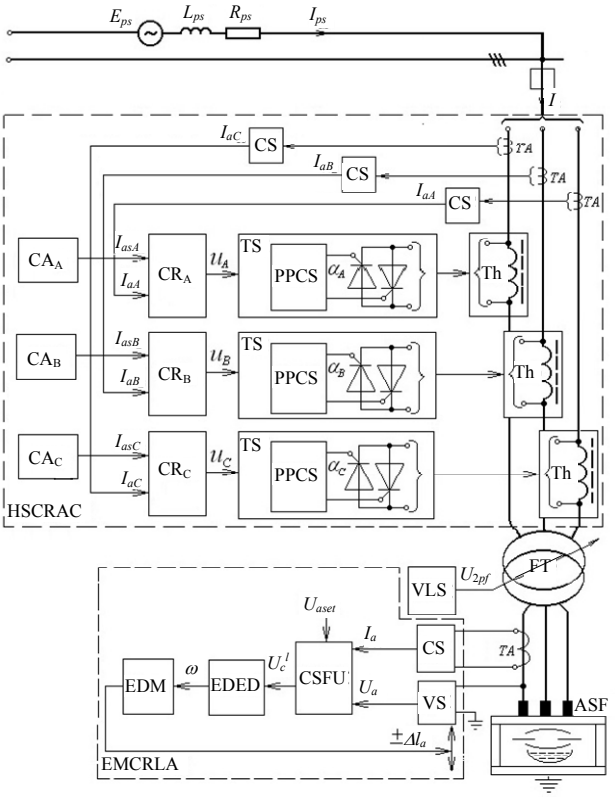

Fig. 2. Functional scheme of the two-circuit control system of the electric mode of the arc furnace

An example of the dynamics of the regulation of arc currents by the electromechanical circuit, performed in the structure of the ACS of the EM of the arc furnace ДСП-200 by the serial regulator of the arcs power of the type АРДМ-Т-12, is illustrated in Fig. 3,*a* by the fragments of the temporal dependencies of the arcs currents $I_{aj}(t)$ (j=A, B, C) (computer experiments were carried out at time intervals of stationary T_c=180-300 s of random processes of perturbations by the lengths of arcs of the furnace ДСП-200 for various technological melting stages).

In the composition of each phase channel of the electric high-speed contour for the regulation of arc current (HSCRAC) there are the arc current sensor (CS), adjuster (CA) and the regulator (CR) of the arc current, the thyristor switch (TS), the control effect of which is the time of the shunting of the throttle (Th) on a certain regulated part of the half-period of the voltage given by the angle α of the control of the parallel thyristor-reactor group. At the joint functioning of these two regulating contour, their advantages are combined: reliable ignition of arcs in the treatment of extreme disturbances – operational short circuits and breakdowns of the arcs of the EMCRLA and high speed of regulation of arc current of the HSCRAC. As a result of such a combination of contours in the two-contour structure of the ACS of the EM of the ASF it is possible to achieve high controllability and dynamic precision of the stabilization of currents (lengths, voltages, powers) of arcs under the conditions of the action of continuous random transient parametric and coordinate disturbances.

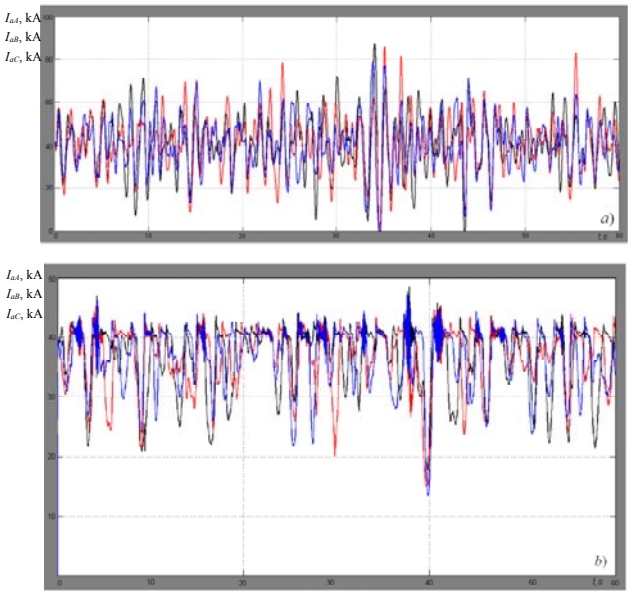

Fig. 3. Temporal dependencies of arc currents of the ДСП-200 furnace at the operation of the regulator АРДМ-Т-12 (*a*) and АРДМ-Т-12 with a high-speed contour at control by the criterion $D_O \Rightarrow \min$ (*b*)

To compare dynamics, as an example, Fig. 3,*b* shows the temporal dependencies of arcs currents in the operation of a two-contour system under the influence of random disturbances with the same parameters of stochastic perturbation characteristics using the proportional integral current regulator CR and EM optimization based on the scalar criterion for the minimum of the dispersion of the reactive power of the furnace $D_O \Rightarrow \min$, which is largely correlated with the criterion for the minimum dispersion of arcs currents. The dispersion of arcs currents in the two-contour structure of the ACS of the EM of the ДСП-200 at the functioning of the proportional-integral regulator was: $D_{I_{aA}} = 2.95 \cdot 10^7$ A^2; $D_{I_{aB}} = 3.15 \cdot 10^7$ A^2; $D_{I_{aC}} = 2.35 \cdot 10^7$ A^2. The average on the phases the dispersion of the currents of arcs was $\overline{D}_{I\,a} = 2.82 \cdot 10^7$ A^2. The presented temporal dependencies illustrate high speed of regulation and high-quality dynamic stabilization of arcs currents in the structure of the two-contour ACS of the EM of the arc furnace. Comparison of dispersions shown in Fig. 3 for processes of the change of arcs currents $I_{aj}(t)$ with the values of dispersions under other parameters of stochastic disturbances by the arcs lengths shows a considerable (almost an order of magnitude) decrease in the dispersion of arcs currents in the joint operation of electromechanical and high-speed electric contours with a proportional integral regulator of arcs currents in the two-contour structure of the ACS of the EM of the arc furnace in comparison with the operation of a one-contour ACS of the EM (regulator АРДМ-Т-12) [10].

For such a two-contour structure of the ACS of the EM of the arc furnace, it is important to develop effective

system-engineering solutions – models of the formation of phase controlling effects of the high-speed contour of regulating the arcs currents of the HSCRAC, which would improve the indicators of the electrical efficiency and electromagnetic compatibility of the arc furnace modes and power grid.

Therefore, it is expedient in the context of the task defined in the work to develop the theoretical bases of a stochastic model of operative synthesis of control influences by a three-dimensional vector of arcs currents in the structure of such a two-contour ACS of the electric mode of the ASF.

For the synthesis of the vector of control effects on the regulation of the arcs currents of the two-contour ACS of the EM of the arc furnace, we apply the principle according to which the optimal change in the distribution density of the three-dimensional arcs currents vector is realized, in particular, in the direction of approximation of this distribution to the form of the δ-function.

So, in the ideal case, the system will better perform its intended purpose, namely, to ensure the state **1** of the three-dimensional vector of phases currents, the sooner it will convert the initial distribution density $p(y_A, y_B, y_C, t_0)$ of the three-dimensional vector of currents of arcs of the furnaces in δ-function, or in the δ-distribution, which is combined with the point $y_A = y_{A.set}$, $y_B = y_{B.set}$, $y_C = y_{C.set}$, where y_A, y_B, y_C, $y_{A.set}$, $y_{B.set}$, $y_{C.set}$ are the current and set values of the regulated coordinates – arcs currents of the arc furnace.

This conclusion corresponds to the principle of the statistical theory of transients, according to which, on the basis of the Fokker-Planck-Kolmogorov equation [16], optimal control is obtained in relation to the ctransient of changing the density of the n-dimensional probability distribution to the density of the form of the δ-function.

For our case, we write the Fokker-Planck-Kolmogorov equation in the form

$$\frac{dp}{dt} = \sum_{i=1}^{3} \frac{d(p \cdot F_i)}{dy_i}, \qquad (3)$$

as an equation for a dynamic system in the absence of noise.

In this equation (3) it is indicated: p is the probability distribution density of a three-dimensional vector $p = p(y_1, y_2, y_3)$; $\dot{y}_i + F_i(y_1, y_2, y_3) = 0$ is the equation describing the system coordinates movement.

For the automatic control system, the functions F_i can be represented as a set of two functions:

$$F_i = f_i(y_1, y_2, y_3) - u(y_1, y_2, y_3),$$

where the function f_i belongs to the control object, and the function u – to the control system.

Synthesized in [16] controls for dynamical systems that provide an optimal change in the density of the distribution of the n-dimensional vector of regulated coordinates y_i are calculated by the expression:

$$u_i = d_i \cdot \text{sign}\left(\frac{\partial \ln(p)}{\partial y_i}\right),$$

where d_i is the maximum permissible or limit value of control influence; y_i is the component of the n-dimensional vector of regulated coordinates.

Such a control on one of the coordinates, for example, on the first, for our case, is written as:

$$u_1 = d_1 \cdot \text{sign}\left(\frac{\partial \ln(p(y_1, y_2, y_3))}{\partial y_1}\right).$$

To find the appropriate control we write down the distribution density (1) of the three-dimensional vector of the regulated coordinate of the electric mode of the ASF in the form convenient for differentiation:

$$p(y_1, y_2, y_3) = \frac{1}{(2/\pi)^{3/2}\sqrt{\det \Lambda_y}} \cdot \exp\left[-\frac{1}{2} \cdot \frac{1}{\det \Lambda_y} \times \right.$$
$$\times \{A_{11}(y_1 - \bar{y}_1)^2 + 2 \cdot A_{12}(y_i - \bar{y}_1) \cdot (y_2 - \bar{y}_2) +$$
$$+ 2 \cdot A_{13}(y_1 - \bar{y}_1) \cdot (y_3 - \bar{y}_3) + A_{22}(y_2 - \bar{y}_2)^2 +$$
$$\left. + 2 \cdot A_{32}(y_2 - \bar{y}_2) \cdot (y_3 - \bar{y}_3) + A_{33}(y_3 - \bar{y}_3)^2\}\right],$$

where $\bar{y}_1$, $\bar{y}_2$, $\bar{y}_3$ are the mathematical expectations of phase regulated coordinates, which for the considered object are given by the values of the currents of arcs of individual phases of the ASF.

If we make the necessary mathematical transformations and substitute currents of arcs I_{aA}, I_{aB}, I_{aC} instead of generalized regulated coordinates y_i ($i = A, B, C$), we obtain the expressions for the mentioned control influences u_A, u_B, u_C for each of the phases of the arc furnace in form:

$$u_A = d_1 \cdot \text{sign}\{\frac{1}{\sqrt{\det \Lambda_I}} \cdot [A_{11}(I_{aA} - \bar{I}_{aA}) +$$
$$+ A_{12}(I_{aB} - \bar{I}_{aB}) + A_{13}(I_{aC} - \bar{I}_{aC})]\};$$
$$u_B = d_2 \cdot \text{sign}\{\frac{1}{\sqrt{\det \Lambda_I}} \cdot [A_{21}(I_{aA} - \bar{I}_{aA}) + \qquad (4)$$
$$+ A_{22}(I_{aB} - \bar{I}_{aB}) + A_{23}(I_{aC} - \bar{I}_{aC})]\};$$
$$u_C = d_3 \cdot \text{sign}\{\frac{1}{\sqrt{\det \Lambda_I}} \cdot [A_{31}(I_{aA} - \bar{I}_{aA}) +$$
$$+ A_{32}(I_{aB} - \bar{I}_{aB}) + A_{33}(I_{aC} - \bar{I}_{aC})]\}.$$

As we see, for the operative formation of the control influences $u_A(t)$, $u_B(t)$, and $u_C(t)$ it is necessary to know the matrix Λ_I of other moments of the three-dimensional vector of the currents of arcs (phases) of the ASF. The operational calculation of control effects by the received model (4) for modern microprocessor devices is a simple (to some extent trivial) technical task.

We note here that the control signals obtained by the equations (4) are formulated as boundary controls and can only be considered as conventionally optimal ones. However, studies [16] show that these controls can be quite close, and even coincide with strictly optimal controls, which translate the n-dimensional distribution of the regulated coordinate into δ-function.

The obtained model (4) of operative synthesis of the vector of control signals u_A, u_B, u_C is realized in the proposed structure of the two-contour adaptive control system of arc furnace electric mode, the functional block diagram of which is shown in Fig. 4.

In the presented scheme of the two-contour adaptive ACS by the values of implementations of the average

rectified currents of the three phases I_{aA}, I_{aB}, I_{aC} of the arc furnace in the block of calculations BC operatively at each interval of stationary (T_c = 3-5 min) of the processes of phases currents changes, the calculation of the matrix $\boldsymbol{\Lambda}_I$ of other moments of the three-dimensional vector of the currents of arcs of arc furnace, its determinant $\det\boldsymbol{\Lambda}_I$ and the values of the elements $\boldsymbol{A}_{i,j}$ of the adjoint matrix $\boldsymbol{A}$ of the inverse matrix $\boldsymbol{\Lambda}_I^{-1}$ is performed.

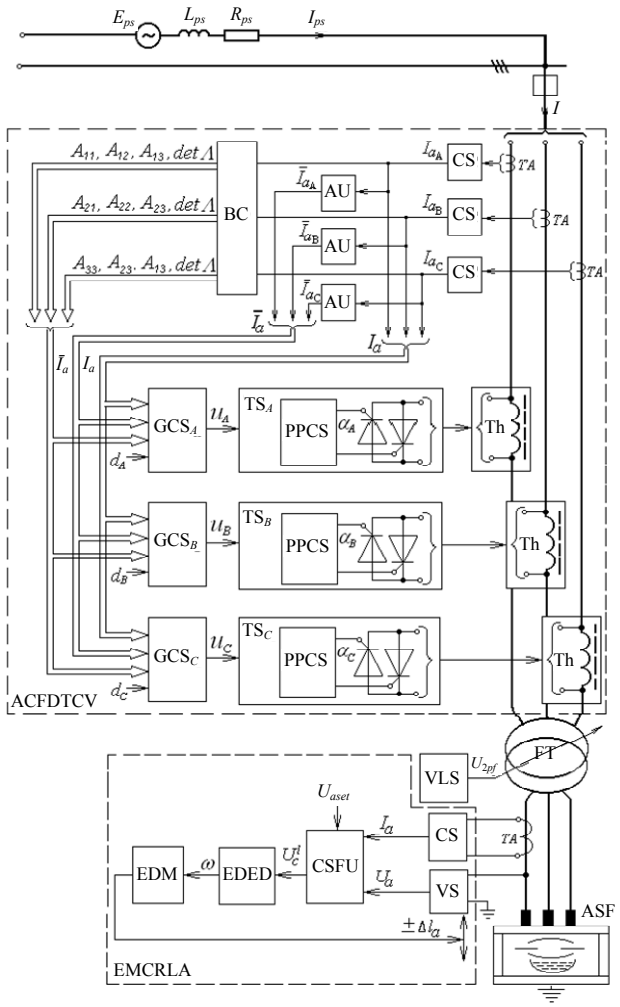

Fig. 4. Functional scheme of the two-contour adaptive control system of arc furnace electric mode for minimization of dispersion of three-dimensional vector of currents

The specified signals from the BC outputs are fed to the third vector input of each phase generator of the control signal for current I_{ai}, namely: A_{11}, A_{12}, A_{13}, $\det\boldsymbol{\Lambda}_I$ – to the third GCS_A input; A_{21}, A_{22}, A_{23}, $\det\boldsymbol{\Lambda}_I$ – to the third GCS_B input; A_{31}, A_{32}, A_{33}, $\det\boldsymbol{\Lambda}_I$ – to the third GCS_C input, and to the first and second vector inputs of GCS_A, GCS_B, GCS_C the three-dimensional vector of currentaverage rectified values of arcs currents I_{ai} from the outputs of currents censors CS and a three-dimensional vector of the averaged on the stationary intervals T_c currents $\bar{\boldsymbol{I}}_{ai}$ are input, respectively. The fourth input of the GCS_i is fed by the scalar signal d of the maximum value of the control influence. On the outputs of the GCS_i continuously online phase control signals u_i are generated based on the obtained control model (4), which are fed to the corresponding phase thyristor switches TS_i. Output signals α_i of pulse-phase control systems (PPCSs) determine the moments of shunting/ switching on in the power circuit of the corresponding phase throttles Th_i.

The proposed procedure for operative synthesis of control effects $u_A(t)$, $u_B(t)$, and $u_C(t)$ is divided into two parallel processes in time: the first process implements the adaptation of the coefficients of the synthesis model (4) to change the parameters of stochastic characteristics of coordinate and parametric perturbations on the time the interval of melting, and the second one performs online operative with discreteness Δt calculation of control effects $u_A(t)$, $u_B(t)$, and $u_C(t)$ in GCS_A, GCS_B, and GCS_C units by this model. The first process involves at each interval of stationary T_c, the duration of which is correlated with the technological stages of melting (the physical and chemical state of the melt) and depends on the types of arc furnaces ((T_c = 180-300 s), the calculation in the BC of the coefficients of the model (4): $\det\Delta_I$, $\bar{I}_{a,j}$, $A_{n,m}$, and the second one implements the process of calculating the control effects u_A, u_B, u_C and is performed with the interval Δt = 0.02 s in the function of averaging the values (rms) of phases currents $I_j(t_k)$ ($t_k = t_{k-1} + \Delta t$, $m = 1, 2, 3$, $n = 1, 2, 3$, $j = A, B, C$) in this interval.

To verify the effectiveness of the proposed stochastic model for synthesizing the control signals $u_A(t)$, $u_B(t)$, and $u_C(t)$, the corresponding mathematical experiments were performed on the three-phase in instantaneous coordinates Simulink model [17, 18] of the two-contour ACS of the EM of the arc furnace ДСП-200 (Fig. 2). The modelling studies were performed at the functioning of the proportional integral arc voltage regulator and using the proposed stochastic model (4) for synthesizing the control signals $u_A(t_i)$, $u_B(t_i)$, and $u_C(t_i)$ which is implemented in the proposed structure of the adaptive ACS of the EM of the arc furnace (Fig. 4), which implements a strategy for minimizing the dispersion of a three-dimensional vector of phases currents.

To do this, a computational block is introduced into the structure of the Simulink model, in which, according to the well-known model [10], on the intervals of stationary $T_{c,i}$, the coefficients of the model (4) $\det\Delta_I$, $\bar{I}_{a,j}$, $A_{n,m}$ are calculated. In the next interval of stationary $T_{c,i+1}$, these coefficients are used in GCS_A, GCS_B, and GCS_C for synthesis of control signals u_A, u_B, u_C by model (4) in the function of current averaged over a period of supply voltage Δt = 0.02 s phase currents I_A, I_B, I_C. Obtained control u_A, u_B, u_C are applied to the inputs of thyristor switches. At the same time, the new values of the coefficients of the model (4) $\det\Delta_I$, $\bar{I}_{a,j}$, $A_{n,m}$, are used in the next $T_{c,i+2}$ interval of online control signal u_A, u_B, u_C, etc. synthesis, are calculated on the current stationary interval $T_{c,i+2}$.

Figure 5 shows the initial fragments of temporal dependencies of phase currents obtained on the Simulink

model at the control by the above model (4), implementing the strategy of minimizing the dispersion of a three-dimensional vector of phases currents.

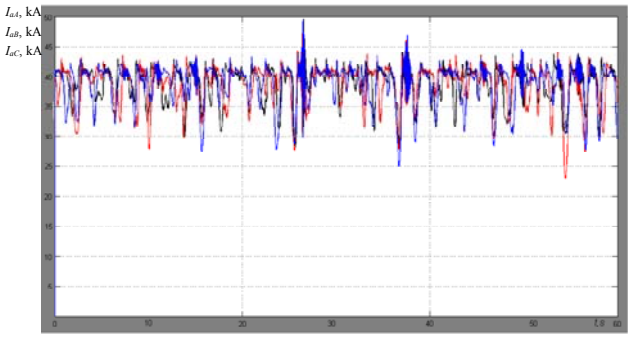

Fig. 5. Temporal dependencies of the arcs currents of the furnace ДСП-200 with the regulation by the obtained model (4) of minimizing the dispersion of the three-dimensional vector of arcs currents in the two-contour structure of the ACS of the EM of the arc furnace ДСП-200

As a result of working out the time dependenceis of the currents of the arcs $I_i(t)$ in Fig. 5, the following values of their dispersions are obtained: $D_{I_A} = 0.95 \cdot 10^7$ A^2; $D_{I_B} = 1.05 \cdot 10^7$ A^2; $D_{I_C} = 1.03 \cdot 10^7$ A^2. The average by the phases the dispersion of the currents of arcs is $\overline{D}_I = 1.01 \cdot 10^7$ A^2.

Comparative analysis of temporal dependencies of arcs currents in Fig. 3,*b* and Fig. 5 shows that the average by phases dispersion of arcs currents at the regulation by the obtained model (4) of minimizing the dispersion of the three-dimensional vector of arcs current in the two-contour structure of the ACS of the EM decreased by 2.73 times. The computer researches for perturbation processes by the lengths of arcs of other technological melting stages, which differ in frequency spectrum and amplitude of oscillations, have shown that the average dispersion of arcs currents at the regulation by the obtained model (4) of the minimization the dispersion of the three-dimensional arcs current vector in the two-contour structure of the ACS of the EM compared with the use of known proportional-integral model of the formation of control signals $u_A(t_i)$, $u_B(t_i)$, and $u_C(t_i)$ decreased in 1.6-3 times.

Due to the cyclical updating of the matrix $\boldsymbol{\Lambda}_I$ of other moments of the three-dimensional vector of arcs currents of the acr furnace in the block BC and elements of the vector I_{ai} on the outputs of the averaging units AU, the adaptation of the vector of control influences $u_A(t_i)$, $u_B(t_i)$, and $u_C(t_i)$ to the change of parameters of stochastic characteristics of coordinate and parametric perturbations in the power circuit and arc gaps of the arc furnaces in the full range of melting is realized.

Thus, due to the obtained model (4) of the operative formation and adaptation of the vector of control effects and their realization through the adaptive contour of the formation of the dispersion of the three-dimensional arcs current vector ACFDTCV of the arc furnace one can obtain a significant approximation of the distribution of the three-dimensional vector of arcs phase currents of the arc furnace to the type of the δ-function. And the fact that the reduction of the dispersion of arcs currents significantly influences the improvement of energy efficiency indicators (electrical efficiency coefficient of the furnace, specific energy consumption, specific ASF productivity, the price of the ton of smelted steel, etc.) of an electro-technological installation, which is an AC arc furnace power is a well-known fact.

It should also be noted that the proposed stochastic model of the regulation of the coordinates of the EM of the arc furnace and the model of adaptive synthesis of control signals based on the three-dimensional vector of phase currents implements a relay, in contrast to the existing control law. Such a law of control of compliance with the conditions of stability, as is known, provides maximum regulation speed and, as a result, high dynamic accuracy of the arc current stabilization at the level of optimal for the selected criterion of values, and also is characterized by a much lower sensitivity to the change of parameters of the control object – the parameters of dynamic volt-ampere characteristics of three-phase arcs and parameters of the elements of the power circuit (short circuit) of an arc furnace. The last feature of the proposed method is particularly important for implementing adaptive optimal control strategies under continuous conditions of intense stochastic parametric perturbations in the power circuit and arc gaps of the furnace during melting.

The stochastic model of operative synthesis and adaptation of the vector of controlling for minimizing the dispersion of the three-dimensional arcs currents vector obtained in the paper is expedient for practical use in the two-contour structures of the ACS of the EM of arc furnaces with a high-speed contour for regulating arc currents.

Conclusions. The developed in the paper the theoretical bases of the method of electric arc furnace control on the basis of the formation of the distribution density of the three-dimensional vector of arc currents make it possible to implement the adaptive optimal control strategy of the electric mode by the criterion of the minimum dispersion of arc currents. As the results of the performed model researches show, the synthesis of the vector of control of arc currents by the obtained stochastic model (4) compared with the use of the proportional-integral regulator of arc current for controlling the EM reduces the dispersion of arc currents by 1.6-3 times. The minimization of the arc current dispersion positively affects the reduction of the power of electrical losses in the elements of the short arc furnace network and, as a result, reduces the specific energy consumption, the corresponding increase in the furnace productivity and the electric efficiency of the arc furnace. In addition, the transformation of the three-dimensional vector of arc currents into the δ-function in the control of the electric mode greatly reduces the consumption of reactive power of the furnace and, accordingly, increases the power factor, reduces the volatility and deviation of the network voltage on the power supply buses of the furnace and accordingly reduces the dose of the flicker.

REFERENCES

1. Lozinskyi O.Yu., Maruschak Y.Yu. Three-dimensional stochastic model of the electric mode regulation of an arc

furnace. *Industrial Process Automation in Engineering and Instrumentation*, 1993, no.31, pp. 7-11. (Ukr).
2. Lozinsky O.Yu., Parancuk Ya.S., Lozinsky A.O. Optimization of dynamic regimes of interconnected electro-mechanical systems. *Bulletin of Lviv Polytechnic National University, «Electric Power and Electromechanical Systems» series*, 2001, no.421, pp. 98-103. (Ukr).
3. Lozynskyi O.Yu., Parancuk Ya.S., Moroz V.I. Synthesis of the control process for electromechanical systems that are under the influence of random perturbations. *Bulletin of NTU «KhPI». Series: Problems of automated electric drive. Theory and practice*, 1994, pp. 104-106. (Ukr).
4. Lozinsky O.Yu., Parancuk Ya.S., Tsyapa V.B. Mathematical description of the dynamics of the regulation of the position of the electrodes of the chipboard model in the space of states. *Bulletin of Lviv Polytechnic National University, «Electric Power and Electromechanical Systems» series*, 2017, no.840, pp. 54-60. (Ukr).
5. Nikolaev A., Povelitsa E., Kornilov G., Anufriev A. Research and Development of Automatic Control System for Electric Arc Furnace Electrode Positioning. *Applied Mechanics and Materials*, 2015, vol.785, pp. 707-713. **doi: 10.4028/www.scientific.net/amm.785.707**.
6. Ghiormez L., Panoiu M. Current control of a 3-phase electric arc furnace using fuzzy logic. *ANNALS of Faculty Engineering Hunedoara – International Journal of Engineering*, 2015, Fascicule 4 Tome XIII, pp. 237-242.
7. Nikolaev A.A., Tulupov P.G. Method of setting optimum asymmetric mode of operation of electric arc furnace. *2016 11th France-Japan & 9th Europe-Asia Congress on Mechatronics (MECATRONICS) / 17th International Conference on Research and Education in Mechatronics (REM)*, Jun. 2016. **doi: 10.1109/mecatronics.2016.7547111.**
8. Zheng T., Makram E.B. An adaptive arc furnace model. *IEEE Transactions on Power Delivery*, 2000, vol.15, no.3, pp. 931-939. **doi: 10.1109/61.871355**.
9. Hooshmand R., Banejad M., Torabian Esfahani M. A New Time Domain Model for Electric Arc Furnace. *Journal of Electrical Engineering*, 2008, vol.59, no.4, pp. 195-202.
10. Pugachov V.S. *Teoriia sluchainykh funktsii i ee primenenie k zadacham avtomaticheskogo upravleniia* [The theory of random functions and its application to problems of automatic control]. Moscow, Fizmatizdat Publ., 1960. 883 p. (Rus).
11. Kazakov V.A. *Vvedenie v teoriiu markovskikh protsessov i nekotorye radiotekhnicheskie zadachi* [Introduction to the theory of Markov's processes and some radio engineering problems]. Moscow, Soviet radio Publ., 1973. 232 p. (Rus).
12. Lozynskyy O., Lozynskyy A., Paranchuk Y., Paranchuk R., Marushchak Y., Malyar A. Analysis and Synthesis of Intelligent System for Electric Mode Control in Electric Arc Furnace. *Part of the Lecture Notes in Electrical Engineering book series (vol.452). Analysis and Simulation of Electrical and Computer Systems*, 2017, pp. 111-130. **doi: 10.1007/978-3-319-63949-9_7**.
13. Lozynskyi O., Lozynskyi A., Paranchuk Y., Paranchuk R., Holovach I., Tsyapa V. Fuzzy extreme control and electric mode coordinates stabilization of arc steel-melting furnace. *2016 XIth International Scientific and Technical Conference Computer Sciences and Information Technologies (CSIT)*, Sep. 2016. **doi: 10.1109/stc-csit.2016.7589866**.
14. Lozynskyy O., Paranchuk Y., Paranchuk R. Fuzzy control law of electrode travel in arc steelmaking furnace. *16th International Conference on Computational Problems of Electrical Engineering (CPEE)*, Sep. 2015. **doi: 10.1109/cpee.2015.7333349.**
15. Lozinskyy O.Yu., Paranchuk Y.S. Optimization of the modes of the process control system for electric steel-melting in arc steel-smelting furnaces. *Electrical engineering*, 2004, no.6, pp. 50-54. (Rus).
16. Krasovskyi A.A. *Statisticheskaia teoriia perekhodnykh protsessov v sistemakh upravleniia* [Statistical theory of transient processes in control systems]. Moscow, Nauka Publ., 1968. 240 p. (Rus).
17. Lozynskyi O.Y., Paranchuk Y.S., Paranchuk R.Y., Matico F.D. Development of methods and means of computer simulation for studying arc furnace electric modes. *Electrical engineering & electromechanics*, 2018, no.3, pp. 28-36. **doi: 10.20998/2074-272X.2018.3.04.**
18. Lozynskyy O., Paranchuk Y., Stakhiv P. The Study of Dynamics of the Two-Loop Arc Furnace Electric Mode ACS on a Simulink-model. *Przegląd Elektrotechniczny*, 2018, vol.1, no.12, pp. 24-27. **doi: 10.15199/48.2018.12.06**.

Received 30.04.2019

O.Y. Lozynskyi[1], *Doctor of Technical Science, Professor,*
A.O. Lozynskyi[1], *Doctor of Technical Science, Professor,*
Y.S. Paranchuk[1], *Doctor of Technical Science, Professor,*
R.Y. Paranchuk[1], *Candidate of Technical Science,*
[1] Lviv Polytechnic National University,
12, S. Bandera Str., Lviv, 79013, Ukraine,
e-mail: yparanchuk@yachoo.com

How to cite this article:
Lozynskyi O.Y., Lozynskyi A.O., Paranchuk Y.S., Paranchuk R.Y. Synthesis and analysis of arc furnace electrical mode control system on the basis of three-dimensional phase currents vector distribution. *Electrical engineering & electromechanics*, 2019, no.4, pp. 26-34. **doi: 10.20998/2074-272X.2019.4.04.**

UDC 621.314.26 **doi: 10.20998/2074-272X.2019.4.05**

O.O Shavelkin, V.V. Kaplun, I.O. Shvedchykova

ERROR ELIMINATION FOR CURRENT CONTROL LOOP FOR MULTI-FUNCTIONAL SINGLE-PHASE GRID-CONNECTED INVERTER

Purpose. Elimination of the error of the inverter current control loop by improving its structure and justifying the parameters, which will ensure compliance with the current quality standard at the common coupling to the distribution grid of the load and the multi-functional grid inverter at the output of the renewable source of electrical energy. Methodology. Synthesis of structure of current control loop based on analysis of processes in electrical circuits and computer simulation. Results. Relationships for determining the input voltage of the inverter, reactor inductance and modulation frequency in accordance with the grid voltage, the maximum values of the inverter current and the amplitude of its ripple when combining the function of the active power filter. Dependencies of the amplitude of the pulsations of the output current of the inverter and the errors in the fundamental harmonic in accordance with the voltage at the input of the inverter, the modulation frequency and inductance of the output reactor are obtained. Originality. The structure of the inverter current control loop has been improved with a combination of proportional, integrating and differentiating links, and their parameters have been determined to ensure compensation of the disturbing action on input of the reference and compensation of the error of current from the disturbing action of the grid voltage regardless of its value. Practical value. The obtained solutions are the basis for the design of converters of electric power systems with renewable sources of electricity with improved energy efficiency. References 10, figures 7.

Key words: **multi-functional single-phase grid-connected inverter, nonlinear load, PWM, current control loop, current error compensation, THD, simulation.**

Мета. Усунення похибки контуру регулювання струму інвертора шляхом удосконалення його структури та обґрунтування параметрів, що сприятиме відповідності стандарту якості струму в точці підключення до розподільчої мережі навантаження і багатофункціонального мережевого інвертора на виході поновлювального джерела електроенергії. Методика. Синтез структури контуру регулювання струму на базі аналізу процесів у електричних колах з використанням комп'ютерного моделювання. Результати. Одержані залежності амплітуди пульсацій вихідного струму інвертора і похибки за основною гармонікою від напруги на вході інвертора, частоти ШІМ і індуктивності реактора. Співвідношення для визначення значень вхідної напруги інвертора, індуктивності реактору та частоти ШІМ згідно напрузі мережі, максимальних значень струму інвертора та амплітуди його пульсацій за суміщенням функції силового активного фільтра. Наукова новизна. Удосконалено структуру контуру регулювання струму зі сполученням пропорційної, інтегруючої та диференціючої ланок і визначені їх параметри для забезпечення компенсації збурюючої дії за завданням і компенсації похибки струму від збурюючої дії напруги мережі незалежно від її значення. Практичне значення. Отримані рішення є основою для проектування перетворювачів для систем з поновлювальними джерелами електроенергії з покращеною енергоефективністю. Бібл. 10, рис. 7.

Ключові слова: **багатофункціональний мережевий інвертор, нелінійне навантаження, ШІМ, контур регулювання струму, компенсація похибки струму, коефіцієнт гармонік, моделювання.**

Цель. Устранение погрешности контура регулирования тока инвертора путем совершенствования его структуры и обоснования параметров, что позволит обеспечить соответствие стандарту качества тока в точке подключения к распределительной сети нагрузки и многофункционального сетевого инвертора на выходе возобновляемого источника электроэнергии. Методика. Синтез структуры контура регулирования тока на базе анализа процессов в электрических цепях с использованием компьютерного моделирования. Результаты. Получены зависимости амплитуды пульсаций выходного тока инвертора и ошибки по основной гармонике от напряжения на входе инвертора, частоты ШИМ и индуктивности реактора. Соотношения для определения значений входного напряжения инвертора, индуктивности реактора и частоты ШИМ в соответствии с напряжением сети, максимальными значениями тока инвертора и амплитуды его пульсаций при совмещении функции силового активного фильтра. Научная новизна. Усовершенствована структура контура регулирования тока инвертора с сочетанием пропорционального, интегрирующего и дифференцирующего звеньев и определены их параметры для обеспечения компенсации возмущающего действия по заданию и компенсации погрешности тока от возмущающего действия напряжения сети независимо от его значения. Практическое значение. Полученные решения являются основой для проектирования преобразователей для систем с возобновляемыми источниками электроэнергии и улучшенной энергоэффективностью. Библ. 10, рис. 7.

Ключевые слова: **многофункциональный сетевой инвертор, нелинейная нагрузка, ШИМ, контур регулирования тока, компенсация ошибки тока, коэффициент гармоник, моделирование.**

Introduction. The use of a renewable energy source (RES) implies the presence of a fairly complex and expensive conversion unit with an output grid-connected autonomous voltage inverter (AVI). Under natural conditions, the use of equipment for a photovoltaic solar cell does not exceed 20 % [1]. For local objects (small enterprise, cottage, mini-hotel, etc.) with power supply from the RES and the distribution grid (DG) of the alternating current, increasing the efficiency of the use of the conversion unit is achieved by the use of a multi-functional grid-connected AVI with a combined function of the power active filter (PAF) [1-9] thanks to its round-the-clock use to maintain the maximum (close to 1) power factor at the point of connection to the DG.

Typical solutions in the current control circuit (CCC) of the multi-functional AVIs are the use of a proportional-integral (PI) regulator [1, 3, 4], the

proportional-resonant regulator [1], the relay current regulator [1, 2], the regulator on the basis of the fuzzy-logic [5]. Solutions using PWM are More widespread [1, 3, 5-9]. The development of the CCC with the use of PWM is quite diverse. So, in [1, 5] the deviation Δi_C of the current i_C of the AVI relative to the given value i^*_C ($\Delta i_C = i^*_C - i_C$) is fed to the proportional-integral (PI) current regulator. Since its efficiency is insufficient, variants are given in [1], where to the output voltage of the current regulator they add the voltage proportional to the DG voltage u_1, or to the output of the current regulator through the corresponding elements they add voltages proportional to i^*_C, i_C and u_1.

The data above is not sufficient for perception and evaluation. For example, oscillograms of currents and indicators of circuits are given, but it is not indicated for which value (nominal, maximum, minimum). Structures are mostly declared, techniques for calculating parameters are absent. For a nonlinear load, the current i_C is non-sinusoidal, compensating for the distortion of the load current form i_L. For this, the DG current $i_1 = i_C - i_L$ contains the first harmonic, and higher (modulation) harmonics are suppressed by the filter. The operation error i^*_C leads to the appearance in the current i_1 of higher harmonics of low order and the deterioration of the harmonic composition of the current, especially for its relatively small values, as evidenced by the oscillograms given in [3, 4]. This complicates the issue of ensuring the correspondence the current harmonic composition to standards [10].

Consequently, the question of the implementation of the CCC of multi-functional grid-connected AVI has not been studied sufficiently and requires additional research.

The goal of the work is to eliminate the error of the inverter current control circuit by improving its structure and justification of the parameters that contributes to compliance with the current quality standard at the point of connection to the distribution grid of the load and the multifunctional grid-connected inverter at the output of the renewable energy source.

Main research materials. Consider the bridge circuit of the grid-connected AVI (Fig. 1) with the output *LC*-filter (C_f with insignificant R_f) at the point of connection to the AC grid with the voltage $u_1 = U_{1m}\sin\omega t$ and load. The input AVI circuit contains a solar cell (SC) with a voltage converter (VC) that supports a given voltage value U at the AVI input.

The operation of the AVI in parallel with the DG in the mode of the current source provides for the fulfillment of the condition $U = aU_{1m}$ (a>1) [6, 9]. The rate of change of the AVI output current di_C/dt in this case must exceed the maximum value for the current setting di^*_C/dt. In the case of the formation of a sinusoidal current, the maximum value $(di^*_C/dt)_{\max} = \omega I_{Cm\max}$ ($\omega = 2\pi f$ is the angular frequency, f = 50 Hz, $I_{Cm\max}$ is the amplitude for the maximum value $I_{C\max}$ of the AVI current). The value of di_C/dt is determined by the voltage at the AVI output reactor

$$u_L = u_C - u_1 = L\frac{di_C}{dt}, \qquad (1)$$

where u_C is the AVI voltage.

The least value of u_L takes place at $u_1 = U_{1m}$ and $U_L = U - U_{1m} = L\omega I_{Cm\max}$. From here $a > 1 + L\omega I_{Cm\max} / U_{1m}$.

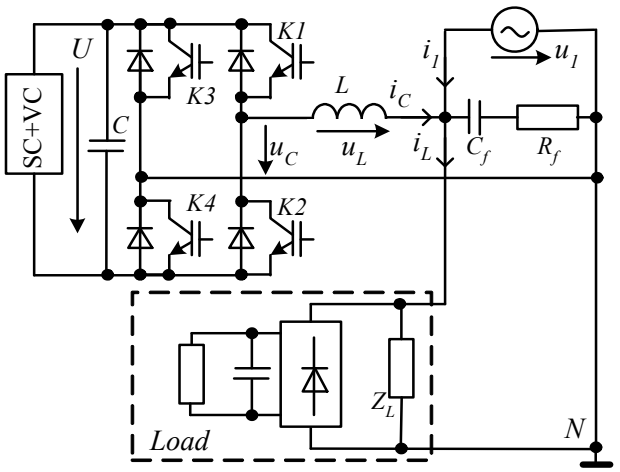

Fig. 1. The structure of the AVI power circles by connecting to grid and load

When combining the PAF function and operation on the nonlinear load, the AVI current shape is distorted, and the value of a determines the possibility of working out the maximum value $(di^*_C/dt)_{\max}$ without error. At non-sinusoidal i_L, harmonics with multiplicity i = 1, 3, 5, ... and the amplitude $I_{m(i)} = I_{m(1)}/i$ are added. For the approximate estimation, let's take into account the largest of them the 3rd harmonic. We accept $I_{m(1)} = I_{Cm\max}$, then

$$a = 1 + \frac{L\omega I_{Cm\max}}{U_{1m}} + \frac{3L\omega I_{Cm\max}}{3U_{1m}} = 1 + 2\frac{L\omega I_{Cm\max}}{U_{1m}}.$$

The inductance L of the AVI reactor according to the relative value of b of the voltage U_L (by the 1st harmonic) for the maximum AVI current $I_{C\max}$ $b = U_L / U_1 = \omega L I_{C\max} / U_1$ (where U_1 is the current value of the DG voltage), we determine as

$$L = \frac{bU_{1m}}{\omega I_{Cm\max}}. \qquad (2)$$

Accordingly, $a > 1 + 2b$.

The simplified structure of the CCC in accordance with (1) is shown in Fig. 2. The dotted line shows the compensation circuits. T_μ is the small uncompensated time constant of the AVI, which is determined by the frequency of PWM. The coefficients k, j, the compensating links of the DC and K are discussed further.

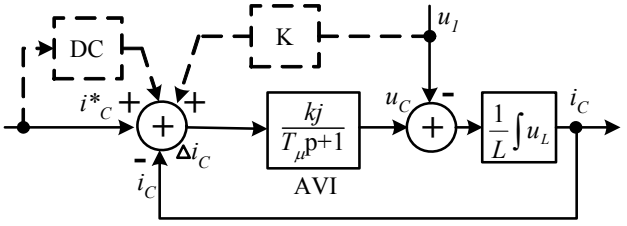

Fig. 2. Current control circuit of the AVI

According to Fig. 2, constantly acting disturbing influence, which causes the «static» error of current processing, is the voltage u_1, even at $i^*_C = 0$.

The typical nonlinear load of local objects is uncontrolled rectifiers (usually with an output capacitive

filter) in the office equipment and household appliances that use the pulsed current i_V. For this, during the switching of the diodes in the AVI current setting, which is determined taking into account the load current, we have the corresponding to i_V current change i^*_C (by a jump-like change in the derivative of the current i^*_C). At a limited frequency of PWM, these current changes are delayed, which results in the appearance of a «dynamic» error and distortion of the current shape of the DG. So, we have a disturbance on the control signal. This leads to a deterioration of the harmonious composition of the grid current, making it difficult to ensure its compliance with the standards for values $I_{1m} \le 0.25 I_{Cm\max}$.

Consider the implementation of PWM for the case when two reference voltages u_{TR} and $(-u_{TR})$ of a triangular shape with a modulation frequency f_M which are symmetric with respect to 0 are used (Fig. 3). Switching of the keys of the first arm (K1, K2) is carried out provided that the given voltage $u^* \ge u_{TR}$, and of the second one (K3, K4) – $u^* \le -u_{TR}$.

In the absence of regulators in the PWM block, the voltage, which is proportional to Δi_C, is compared with u_{TR}. In the case of the formation of positive half-wave of u_C, two voltage values U and 0 (for negative half-wave, respectively, $-U$ and 0) are used and the voltage u_L takes the value:

- if $u_C = U$, then the value $u_L = U - u_1 = L\dfrac{di_C}{dt}$ and the current i_C increases (the initial deviation Δi_C relative to the average value of Δi_{CAV} (error of current processing) is positive ($i^*_C > i_C$) and decreases to zero and then becomes negative ($i^*_C < i_C$)) (Fig. 3);

- if $u_C = 0$, then the value $u_L = 0 - u_1 = L\dfrac{di_C}{dt}$ and the current decreases (Δi_C increases to zero, and then becomes positive). Since f_M is large enough, it can be assumed that on the modulation interval T the voltage u_1 and current i^*_C are unchanged. Consequently, the current fluctuates relative to the given value and changes according to the linear law, the rate of its change depends on the values u_1 and u_C.

We assume that the current i_C and, accordingly, di_C/dt vary according to the harmonic law. The amplitude of current pulsations ΔI_{Cm} is determined by the coefficient of filling the pulses of the AVI voltage $\gamma = t_{on} / T$ (t_{on} is the key activation time, T is the modulation period) and does not depend on the current value. Therefore, we assume that the given value of the AVI current is zero. So, we have:

- at $u_1 \to 0$, the value $\gamma \to 0$, accordingly, $\Delta I_{Cm} \to 0$ (Fig. 3,*a*). For this, the mean value of the current deviation during the modulation period is $\Delta i_{CAV}(t) = 0$. The rates of growth and decrease of current are different, which in the case of $\gamma > 0$ leads to an increase $|\Delta i_{CAV}(t)| > 0$. That is, the mean value $|\Delta i_{CAV}(t)|$ gradually increases;

- the value $\gamma = 0.5$, when ΔI_{Cm} is the maximum (Fig. 3,*b*), meets the condition

$$aU_{1m} - U_{1m}\sin\omega t = |-U_{1m}\sin\omega t)|, \text{ and}$$

$$\Delta I_{Cm} = \Delta I_{Cm\max} = \frac{aU_{1m}}{16Lf_M}; \quad (3)$$

- at $u_1 = U_{1m}$, the value of γ is maximal (Fig. 3,*c*), it can be found under the condition that $\int_0^T u_L dt = 0$, or

$$U_{1m}(a-1)\gamma + U_{1m}(0-1)(1-\gamma) = 0.$$

Accordingly, $\gamma_{\max} = 1/a$ and

$$\Delta I_{Cm1} = \frac{\gamma(a-1)U_{1m}}{4Lf_M}. \quad (4)$$

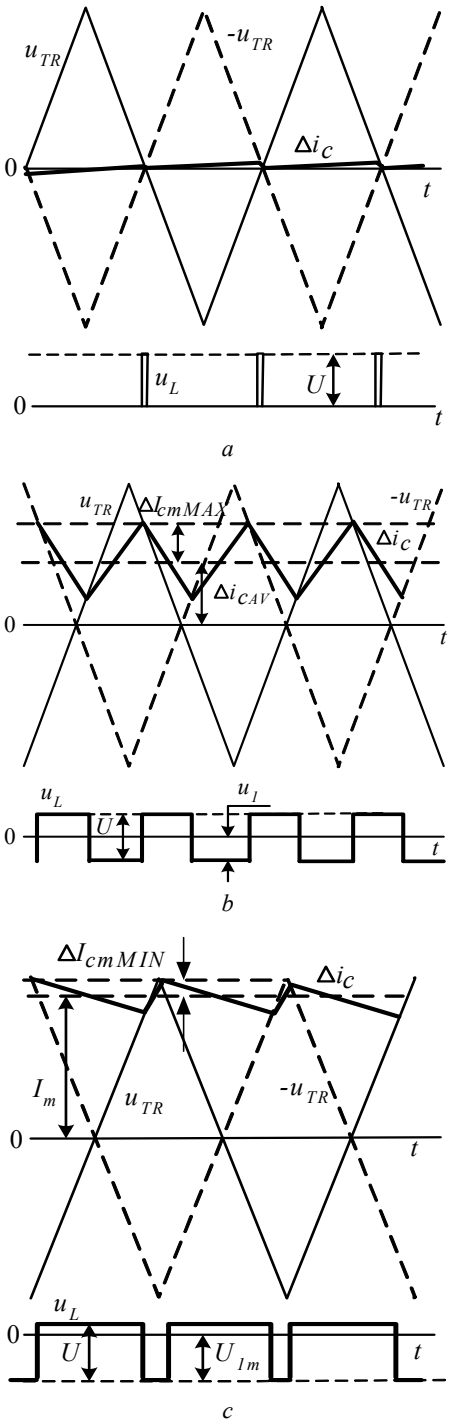

Fig. 3. Determination of amplitude of pulsations and error of current processing of the AVI with PWM

We take into account the relation of the rate of change of i_C and the reference voltage $\frac{du_{TR}}{dt} > \frac{di_C}{dt}$. The value $\frac{du_{TR}}{dt} = 4u_{TRm}f_M$. The maximum value di_C/dt takes place, when $u_L = 0 - U_{1m} = -U_{1m}$ and equal to $\frac{di_C}{dt} = \frac{U_{1m}}{L}$. So, $\frac{du_{TR}}{dt} = 4u_{TRm}f_M \geq \frac{U_{1m}}{L}$ (u_{TRm} – amplitude of u_{TR}), from here

$$f_M \geq \frac{U_{1m}}{4u_{TRm}L}. \quad (5)$$

Based on the condition $\int_0^T u_L dt = 0$, we can determine dependencies $\gamma(t)$ and $\Delta I_{Cm}(t)$. So, for $u_C > 0$ we have $U_{1m}(a - \sin\omega t)\gamma + U_{1m}(0 - \sin\omega t)(1 - \gamma) = 0$. From here

$$\gamma = \frac{\sin\omega t}{a}.$$

Current deviation amplitude $\Delta I_{Cm} = \frac{\gamma(1-\gamma)aU_{1m}}{2Lf_M}$. Taking into account the value of γ we obtain $\Delta I_{Cm}(t) = \frac{U_{1m}}{2aLf_M}(a\sin\omega t - 0.5 + 0.5\cos 2\omega t)$. For $u_C < 0$ we have the same situation. So,

$$\Delta I_{Cm}(t) = \frac{U_{1m}}{2aLf_M}(|a\sin\omega t| - 0.5 + 0.5\cos 2\omega t),$$

$$\Delta i_{CAV}(t) = \frac{u_{TRm}}{a}\sin\omega t.$$

The boundary is the mode where the current error amplitude I_m approaches u_{TRm} and $\Delta I_{Cm1} = 0$ at $a = 1$. In general, it is necessary to fulfill the condition

$$I_m + \Delta I_{Cm1} \leq u_{TR}. \quad (6)$$

Otherwise there is an additional (superfluous) switching of the keys of the inverter.

The amplitude u_{TRm} can be determined according to (5), then the amplitude of the fundamental harmonic of the current error, accordingly to (4) and (6) $I_m \leq \frac{U_{1m}}{a4Lf_M}$, or

$$I_m \leq \frac{u_{TRm}}{a}. \quad (7)$$

Values ΔI_{Cm} at $\gamma = 0.5$ and $\gamma_{\max}$ are, respectively, $\Delta I_{Cm\max} \leq \frac{a}{4}u_{TRm}$, $\Delta I_{Cm1} = \frac{(a-1)}{a}u_{TRm}$.

Let's turn to relative value $\Delta I_{Cm\max}$ (to the amplitude $I_{Cm\max}$) $c = \frac{\Delta I_{Cm\max}}{I_{Cm\max}}$, then accordingly to (2), (3)

$$f_M \geq \frac{a\omega}{16bc}. \quad (8)$$

So, for example, at $b = 0.15$, $c = 0.05$, $a = 1.3$ values $I_m = 0.77u_{TRm}$, $\Delta I_{Cm\max} = 0.325u_{TRm}$, $\Delta I_{Cm1} = 0.23u_{TRm}$. If $I_{C\max} = 25$ A ($I_{Cm\max} = 35.35$ A), the modulation frequency by (8) $f_M = 3400$ Hz, then $\Delta I_{Cm\max} = 1.77$ A. Here $I_m = \frac{4}{a^2}\Delta I_{Cm\max} = 4.19$ A.

To reconcile the scale of the quantities in the direct channel of deviation, coefficients are introduces (Fig. 2): $k = \frac{a}{4\Delta I_{Cm\max}}$ (without taking into account transmission coefficients of sensors and $u_{TRm} = 1$) and $j = U/u_{TRm}$.

Without taking into account the modulation components, the «smooth» component of the reactor voltage according to (1)

$$u^1L = u^1C - u_1 = L\frac{di^1C}{dt} = ju_K - u_1$$ (u_K is the control voltage varying within ($-u_{TRm}$, u_{TRm}), $u^1{}_C$, $i^1{}_C$ are the voltage and current without taking into account modulation components). From here $u_K = \frac{L}{j}\frac{di^1C}{dt} + \frac{u_1}{j}$. Error $\Delta i_{CAV} = 0$ provided that $i^*{}_C = i^1{}_C$, respectively, $\frac{di^*C}{dt} = \frac{di^1C}{dt}$. From here

$$u_K = \frac{L}{J}\frac{di^*{}_C}{dt} + \frac{u_1}{j}. \quad (9)$$

In the case $i^*{}_C = 0$, the value $u_K = u_1/j$. The voltage u_1 is measurable and the static error can be compensated by the introduction of the corresponding connection (link K in Fig. 2).

The exclusion of the current error caused by the perturbation by the control signal is possible using the differential link of dynamic compensation (DC) according to (9) in the AVI current assignment channel.

In real conditions, U_1 varies in certain limits. With the change of U_1 at constant f_M (8) $b' = b/U_1{}^*$ ($U_1{}^* = U_1/U_{1N}$, where U_{1N} is the nominal voltage), $a' = a/U_1{}^*$, $c' = \frac{a'bc}{b'a}$, which requires readjustment of the CCC. Another version of the compensation of static error is the introduction of the integrative link (Fig. 4) with the coefficient $g = f_M/k$, which calculates the actual value of $\Delta i_{CAV}(t)$ and adds it to the signal of deviation of current.

The proposed structure of the CCC of the AVI (Fig. 4) contains final devices, a proportional link with coefficient k, an integrative link, multipliers, a block of comparators BC, a generator of reference voltage GRV, a block of phase auto-adjustment of frequency PLL, a link of dynamic compensation DC. According to the signal of the setting of the amplitude of the current of the grid $I^*{}_{1m}$ from the output of the external voltage regulator OR (it supports the voltage at the AVI input at a given level $U = U^*$) a sinusoidal signal of the grid current setting $i^*{}_1$ is formed, which, when generating energy of the SC to the grid is shifted relative to voltage u_1 by 180°, and in the case of power consumption from the grid coincides by the phase. The AVI current setting is determined taking into account i_L and the capacitive current component of the filter with the amplitude $I_{fm(1)} = \omega C_f U_{1m}$. PLL according to the DG voltage $u_1 = U_{1m}\sin\omega t$ and the given value of the angular frequency ω_0 forms signals $\sin\omega t$, $\cos\omega t$.

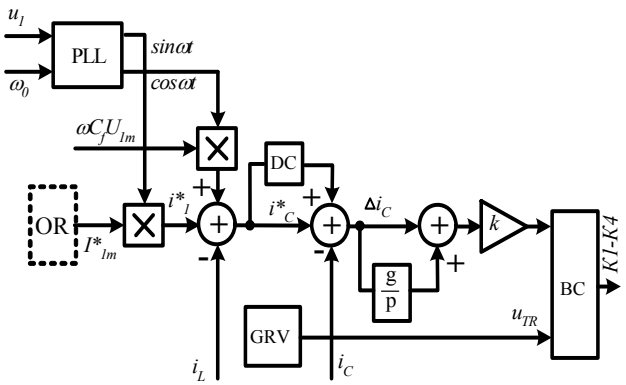

Fig. 4. CCC structure

Simulation in Matlab and its results. It made with combination of nonlinear load (uncontrolled rectifiers with output capacitance filter and *RL*-load) and *RL*-load ($I_{Lm(1)}$ = 19.6 A, $\varphi_{(1)}$ = 27°). The DG contains the resistances R = 0.02 Ω, X_L = 0.02 Ω. Reactor with L = 0.0042 H and R = 0.1 Ω, R_f = 0.3 Ω, C_f = 60μF. AVI parameters: $I_{C\max}$ = 25 A, f_M = 6800 Hz, U = 405 V (a = 1.3).

Three variants of CCC are considered: variant 1 – with DC and compensatory connection by u_1; variant 2 – with DC and the integrating link; variant 3 – using PI-regulator with adjustment on the symmetric optimum

$$W(p)=\frac{4L}{8KT_\mu}+\frac{L}{8KT_\mu^2 p}\left(T_\mu=1/f_M,\ K=k\cdot j\right).$$

Variant 3 at nonlinear load is operational only with DC and compensating link by u_1 and has the worst performance at small DG current values.

For example, in the case of I^*_{1m} = 3 A, the value $I_{1m(1)}$ = 2.973 A, THDi_1 = 4.79 %. Under the same conditions for variant 1 $I_{1m(1)}$ = 2.943 A, THDi_1 = 3.41 %, for variant 2 $I_{1m(1)}$ = 2.966 A, THDi_1 = 2.68 %. In addition, variant 2 has the best DG current spectrum (Fig. 5) and provides THD$i_1 \le 5$ % in the range of values of I_{1m} up to 0.05 $I_{1m\max}$ ($I_{1m\max}$ in this case is 35.35 A). In the case of change of u_1, variant 2 does not need to be readjusted, so by U^*_1 = 0.85 at I^*_{1m} = 3 A, $I_{1m(1)}$ = 2.97 A, THDi_1 = 2.5 %. In variant 1, under the same conditions, $I_{1m(1)}$ = 3.3 A, THDi_1 = 2.83 %, which implies a change in the coefficient in the link K (Fig. 2).

Oscillograms of u_1, u_C, i_1, $\Delta I_{Cm}(t)$ at the linear load with the DC are shown in Fig. 6. Oscillograms of u_1, u_C, i_1, i_C, i_L for I^*_{1m} = 3 A at the combined linear and nonlinear load (rectifiers with capacitive filter and *RL*-load) for variant 2 are shown in Fig. 7 (I^*_{1m} = 3 A, $I_{1m(1)}$ = 2.97 A, THDi_1 = 2.97 %).

For comparison in [3] with use in the CCC of the PI-regulator at f_M = 20 kHz, I_{1m} = 10 A (I_{Cm} = 20 A, current amplitude of the nonlinear load I_{Lm} = 9 A), the value of THDi_1 = 4.8 %.

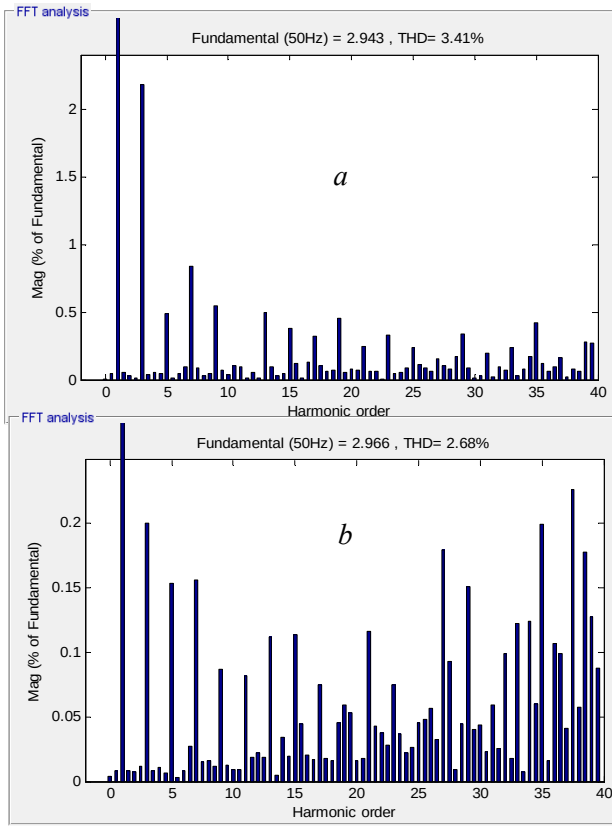

Fig. 5. DG current spectra: *a* – variant 1; *b* – variant 2

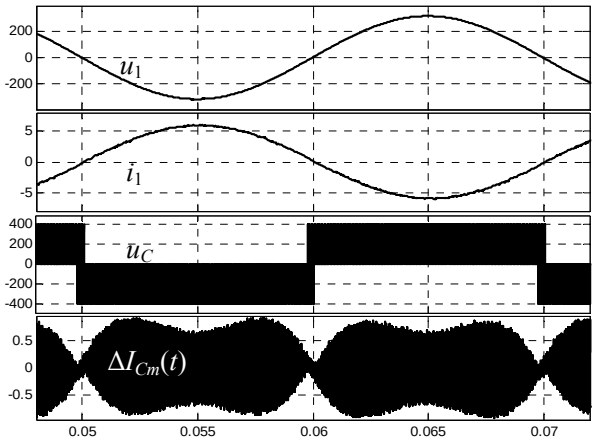

Fig. 6. Oscillograms of voltage and currents at linear load

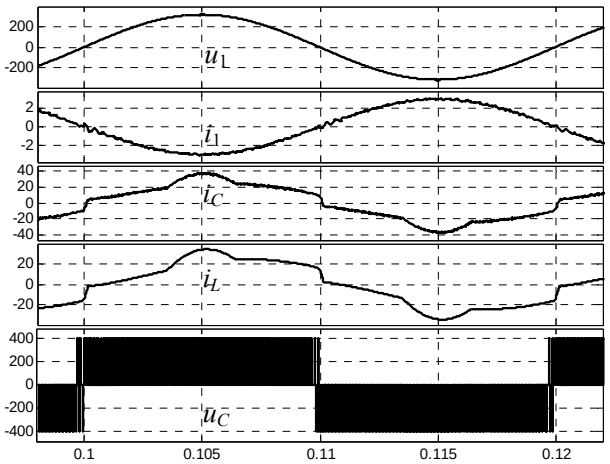

Fig. 7. Oscillograms of voltage and currents at combined load

Conclusions.

Based on the received dependencies of the amplitude of the pulsations of the AVI output current and the fundamental harmonic error according to the voltage at the AVI input, the PWM frequency and the inductance of the output reactor, the parameters of the links to compensate for disturbing influences are justified. It is shown that the compensation of the perturbation of the DG voltage using in the channel of the current deviation of the integral link does not require readjustment in the event of a change in the voltage of the grid. The proposed structure of the CCC of the multifunctional AVI with a combination of proportional, integrative and differential links with their respective parameters allows for a limited value of PWM frequency of 6800 Hz to expand the range of current values i_1 at the point of connection to the grid in the direction of lower values up to 0.05 from the maximum current value at the value of THD$i_1 \leq 5$ % In this case, the value of the inverter voltage and the PWM frequency are determined according to the DG voltage, the reactor inductance, the maximum values of the AVI current and the amplitude of its pulsations. The results are obtained for relative values: amplitude of current pulsations $c = 0.0025$, the voltage drop on the reactor at the maximum current (for the 1st harmonic) $b = 0.15$ and $a = 1.3$. A further direction of work is the development of a model for researching the AVI operation, taking into account the discreteness of the operation of the digital control system, to clarify the requirements for its elements and to assess real indicators.

REFERENCES

1. Zeng Z., Yang H., Zhao R., Cheng C. Topologies and control strategies of multi-functional grid-connected inverters for power quality enhancement: A comprehensive review. *Renewable and Sustainable Energy Reviews*, 2013, vol.24, pp. 223-270. **doi: 10.1016/j.rser.2013.03.033.**

2. Vaquero J., Vázquez N., Soriano I., Vázquez J. Grid-Connected Photovoltaic System with Active Power Filtering Functionality. *International Journal of Photoenergy*, vol. 2018, pp. 1-9. **doi: 10.1155/2018/2140797.**

3. Da Silva S.A.O., Sampaio L.P., Campanhol L.B.G. Single-phase grid-tied photovoltaic system with boost converter and active filtering. *2014 IEEE 23rd International Symposium on Industrial Electronics (ISIE)*, Jun. 2014. **doi: 10.1109/isie.2014.6865013.**

4. Denizar C. Martins, Kleber C. A. de Souza. A single-phase grid-connected PV system with active power filter. *International journal of circuits, systems and signal processing*, 2008, iss.1, vol.2, pp. 50-55.

5. Vigneysh T., Kumarappan N. Grid interconnection of renewable energy sources using multifunctional grid-interactive converters: A fuzzy logic based approach. *Electric Power Systems Research*, 2017, vol.151, pp. 359-368. **doi: 10.1016/j.epsr.2017.06.010**.

6. Shavelkin A., Shvedchykova I. Multifunctional converter for single-phase combined power supply systems for local objects with a photovoltaic solar battery. *Technical electrodynamics*, 2018, no.5, pp. 92-95. **doi: 10.15407/techned2018.05.092**.

7. Wu T.-F., Nien H.-S., Shen C.-L., Chen T.-M. A Single-Phase Inverter System for PV Power Injection and Active Power Filtering With Nonlinear Inductor Consideration. *IEEE Transactions on Industry Applications*, 2005, vol.41, no. 4, pp. 1075-1083. **doi: 10.1109/tia.2005.851035**.

8. Mendez I., Vazquez N., Vaquero J., Vazquez J., Hernandez C., Lopez H. Multifunctional grid-connected photovoltaic-system controlled by sliding mode. *IECON 2015 – 41st Annual Conference of the IEEE Industrial Electronics Society*, Nov. 2015. **doi: 10.1109/iecon.2015.7392286**.

9. Shavelkin A.A. Structures of single-phase converters units for combined electrical supply systems with photoelectric solar panels. *Technical electrodynamics*, 2018, no.2, pp. 39-46. (Rus). **doi: 10.15407/techned2018.02.039.**

10. *1547-2018 – IEEE Standard for Interconnection and Interoperability of Distributed Energy Resources with Associated Electric Power Systems Interfaces*. Date of Publ. 6 April 2018. **doi: 10.1109/IEEESTD.2018.8332112**.

Received 07.02.2019

O.O Shavelkin[1]*, Doctor of Technical Science, Professor,*
V.V. Kaplun[1]*, Doctor of Technical Science, Professor,*
I.O. Shvedchykova[1]*, Doctor of Technical Science, Professor,*
[1] Kyiv National University of Technologies and Design,
2, Nemirovich-Danchenko Str., Kyiv, 01011, Ukraine,
phone +380 50 9720629,
e-mail: shavolkin@gmail.com, ishved89@gmail.com

How to cite this article:
Shavelkin O.O, Kaplun V.V., Shvedchykova I.O. Error elimination for current control loop for multi-functional single-phase grid-connected inverter. *Electrical engineering & electromechanics*, 2019, no.4, pp. 35-40. **doi: 10.20998/2074-272X.2019.4.05.**

UDC 621.3.022: 621.315.3: 537.311.8 **doi: 10.20998/2074-272X.2019.4.06**

M.I. Baranov

PECULIARITIES OF THE MANIFESTATION AND INFLUENCE ON THE ELECTROMAGNETIC PROCESSES OF THE TRANSIENT SKIN EFFECT IN METAL CONDUCTORS WITH PULSED CURRENT

Purpose. ***Preparation of brief scientific review of basic results of the known theoretical researches of the electrophysics phenomenon of linear transient skin effect (TSE) in the non-magnetic homogeneous massive conductors of flat and cylindrical configurations on which in the discharge electric circuits of high-voltage electrophysical installations (EPHI) the pulsed currents $i_p(t)$ flow with given amplitude-temporal parameters (ATPs).*** ***Methodology.*** ***Theoretical bases of electrical engineering, bases of theoretical electrophysics, electrophysics bases of technique of high-voltage and high pulsed currents.*** ***Results.*** ***The brief scientific review of results of the known theoretical researches of the electrophysical phenomenon of linear TSE in non-magnetic homogeneous massive flat and cylindrical metal conductors with pulsed axial (azimuthal) current $i_p(t)$, formed in the discharge circuit of powerful high-voltage EPHI. In the generalized and systematized form the basic features of manifestation of linear TSE in the indicated conductors and influence of the considered skin effect on electromagnetic processes are presented at flow in conductors and discharge circuit of a high-voltage EPHI with the pulsed current $i_p(t)$ time-varying by law of attenuated sinewave. Influence of linear TSE is described in non-magnetic massive conductors during transient in a discharge circuit of EPHI with the pulsed current $i_p(t)$ of given ATP, depth of penetration of the electromagnetic field in materials of the indicated conductors, own integral electric parameters of the considered conductors and their good quality in the high-current discharge circuit of high-voltage EPHI. It is shown that at the analysis of electromagnetic transients in high-current discharge electric circuits of powerful high-voltage EPHI it is necessary to take into account flowing in materials of the examined massive conductors of such known electrophysical phenomenon as linear TSE.*** ***Originality.*** ***Generalization and systematization is first executed regarding domestic and foreign scientists-electrical engineers' results of theoretical researches for long-term period of the electrophysics phenomenon of linear TSE in the flat and cylindrical metallic conductors of different thickness with the pulsed current $i_p(t)$of given ATP.*** ***Practical value.*** ***The results presented in the generalized and systematized form will be useful for electrical engineers in deepening of understanding of basic features of manifestation in non-magnetic massive homogeneous conductors with the pulsed current $i_p(t)$ of given ATP of such widely widespread in area of high-voltage high-current pulsed technique electrophysics phenomenon as linear TSE and its influences on electromagnetic transients in similar metallic conductors and high-current discharge circuits of high-voltage EPHI.*** References 28, figures 2.

Key words: **metal conductors, pulsed current, linear transient skin effect, features of the manifestation of linear skin effect in conductors and its influence on electromagnetic processes.**

Приведений короткий огляд результатів відомих теоретичних досліджень електрофізичного явища лінійного нестаціонарного поверхневого ефекту (НПЕ) в немагнітних однорідних масивних плоских і циліндричних металевих провідниках з імпульсним аксіальним (азимутним) струмом, що формується в розрядному колі високовольтної електрофізичної установки (ЕФУ). ***У узагальненому і систематизованому вигляді представлені основні особливості прояву лінійного НПЕ у вказаних провідниках і впливу даного скін-ефекту на електромагнітні процеси, що протікають в провідниках і розрядному колі ЕФУ з імпульсним струмом, що змінюється в часі за законом затухаючої синусоїди.*** ***Описаний вплив лінійного НПЕ на тривалість перехідного процесу в розрядному колі ЕФУ, глибину проникнення електромагнітного поля в матеріал провідників, власні електричні параметри провідників і їх добротність в розрядному колі ЕФУ.*** Бібл. 28, рис. 2.

Ключові слова: **металеві провідники, імпульсний струм, лінійний нестаціонарний поверхневий ефект, особливості прояву лінійного скін-ефекту в провідниках і його впливу на електромагнітні процеси**.

Приведен краткий обзор результатов известных теоретических исследований электрофизического явления линейного нестационарного поверхностного эффекта (НПЭ) в немагнитных однородных массивных плоских и цилиндрических металлических проводниках с импульсным аксиальным (азимутальным) током, формируемым в разрядной цепи высоковольтной электрофизической установки (ЭФУ). ***В обобщенном и систематизированном виде представлены основные особенности проявления линейного НПЭ в указанных проводниках и влияния рассматриваемого скин-эффекта на электромагнитные процессы, протекающие в проводниках и разрядной цепи ЭФУ с импульсным током, изменяющимся во времени по закону затухающей синусоиды.*** ***Описано влияние линейного НПЭ на длительность переходного процесса в разрядной цепи ЭФУ, глубину проникновения электромагнитного поля в материал проводников, собственные электрические параметры проводников и их добротность в разрядной цепи ЭФУ.*** Библ. 28, рис. 2.

Ключевые слова: **металлические проводники, импульсный ток, линейный нестационарный поверхностный эффект, особенности проявления линейного скин-эффекта в проводниках и его влияния на электромагнитные процессы.**

Introduction. In high-voltage high-current pulse technology, electrophysical installations (EPHI) have been widely used, which are designed to achieve various scientific and electrotechnological goals in practice [1-6]. In this case, non-metallic and insulated conductors are

commonly used in electric power circuits of such EPHI, the current-carrying parts of which contain non-magnetic conductors made of materials with high electrical conductance γ_C (for example, copper and aluminum) and through which pulsed currents $i_p(t)$ with different amplitude-temporal parameters (ATPs). The sources of generation in EPHI circuits of pulsed axial (longitudinal) and azimuthal (circular) currents $i_p(t)$, as a rule, are powerful capacitive (CES) or inductive (IES) energy storages [1-3]. Considering the physical nature of the formation and flow of a pulsed current $i_p(t)$ in conducting media, in these materials of conductors of discharge circuits of EPHI with CES (IES), transient skin effect (TSE) appears, the study of which was given quite a lot of attention [2, 7-19]. Nevertheless, today there are practically no publications in the scientific world devoted to the generalization and systematization of the results of theoretical studies of the phenomenon of TSE in metal conductors with a pulsed current $i_p(t)$ of various ATPs for many years obtained by domestic and foreign scientists in the area of electrical engineering. Therefore, the preparation at the first stage of even a brief overview of the main publications on TSE in conductors is of scientific and practical interest. We also indicate that the available foreign publications (for example, [20-22]) are mainly devoted to the study of the stationary skin effect in metallic conductors. In this regard, the preparation of a brief review of well-known works on the phenomenon of TSE in conductors of EPHI with a pulse current $i_p(t)$, containing the main results of its manifestation and influence on the electromagnetic processes occurring in them and in the discharge circuits of EPHI, is an important task.

The goal of the paper is performing a brief scientific review of the main results of the well-known theoretical studies of the electrophysical phenomenon of linear TSE in nonmagnetic homogeneous massive conductors of flat and cylindrical configurations, along which pulsed currents $i_p(t)$ with given ATPs flow in the discharge electric circuits of high-voltage high-current EPHIs.

1. Problem definition. Consider non- and insulated solid non-magnetic homogeneous conductors with flat (Fig. 1) or cylindrical configuration (Fig. 2) [2, 13] that are widely used in high-voltage EPHIs. We assume that for the considered conductors with thickness h or b (see Fig. 1, 2), inequalities of the form $h/\Delta_C>>1$ and $b/\Delta_C>>1$ are satisfied, where $\Delta_C=[2/(\omega_p\mu_0\gamma_C)]^{1/2}$ is the penetration depth in the stationary (steady-state) mode of the external electromagnetic field with the circular frequency ω_p in time t into the conductor material with electrical conductance γ_C, and $\mu_0=4\pi\cdot10^{-7}$ H/m is the magnetic constant [2]. In this regard, a sharp manifestation of the skin effect takes place in the indicated conductors of the discharge circuit of the EPHI, and the conductors can be considered massive [2, 9, 13]. The cases when $h/\Delta_C\le1$ and $b/\Delta_C\le1$ are atypical for conductors used in high-current discharge circuits of the EPHI, and therefore they are not of particular interest.

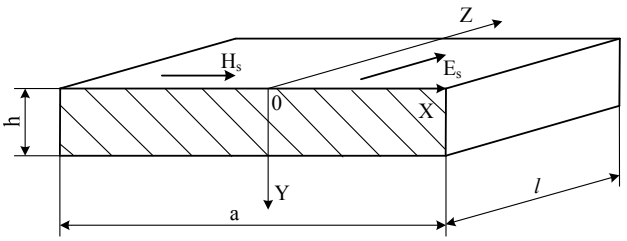

Fig. 1. Flat massive non-insulated metal conductor with pulsed axial electric conduction current $i_p(t)$ flowing along its longitudinal axis OZ (E_S, H_S are, respectively, the strength of the pulsed electric and magnetic fields on the outer flat surface of the conductor) [13]

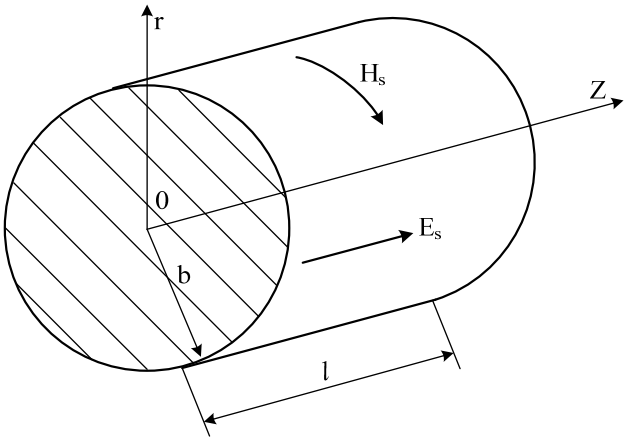

Fig. 2. Cylindrical massive non-insulated metal conductor with pulsed axial electric conduction current $i_p(t)$ flowing along its longitudinal axis OZ (E_S, H_S are, respectively, the strength of the pulsed electric and magnetic fields on the outer cylindrical surface of the conductor) [13]

We believe that the electrical conductance γ_C of the material of the conductors is almost the same in time t value, and the linear dimensions of the conductors (their length l and width a) significantly exceed their thickness h or radius b. The displacement currents in the Maxwell equations for the studied conductors are neglected [2, 12]. Let in considered conductors along their longitudinal axes OZ only pulsed conduction currents $i_p(t)$ with arbitrary ATPs flow. It is required, based on the published results of investigations of linear TSE in the considered non-magnetic homogeneous massive metal conductors of the discharge circuit of the EPHI with pulsed current $i_p(t)$ of specified ATPs, to formulate in generalized and systematic form the main features of the specified skin effect manifestation and its influence on the electromagnetic processes occurring in the material of conductors and discharge electric circuit of the EPHI.

2. The main features of the manifestation of linear TSE in massive conductors with pulsed current. We confine ourselves to the case typical for high-power high-voltage EPHI, when the pulsed current $i_p(t)$ in the

studied conductors changes in time t according to the law of a damped sinusoid and is described by the well-known relation of the form [9, 13]:

$$i_p(t) = k_p I_{mp1} \exp(-\delta_p t) \sin(\omega_p t) , \qquad (1)$$

where I_{mp1}, δ_p, ω_p are, respectively, the first amplitude, attenuation coefficient and circular frequency of oscillations of the pulsed current in the discharge electric circuit of the EPHI; $k_p=[\exp(-\delta_p/\omega_p \cdot \text{arcctg}\delta_p/\omega_p)\times \times\sin(\text{arcctg}\delta_p/\omega_p)]^{-1}$ is the normalization factor ($k_p \geq 1$).

The temporal dependence (1) for the current $i_p(t)$ makes it possible to establish the main and characteristic features of the space-temporal distributions of the strengths of the pulsed electromagnetic field in the materials of the studied massive conductors and their influence on the electrical parameters of the conductors, as well as on the behavior of transient electromagnetic processes in the discharge circuits of high-voltage EPHIs.

2.1. Features of the distribution of the strength of a pulsed electric field in the material of conductors. The data of analytical solutions of linear diffusion problems for penetration into a cylindrical tubular metal conductor, often used in the discharge circuit of EPHI with a pulse current $i_p(t)$ of a temporary form (1), the strengths of a pulsed axial E_Z and azimuthal E_θ electric fields given in [14, 15] makes it possible to formulate the following main features of the manifestation of linear TSE in the specified conductor:

- the first amplitude of the strength E_Z of the pulsed axial electric field in the outer layers of the massive conductor wall is significantly less than the corresponding strength characteristic of the steady-state (stationary) electromagnetic process in the conductor material. For the outer surface of a massive conductor, this discrepancy between the non- and stationary modes of penetration of this field is approximately 33 %;
- the amplitude of the first half-wave E_θ of the pulsed azimuthal electric field strength on the outer surface of the massive conductor wall is approximately 31 % less than in the stationary mode of penetration of a similar field into it;
- the strengths E_Z and E_θ of the pulsed electric field on the outer surface of the massive conductor wall are characterized by an increased slew rate on the frontal parts of their first half-waves, the duration of which turns out to be significantly less (from 30 to 35 %) to the duration of the next half-waves of this field change;
- the strengths E_Z and E_θ of the pulsed electric field faster become steady in the inner layers of the wall of a non-magnetic massive conductor with pulsed axial or azimuthal current;
- full attenuation in the material of the massive conductor of the indicated strengths E_Z and E_θ of the pulsed electric field occurs almost at the depth of its wall, approximately equal to $5\Delta_C$.

2.2. Features of the distribution of the strength of a pulsed magnetic field in the material of conductors. The results of a linear TSE study in the specified massive cylindrical conductor, presented in [14, 15], indicate that:

- the first amplitude of the strength H_θ of the pulsed azimuthal magnetic field across the entire wall thickness of the massive conductor in the transient penetration mode is much larger than in the stationary one. This discrepancy in the values of the strength H_θ for the inner layers of the wall of the conductor considered reaches up to 35 %;
- the first half-waves of the strengths H_θ и H_Z of the pulsed magnetic field as it penetrates into the inner layers of the wall of a non-magnetic massive conductor undergo a considerable attenuation in amplitude and change in shape. There is a smoothing of their frontal parts and a shift of their amplitude values towards longer times;
- the first amplitude of the strength H_Z of the pulsed axial field into the inner layers of the conductor wall is approximately 32 % higher than its corresponding values, determined from the condition of the steady-state (stationary) electromagnetic mode of its penetration into the conductor material;
- the strengths H_θ and H_Z of the pulsed magnetic field faster become steady in the outer layers of the wall of the massive conductor with pulsed current;
- full attenuation in the non-magnetic material of the massive conductor of the indicated strengths H_θ and H_Z of the pulsed magnetic field practically occurs at a depth of its wall equal to about $5\Delta_C$.

3. Main features of the influence of linear TSE in massive conductors with pulsed current on the electromagnetic processes in them and in the discharge electric circuit of the EPHI. Based on presented in [2, 8-10, 12-19] the results of studies of linear TSE in flat and cylindrical conductors with pulse current $i_p(t)$ varying in time t according to (1), it can be concluded that its (skin effect's) the main effects are as follows.

3.1. The effect on the duration of the transient in the discharge electric circuit of the EPHI. Analysis of the obtained data for linear TSE in massive conductors with pulsed axial (azimuthal) current $i_p(t)$ of the form (1) indicates that the transient process of becoming steady of the strengths of the pulsed electromagnetic field in their non-magnetic homogeneous (isotropic) material lasts almost one and a half period T_p (no more than $3\pi/\omega_p$) of changes of the external field generated by the considered discharge current of the EPHI near their outer surfaces. This circumstance is clearly indicated by the results of studies in [9, 16] of pulsed penetration of plane electromagnetic waves into a flat non-magnetic massive wall of a tubular conductor of unlimited radial dimensions, as well as by theoretical data from [14, 15] on the study of linear TSE in a non-conductive cylindrical tubular conductor with arbitrary wall thickness with

pulsed axial or azimuthal current $i_p(t)$ of a temporary form (1). Therefore, the duration of the transient electromagnetic process in the discharge circuit of a high-voltage EPHI with massive metal conductors (tires), due to transient diffusion in their walls of the external pulsed electromagnetic field strengths with an oscillation period T_p, practically does not exceed the value $1{,}5 \cdot T_p = 3\pi/\omega_p$.

3.2. The effect on the depth of penetration of the electromagnetic field into the material of conductors. As is known, to calculate the depth of penetration Δ_N in the transient (unsteady) mode of the external pulsed electromagnetic field into the considered non-magnetic massive homogeneous conductors of the discharge circuit of the EPHI, the following analytical relation can be used [13, 23]:

$$\Delta_N = H_S /(\gamma_C E_S), \qquad (2)$$

where E_S, H_S are, respectively, the strengths of the pulsed electric and magnetic fields on the outer surface of a flat (cylindrical) conductor (see Fig. 1, 2), the non-ferromagnetic material of which has a constant electrical conductance γ_C.

Knowing in (2) the temporal dependencies of the surface strengths E_S and H_S of the pulsed electric and magnetic fields for the considered flat and cylindrical conductors included in the discharge circuit of EPHI with time-varying in t according to the law (1) the pulsed axial (azimuthal) current $i_p(t)$, it is relatively easy to determine the desired penetration depth Δ_N for transient process of diffusion of the external pulsed electromagnetic field into their walls and is compared with the known classical penetration depth Δ_C characteristic of the steady-state (stationary) field diffusion mode.

From the analysis of the results obtained in [13, 23], it follows that in the area of the first half-wave of a pulsed damped sinusoidal axial current $i_p(t)$ according to (1) (δ_p/ω_p=0,3; ω_p=666,58 kHz; T_p=9,42 μs) flowing through a round solid copper tire (b=2,5 mm; $\gamma_C=5{,}81 \cdot 10^7$ S/m; Δ_C=0,202 mm; b/Δ_C=12,37) of the radio frequency cable brand PK 75-33-17 [24], the value of the depth of penetration Δ_N of the field into this core for the transient mode, compared with the value of the depth of penetration Δ_C into it of a similar field for the stationary mode, is approximately 37 % larger. For the area of the second half-wave of the pulsed electromagnetic field penetrating into a cylindrical tire, the value of Δ_N becomes 19 % less than the value of Δ_C characteristic of the stationary mode of penetration of the external electromagnetic field into the specified massive conductor. In the area of the third half-wave of the investigated type of electromagnetic field, the ratio Δ_N/Δ_C approaches almost 1. Therefore, for the analyzed case, the depth of penetration Δ_N of the pulsed electromagnetic field into the massive cylindrical conductor varies most noticeably in the interval of the first two half-waves of this field or the pulsed current $i_p(t)$ described by (1).

The above feature for the temporal distribution of Δ_N allows to explain from electrophysical positions the nature of the value of the intensity E_{ZS} of the pulsed axial electric field on the outer surface of the massive cylindrical conductor during a transient in the discharge circuit of the EPHI (see subsection 2.1). It is a mentioned increase in Δ_N (by about 37 %) in the first half-wave area of the penetrating pulsed electromagnetic field, in transient mode, by reducing the instantaneous value of active resistance R_N of the current skin layer in the massive cylindrical conductor, results in a corresponding decrease (approximately by 33 %) in the first half-wave amplitude of the surface strength E_{ZS} of the pulsed axial electric field (respectively, also the drop of the pulsed electric voltage on this conductor [25]) by comparing to its value in the steady state diffusion mode of similar alternating field into the consideration conductor. In the area of the second half-wave of the discharge current $i_p(t)$ of the form (1), the decrease in Δ_N (by about 19 %) results, due to an increase in the instantaneous value of the active resistance R_N of the current skin layer in the massive cylindrical conductor, in a corresponding increase in the transient penetration mode into it of the analyzed field of the specified amplitude of the strength E_{ZS} of the axial electric field on the outer surface of the conductor.

Therefore, it can be stated that the nature of the penetration mode (transient or steady state in the electrodynamic sense) into the indicated massive flat and cylindrical conductors of the discharge circuit of the EPHI of the external electromagnetic field significantly affects the calculation of its penetration depth into their non-magnetic materials.

3.3. Influence on the intrinsic electrical parameters of the conductors of the discharge circuit of the EPHI. The values of active resistances R_{Na} and internal inductances L_{Na} (external inductances determined by the geometry of the conductors and not dependent on the electrodynamic mode of current propagation in them, are not considered) for non- and massive flat and cylindrical conductors, averaged over an arbitrary time interval $[t_s, t_e]$ used in the discharge circuits of high-voltage EPHIs with pulse current $i_p(t)$, can be represented in a generalized electrical engineering form [26, 27]:

$$R_{Na} = k_R R_0; \qquad (3)$$

$$L_{Na} = k_L L_0, \qquad (4)$$

where R_{Na}, L_{Na} are, respectively, the active resistance and internal inductance of the conductor, taking into account the influence of the apparent TSE in them; R_0, L_0 are, respectively, the known values of active resistance and internal inductance of a conductor when DC flows through it [2, 28]; k_R, k_L are the dimensionless coefficients that take into account the influence of the transient mode of penetration of the external electromagnetic field into the conductor material, respectively, on the values of its active resistance and internal inductance.

It is interesting to note that according to data from [26, 27] for a non-massive continuous cylindrical conductor of radius b with pulsed axial current $i_p(t)$ of the form (1) with $b/\Delta_C \leq 1$, the coefficients k_R and k_L in (3), (4) become equal to 1 and its pulsed electrical parameters R_{Na} and L_{Na} take values characteristic of DC in it. This circumstance, corresponding to the well-known provisions of theoretical electrophysics [2, 6], may additionally indicate the reliability of both the approach used in [26, 27] and the results obtained on its basis for the electrical parameters of the studied conductors with pulsed current $i_p(t)$.

In (3), (4), the electrical parameters of R_{Na} and L_{Na} are understood to be constant over the time interval $[t_s, t_e]$ the values of active resistance and internal inductance of the conductor under consideration, which by the time point $t_e > t_s$ cause in its material the same changes of energy of thermal (Joule) losses and magnetic field energy, as the time variable values of active resistance R_N and internal inductance L_N of the conductor. Note that in [28] for the case of a sharp manifestation of a stationary skin effect in a nonmagnetic massive solid cylindrical wire of radius b (see Fig. 2) with a variable sinusoidal axial current of frequency f, the following classical calculation relations were obtained for its current oscillations averaged over a half-period's area duration $0{,}5f^{-1}$ values of active resistance R_C and internal inductance L_C:

$$R_C = 0{,}5l(\pi b \gamma_C \Delta_C)^{-1}; \quad (5)$$

$$L_C = 0{,}25\mu_0 l \Delta_C (\pi b)^{-1}. \quad (6)$$

For comparison at $\delta_p/\omega_p=0$ of the values of the active resistance R_{Na} and the internal inductance L_{Na} of the massive continuous cylindrical conductor of radius b with apulsed axial current $i_p(t)$, found taking into account the influence of the TSE, with the corresponding values of its active resistance R_C and internal inductance L_C, calculated in the stationary mode, at $b/\Delta_C >> 1$ the following relations can be used [26]:

$$R_{Na}/R_C = 2\Delta_C k_R / b; \quad (7)$$

$$L_{Na}/L_C = 0{,}5b k_L / \Delta_C. \quad (8)$$

Analytical and graphical dependencies for the coefficients $k_R > 1$ and $k_L < 1$ as applied to flow through the considered massive cylindrical conductor of pulsed axial current $i_p(t)$ of the form (1) are presented in [12, 26]. We now turn to the analysis of the effect of the TSE on the active resistance R_{Na} and the internal inductance L_{Na} of a nonmagnetic massive cylindrical conductor with pulsed axial current $i_p(t)$ according to (1).

The results obtained in [12, 26] for the conductor considered indicate that the averaged in the area of the first half-wave ($t_s=0$; $t_e=\pi/\omega_p$) of the damped sinusoidal current $i_p(t)$ of the form (1) values of the active resistance R_{Na} taking into account the linear TSE are much smaller, and the averaged in this area values of the internal inductance L_{Na} are larger than at the stationary skin effect in the material of such a conductor. So, at $b/\Delta_C=10$ and $\delta_p/\omega_p=0$ for a non-magnetic continuous cylindrical conductor with pulsed axial current $i_p(t)$, the ratio R_{Na}/R_C by (7) is numerically about 0.75, and the ratio L_{Na}/L_C by (8) takes a value numerically equal to about 1.14. It can be seen that for a massive cylindrical conductor, taking into account the influence of the linear TSE leads to a decrease (by about 25 %) of its average active resistance value R_{Na} and an increase (by about 14 %) of its average internal inductance L_{Na}. It is important to point out that according to the calculation data from [12, 26] for relatively thin (non-massive) cylindrical conductors ($b/\Delta_C \leq 1$) with pulsed axial damped sinusoidal current $i_p(t)$ in the discharge circuit of the high-voltage EPHI, the transient electromagnetic process in their non-magnetic homogeneous material has practically no effect on the values of such integral electrical parameters as active resistance and internal inductance.

3.4. Influence on the quality factor of conductors of the discharge circuit of the EPHI. The quality factor (Q-factor) Q_N of the considered flat and cylindrical conductors with pulsed current $i_p(t)$ of the form (1) in the discharge circuit of the EPHI is understood as the physical quantity determined by the ratio of their internal reactances to their active resistances and calculated by the following expression [12]:

$$Q_N = \omega_p L_N / R_N. \quad (9)$$

For a non-magnetic massive solid cylindrical conductor with a pulsed axial current $i_p(t)$ of the form (1), expression (9) according to [12] can be written as follows:

$$Q_N = 0{,}25b^2 k_L / (\Delta_C^2 k_R). \quad (10)$$

Based on (9) and taking into account (5) and (6), for the specified massive ($b/\Delta_C >> 1$) cylindrical conductor at a stationary mode of manifestation in its non-magnetic material of the skin effect, the value of quality factor takes a numerical value equal to $Q_N=1$. This result corresponds to the well-known classical provisions of theoretical electrical engineering [28]. And how does the linear TSE, which manifests itself in their materials, affect the Q-factor Q_N of the considered conductors? From (10) and analysis of the results of theoretical studies of this skin effect in nonmagnetic massive conductors with pulsed axial current $i_p(t)$ of a temporary form (1), presented in [12, 26], it follows that for a massive solid cylindrical conductor with $b/\Delta_C=10$ (in the case of $\delta_p/\omega_p=0$) its Q-factor in the transient mode becomes numerically equal to about $Q_N=1.52$. It can be seen that linear TSE compared with the steady-state (stationary) skin effect leads to a significant increase (by about 52 %) of the value of Q-factor Q_N of the specified massive conductor with pulsed current $i_p(t)$, connected in the high-current discharge circuit of the EPHI. Note that a similar result for the quality factor Q_N was also obtained when calculating the integral

electrical parameters for an infinitely thick flat conductor with a pulsed sinusoidal current in a transient mode [8]. From this we can conclude that in order to achieve in the discharge circuit of the powerful high-voltage EPHI that generates high pulsed currents and high pulsed magnetic fields on an electrical load, high values of Q-factor of its current-carrying busbar, in it (in this busbar) non-magnetic massive conductors must be used.

Conclusions.

1. From the presented data of the review, it follows that the linear transient skin effect in the metal conductors under consideration, compared with the stationary skin effect in them, in the first half-wave of the damped sinusoidal pulsed current $i_p(t)$ leads to a significant decrease (up to 33 %) on the outer surface of the conductors of the value of the strength of the pulsed electric field, a significant increase (up to 35 %) in the inner layers of the conductors of the value of the strength of the pulsed magnetic field, a noticeable increase (up to 37 %) in the depth of penetration of the external electromagnetic field into the conductor material, a decrease (up to 25 %) in the average active resistances of the conductors, an increase (up to 14 %) in the average internal inductance of the conductors and an increase (up to 52 %) in the Q-factor of the conductors, as well as to the flow in the discharge circuit of a high-voltage high-current electrical installation of a transient electromagnetic process with a duration of up to one and a half period of change of its pulsed current $i_p(t)$ of the specified temporary type.

2. The above-described features of the manifestation and influence of a linear transient skin effect in indicated non-magnetic homogeneous massive conductors of discharge electric circuits of high-voltage high-current electrical installations must be taken into account when designing and choosing the design of flat (cylindrical) busbar of discharge circuits of similar electrophysical installations, as well as when solving applied problems of obtaining on certain electrical loads of specified current (voltage) pulses with the specified parameters.

REFERENCES

1. Dashuk P.N., Zayents S.L., Komel'kov V.S., Kuchinskiy G.S., Nikolaevskaya N.N., Shkuropat P.I., Shneerson G.A. *Tehnika bol'shih impul'snyh tokov i magnitnyh polej* [Technique large pulsed currents and magnetic fields]. Moscow, Atomizdat Publ., 1970. 472 p. (Rus).

2. Knopfel' G. *Sverkhsil'nye impul'snye magnitnye polia* [Ultra strong pulsed magnetic fields]. Moscow, Mir Publ., 1972. 391 p. (Rus).

3. Bostic W., Nardi V., Zucker O. *Nakoplenie i kommutacija energii bol'shih plotnostej* [Accumulation and commutation of energy of high densities]. Moscow, Mir Publ., 1979. 474 p. (Rus).

4. Gulyi G.A. *Nauchnye osnovy razriadno-impul'snykh tekhnologii* [Scientific basis of the discharge-pulse technology]. Kiev, Naukova Dumka Publ., 1990. 208 p. (Rus).

5. Mesiats G.A. *Impul'snaia energetika i elektronika* [Pulsed power and electronics]. Moscow, Nauka Publ., 2004. 704 p. (Rus).

6. Baranov M.I. *Izbrannye voprosy elektrofiziki. Monografija v 3-h tomah. Tom 3: Teoriya i praktika electrofizicheskih zadach* [Selected topics of electrophysics. Monograph in 3th vols. Vol. 3. Theory and practice of electrophysics tasks]. Kharkiv, Point Publ., 2014. 400 p. (Rus).

7. Timofeev B.B. *Spetsial'nye zadachi teorii poverhnostnogo effekta* [Special tasks of theory of superficial effect]. Kyiv, Naukova dumka Publ., 1966. 192 p. (Rus).

8. Bondaletov V.N. Equivalent parameters at non-stationary distribution of the impulsive electromagnetic field in an explorer. *Electricity*, 1975, no.8, pp. 55-58. (Rus).

9. Mihaylov V.M. *Impul'snye elekromagnitnye polya* [Impulsive electromagnetic fields]. Kharkiv, Higher School Publ., 1979. 140 p. (Rus).

10. Shneerson G.A. *Polya i perehodnye processy v apparature sverhsilnyh tokov* [Fields and transients in equipment ultra strong currents]. Leningrad, Energoizdat Publ., 1981. 200 p. (Rus).

11. Batygin Yu.V., Lavinskyi V.I., Khimenko L.T. *Impul'snye magnitnye polya dlya progressivnyh tehnologiy* [Impulsive magnetic fields for progressive technology]. Kharkiv, MOST-Tornado Publ., 2003. 288 p. (Rus).

12. Baranov M.I. *Izbrannye voprosy elektrofiziki: Monografija v 2-h tomah. Tom 2, Kn. 1: Teorija elektrofizicheskih effektov i zadach* [Selected topics of Electrophysics: Monograph in 2 vols. Vol. 2, book. 1: Theory of electrophysics effects and tasks]. Kharkov, NTU «KhPI» Publ., 2009. 384 p. (Rus).

13. Baranov M.I. *Izbrannye voprosy elektrofiziki. Monografiya v 3kh tomakh. Tom 2, Kn. 2: Teoriia elektrofizicheskikh effektov i zadach* [Selected topics of Electrophysics. Monograph in 3 Vols. Vol.2, Book 2. A theory of electrophysical effects and tasks]. Kharkiv, Tochka Publ., 2010. 407 p. (Rus).

14. Baranov M.I., Belyi I.V., Khimenko L.T. Superficial effect and distributing of electrodynamic efforts in cylindrical current-wires of the coaxial system with an impulsive current. *Electricity*, 1976, no.10, pp.1-8. (Rus).

15. Baranov M.I. Superficial effect in a hollow conducting homogeneous cylinder with the axial-flow impulsive magnetic field. *Technical electrodynamics*, 1999, no.2, pp. 3-6. (Rus).

16. Mihaylov V.M. About distribution of the impulsive electromagnetic field in the system «inductor – workpart». *Bulletin of «KhPI». Series: «Magnetic-impulsive metal forming»*, 1971, iss.1, no.53, pp. 15-23. (Rus).

17. Mihaylov V.M. Calculation of inductance and distributing of current at a sharp skin-effect. *Electricity*, 1978, no.8, pp. 27-33. (Rus).

18. Vitkov M.G. Penetration of impulsive magnetic field into a cylindrical screen. *Technical physics*, 1965, vol.35, iss.3, pp. 410-413. (Rus).

19. Podoltsev A.D., Pignastiy S.S. Influence of skin-effect on the power indexes of impulsive without ferum-transformer. *Electricity*, 1985, no.7, pp. 56-59. (Rus).

20. Wheeler H.A. Formulas for the skin-effect. *Proceedings of the IRE*, 1942, vol.30, pp. 412-424.

21. Kaden G. *Elektromagnitnyie ekrany v vyisokochastotnoy tehnike i tehnike elektrosvyazi* [Electromagnetic shields in high-frequency technology and communication technology]. Moscow-Leningrad, Gosenergoizdat Publ., 1957. 327 p. (Rus).

22. Waldow P., Wolff I. The Skin-Effect at High Frequencies. *IEEE Transactions on Microwave Theory and Techniques*,

1985, vol.33, no.10, pp. 1076-1082. **doi: 10.1109/tmtt.1985.1133172**.

23. Baranov M.I., Kravchenko V.I., Medvedeva V.A. Calculation of depth of penetration of the impulsive electromagnetic field in massive explorer. *Technical electrodynamics*, 2001, no.3, pp.13-16. (Rus).

24. Belorussov N.I., Saakjan A.E., Jakovleva A.I. *Elektricheskie kabeli, provoda i shnury. Spravochnik* [Electrical cables, wires and cords. Directory]. Moscow, Energoatomizdat Publ., 1988. 536 p. (Rus).

25. Baranov M.I. Close scope terms for the impulsive electromagnetic field on-the-spot homogeneous conducting bodies. *Technical electrodynamics*, 1996, no.6, pp. 3-10. (Rus).

26. Baranov M.I., Bondina N.N. Calculation of active resistance and inductance of cylindrical explorer with an impulsive current. *Electricity*, 1990, no.1, pp. 81-87. (Rus).

27. Baranov M.I., Bondina N.N. Impulsive resistance of cylindrical wire with the current of lightning. *Technical electrodynamics*, 1996, no.3, pp. 3-9. (Rus).

28. Neyman L.R., Demirchyan K.S. *Teoreticheskie osnovy elektrotechniki. V 2-h tomah. Tom 2* [Theoretical bases of the Electrical Engineering. In 2 vols. Vol.2]. Leningrad, Energoizdat Publ., 1981. 416 p. (Rus).

Received 09.01.2019

M.I. Baranov, *Doctor of Technical Science, Professor,*
Scientific-&-Research Planning-&-Design Institute «Molniya»,
National Technical University «Kharkiv Polytechnic Institute»,
47, Shevchenko Str., Kharkiv, 61013, Ukraine,
phone +380 57 7076841,
e-mail: baranovmi@kpi.kharkov.ua

How to cite this article:

Baranov M.I. Peculiarities of the manifestation and influence on the electromagnetic processes of the transient skin effect in metal conductors with pulsed current. *Electrical engineering & electromechanics*, 2019, no.4, pp. 41-47. **doi: 10.20998/2074-272X.2019.4.06.**

UDC 621.315.2 **doi: 10.20998/2074-272X.2019.4.07**

Y.A. Antonets, L.A. Shchebeniuk, O.M. Grechko

TECHNOLOGICAL MONITORING OF ELECTRICAL RESISTANCE OF PRESSED CABLE CONDUCTORS IN PRODUCTION CONDITIONS

This paper presents results of control of electrical resistance R production pressed aluminum cable conductors. Control of electrical resistance in manufacturing of cable production is the most massive non-destructive test, which provides a compromise between the manufacturer's costs for a high-conductivity material on the one hand and the user's operating costs from conducting heating losses on the other. For the adoption of technological solutions for the use of hot compression of solid aluminum wires (instead of cold drawing technology) for a specific size, a reliable determination of the probability of unacceptable values of electrical resistance R > Ř (probability of claims) in large masses of products is necessary. The application of statistical analysis of measurement results using the mathematical apparatus of boundary distributions is considered. In this case, the subject matter of the analysis is the distribution of the limit values of the control parameter, which makes it possible to reliably estimate the likelihood of the appearance of inadmissible values (probability of claims). An algorithm for determining the probability of the appearance of impermissible values of the electrical resistance R > Ř (probability of claims) for solid aluminum wires of low and medium voltage cables in the range of the cross-sectional area (120...240) mm^2 based on the analysis of the results of control of the electrical resistance during a long technological period (18 months) manufacturing in production conditions. The use of the appeal potential of the technological solution as the cost of products, for which R > Ř is used, is proposed. The comparison of the appeal potential of the technology of hot pressing of solid aluminum and the technology of cold drawing (dragging) provided the same level of specific electrical conductivity of the metal is achieved. References 8, figures 5.

Key words: **control of electrical resistance, aluminum cable conductors, technological monitoring, probability of claims, mathematical apparatus of boundary distributions.**

Представлено результати контролю в умовах виробництва електричного опору R пресованих алюмінієвих кабельних провідників. Контроль R в кабельному виробництві є наймасовішим неруйнівним випробуванням, яке забезпечує компроміс між затратами виробника на матеріал високої електропровідності з одного боку, і експлуатаційними затратами користувача від втрат на нагрівання провідників з іншого. Для прийняття технологічних рішень щодо використання гарячого пресування суцільних алюмінієвих жил (замість технології холодної витяжки) для конкретних розмірів жили необхідне надійне визначення ймовірності появи недопустимих значень електричного опору R > Ř (ймовірності рекламацій) у великих масивах продукції. Розглянуто застосування статистичного аналізу результатів вимірювання за допомогою математичного апарату граничних розподілів. При цьому предметом аналізу стає розподіл граничних значень контрольного параметру, що дає можливість надійного оцінювання ймовірності появи недопустимих значень (ймовірності рекламацій). Розроблено алгоритм визначення ймовірності появи недопустимих значень електричного опору R > Ř (ймовірності рекламацій) для суцільних алюмінієвих жил силових кабелів низької і середньої напруги в діапазоні площі поперечного перерізу (120…240) мм^2 на основі аналізу результатів контролю електричного опору впродовж тривалого технологічного періоду (18 місяців) виготовлення в умовах виробництва. Запропоновано використання рекламаційного потенціалу технологічного рішення як вартості продукції, для якої R > Ř. Виконане порівняння рекламаційного потенціалу технології гарячого пресування суцільних алюмінієвих і технології холодної витяжки (волочіння) за умови досягнення однакового рівня питомої електропровідності металу. Бібл. 8, рис. 5.

Ключові слова: **контроль електричного опору, алюмінієві кабельні провідники, технологічний моніторинг, ймовірність рекламацій, математичний апарат граничних розподілів.**

Представлены результаты контроля электрического сопротивления R в условиях производства прессованных алюминиевых кабельных жил. Контроль R в кабельном производстве являться наиболее массовым неразрушающим испытанием, которое обеспечивает компромисс между затратами изготовителя на материал высокой электропроводности, с одной стороны, и эксплуатационными затратами пользователя от потерь на нагрев проводников, с другой. Для принятия технологических решений относительно использования горячего прессования сплошных алюминиевых жил (вместо технологии холодной вытяжки) для конкретных размеров жилы необходимо надежное определение вероятности появления недопустимых значений электрического сопротивления R > Ř (вероятности рекламаций) в больших массивах продукции. Рассмотрено использование статистического анализа результатов измерений с помощью математического аппарата предельных распределения. При этом предметом анализа становится распределение предельных значений контрольного параметра, что дает возможность надежного определения вероятности появления недопустимых значений (вероятности рекламаций). Разработан алгоритм определение вероятности появления недопустимых значений электрического сопротивления R > Ř (вероятности рекламаций) для сплошных алюминиевых жил силовых кабелей низкого и среднего напряжения в диапазоне площади поперечного сечения (120…240) мм^2 на основе анализа результатов контроля электрического сопротивления в течение длительного технологического периода (18 месяцев) изготовления в условиях производства. Предложено использование рекламационного потенциала технологического решения как стоимости продукции, для которой R > Ř. Произведено сравнение рекламационного потенциала технологии горячего прессования сплошных алюминиевых жил и технологии холодной вытяжки (волочения) при условии достижения одинакового уровня удельной электропроводности металла. Библ. 8, рис. 5.

Ключевые слова: **контроль электрического сопротивления, алюминиевые кабельные проводники, технологический мониторинг, вероятность рекламаций, математический аппарат граничных распределений.**

Introduction and problem definition. The introduction of technological changes in the production of cable and wire products, which increase the economic efficiency of production, always requires the analysis of the impact of these changes on the relation of interests of the manufacturer and consumer of products. Here, it is a matter of solid aluminum wires made by hot pressing (SSAP – **s**olid **s**oft **a**luminum **p**ressed), instead of the technology of cold drawing, which in practice of cable technology is called dragging. Hot pressing provides the highest electrical conductivity of the metal with the simultaneous elimination of the cost of annealing, which is necessary for recrystallization of the structure of the conductor due to the cold deformation of compression during dragging. Providing a high level of electrical conductivity corresponds both to the interests of the manufacturer and to the interests of the consumer, since this characteristic is the basis for providing the electrical resistance R of conductors. But the value of R is influenced by a number of structural and technological factors. Therefore, the monitoring of the electrical resistance R for conductors is the most massive non-destructive test in the cable industry, which provides a compromise between the manufacturer's costs on the material of high electrical conductivity on the one hand and the user's operating costs from the losses of heating of conductors on the other.

Corresponding maximum limit values $\check{R}$ are normalized to provide a sufficiently small electrical resistance, which determines the energy losses in the cable, and hence the temperature of its elements and by it, the durability and reliability of cable insulation in both operating and emergency modes [1]. In order to make technical decisions on the use of hot pressing of solid aluminum wires (instead of the cold drawing technology) for a specific size of the wire, it is necessary to reliably determine the probability of unacceptable values of electrical resistance $R > \check{R}$ (probability of claims) in large masses of products based on the results of technological monitoring of R.

Analysis of literature. Cable production is characterized by significant lengths of products with high requirements for the uniformity of length parameters, therefore the value of $\check{R}$ per unit of length is standardized [2]. The monitoring of homogeneity of R in length is the subject of technological monitoring. The problem of organizing active technological monitoring is conceptual for automated mass production not only in cable technology, since between the tasks of receiving and current technological monitoring there is a significant theoretical and technical difference [3]. For the key electrical engineering parameters of mass production, one-way restrictions are used: for electrical resistance of conductors – no more than; for electric strength – not less than, etc. Therefore, for the evaluation of the guaranteed level of technical parameters of products that ensure its reliable functioning, it is expedient to use the mathematical apparatus of boundary distributions [4]. The difference in the technological monitoring from the receiving one is that possible changes in the technological process should be recorded by it [4]. That is, the measurement result is an element of an unknown statistical array. Therefore, for the purposes of technological monitoring, it is expedient to use the mathematical apparatus of the boundary distributions. In this case, the subject matter of the analysis is the distribution of the limit values of the control parameter, which makes it possible to reliably estimate the probability of the appearance of inadmissible values (probability of claims).

The number of structural and technological factors that affect the value of R is very significant. The first is the cross-sectional area of the conductor. The larger the area of the section of the continuous wire, the economic efficiency of the application of hot pressing technology is higher because of the unnecessary further annealing. On the other hand, in the process of crystallization of the metal, after compression its density changes and its shrinkage [5] is observed, which depend on the compression mode and the cross-sectional area of the wire. For a specific size of the wire, a reliable determination of the probability of the occurrence of impermissible values of electrical resistance $R > \check{R}$ in large masses of products based on the results of technological monitoring of R is necessary.

Reliable determination of the probability of the appearance of inadmissible values of random variable is still the subject of the search for specific solutions for specialists in the field of mathematical statistics [6]. It is obvious that such a determination in production conditions should take into account the volume of output and be based on sufficiently well-known and indisputable statistical models. Known statistical models of distribution of boundary values correspond to these obvious requirements [4]. The one-time, even massive, statistical stability study can not be practically carried out, the concept of solving applied probabilistic problems is the well-known Mises concept [7]: the frequency $f^*(A)$ of event A is the proportion of the number of events $m^*(A)$ arising from the number of independent attempts n^* under the identical conditions that they may have occurred in: $f^*(A) = m^*(A)/n^*$. Here and further the mark «*» is used for the values determined experimentally. The requirement of reproducibility of a phenomenon with the definition of frequency acquires a quantitative expression in the form of the principle of constancy of frequencies:

$$m_1^*(A)/n_1^* \cong m_2^*(A)/n_2^* \cong m_3^*(A)/n_3^* \cong .. m_k^*(A)/n_k^*, \quad (1)$$

that is, the frequency of this event in a series of independent attempts must be sufficiently identical.

The relation (1) is precisely the principle, since sufficient uniformity of frequencies can be accepted only within the framework of a specific problem, but the requirement of constancy of frequencies naturally follows from the requirement of the reproducibility of the event. This requirement is successfully used in practical statistics [8]. Therefore, it is necessary to reliably determine the probability of the occurrence of impermissible values of resistance $R > \check{R}$ that should be performed for the largest cross-sectional area produced and tested during a long technological period in a series of independent attempts.

The goal of the work is the development of an algorithm for determining the probability of the

appearance of impermissible values of the electrical resistance $R > \check{R}$ (probability of claims) for solid aluminum wires of low and medium voltage cables in the range of the cross-sectional area (120 ... 240) mm^2 based on the analysis of the results of the electrical resistance monitoring during a long technological manufacturing period in a production environment. Determination of the probability of unacceptable values of electrical resistance in the current production conditions is the basis for establishing economically justified guarantees for the user, first of all, regarding the bandwidth of the cable, which is guaranteed by the manufacturer in nominal operating conditions.

Main results. Figure 1 shows the results of the monitoring of the electrical resistance R under the conditions of production and, in accordance with the current certification documentation, for 18 months of 2017 and 2018, of solid aluminum wires of low and medium voltage power cables made by pressing in the range of the cross-sectional area (120 ... 240) mm^2.

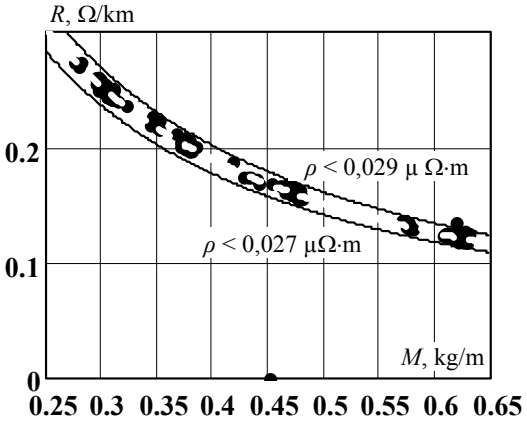

Fig. 1. The dependence of the electric resistance R on the unit length of the aluminum wire, made by hot pressing, from the mass M in the range of the cross-sectional area (120 ... 240) mm^2: points – experimental values; solid curves – the dependencies $R = f(M)$, calculated for the specific electric resistance of 0.027 μΩ·m (lower) and 0.029 μΩ·m (upper)

The dependence $R = f(M)$ of the lateral resistance R on the particle mass of the conductor is universal, inversely proportional and its parameter is the specific electrical resistance ρ of the wire metal. The results of the control over 18 months are in accordance with the current standards regarding the specific electrical resistance of the wire metal, which confirms the starting thesis that pressing provides the necessary electrical conductivity of the metal with the simultaneous exclusion of the cost of annealing.

A feature is the presence of samples with an abnormally low mass for each of the nominal cross sections studied. Such samples appear evenly throughout the long technological observation period, representing a relatively small, but substantial part of the tested samples (from 5 % to 8 %). In accordance with the principle of the reproducibility of the Mises, the technology of manufacturing of continuous aluminum wires by hot pressing ensures the reproducibility of the electrical conductivity of the metal, but in this particular case does not ensure the reproducibility of the particle mass of the metal.

Therefore, in the further development of the algorithm for determining the probability of the appearance of impermissible values of electrical resistance $R > \check{R}$ (probability of claims) for solid aluminum wires of low and medium voltage cables, has been carried out on the basis of analysis of the data array (238 values), which corresponds to the principle of the reproducibility of the event. Data that does not correspond to the principle of reproducibility of an event are used to analyze the reasons for the appearance of specimens with an abnormally low mass.

Figure 2 shows the characteristic functions of the distribution of electrical resistance of SSAP samples. The functions of the distribution of the maximum values of R_{max} are obtained in two ways: analytically by the formula (2) and by the computer statistical experiment as the distributions of the largest values in the corresponding normally distributed random variables. Both methods gave the same result, presented in Fig. 2.

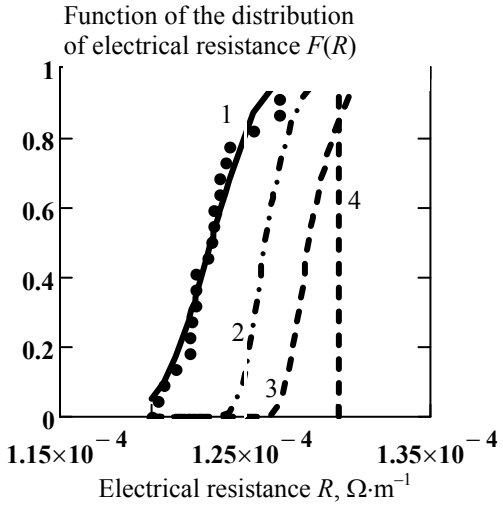

Fig. 2. Functions of the resistance R distribution of SSAP samples: 1 – empirical distribution function (points) and its approximation by normal distribution (solid line); 2 – function of distribution of maximum values R_{max} in 24 samples at 24 normally distributed values; 3 – function of distribution of maximum values R_{max} in the corresponding 250 samples; 4 – arbitrarily selected impermissible value

The results presented in Fig. 2 testify:

1) according to the results of measurements of the electrical resistance, it is possible to determine the probability of the appearance of impermissible values of the electrical resistance $R > \check{R}$ (probability of claims) by means of the known mathematical apparatus of distributions of maximum values R_{max} for solid aluminum wires of low and medium voltage cables;

2) parameters of the boundary function of the distribution of the maximum values R_{max} [4]:

$$F(R_{max}) = \exp\{-\exp[-(R_{max} - B_n)/A_n]\}, \quad (2)$$

where B_n is the shift parameter equal to R_{max}, less than 37 % of the samples with n; A_n is the scale parameter that depends on the initial distribution and does not depend on n; the parameters of the function (2) depend on the

division of the batch into statistical groups according to the requirement of constancy of frequencies (1); to determine the parameters we double-log the function $F(R_{max})$, obtain a linear relationship between the double logarithms of the distribution function and the values of R_{max};

3) the larger the statistical groups in accordance with the requirement of constancy of frequencies (1), the greater the number of inadmissible values of the electrical resistance on the curve of the function of the distribution of maximum values (see curves 2 and 3 in Fig. 2), but this increase is rather fast decelerating and there is a limit distribution and, accordingly, the boundary parameters that do not depend on the volume of the batch of products or its division into statistical groups.

Dependencies of the parameters of the distribution function (3) of the maximum values R_{max} on the division of a batch into statistical groups by the results of measurements of electrical resistance (1 in Fig. 2) are presented in Fig. 3.

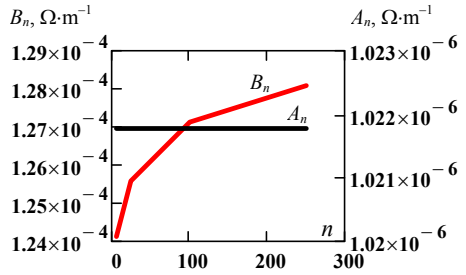

Fig. 3. Dependences of the parameters of the distribution function $F(R_{max})$ (3) on the division of a batch into statistical groups by the results of measurements of electrical resistance: dependence $B_n(n)$ – nonlinear, the value of the parameter B_n reflects the maximum distribution density $F(R_{max})$ (see Fig. 4)

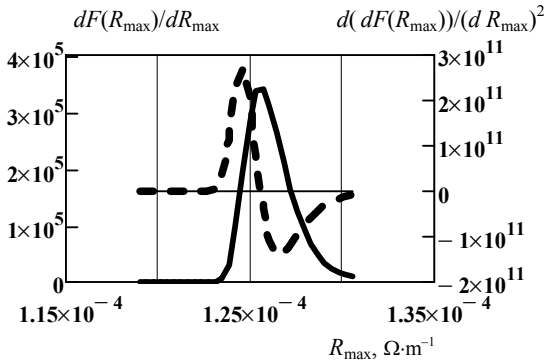

Fig. 4. Characteristic points of the first (solid line $f(R_{max})$) and the second derivative (dashed line $df(R_{max})/dR_{max}$) of the distribution of the maximum values of electrical resistance reflect the unambiguous technical meaning of the corresponding values of R_{max}: the minimum of the second derivative – the appropriate technical characteristic of the upper bound for technological monitoring by R_{max} depends on n, but the corresponding probability of exceeding this bound does not depend on n, which gives an opportunity to analytically assess the appropriate level of technical guarantee

Figure 5 illustrates the application of different upper bounds for technological monitoring of the distribution function of R_{max} in 24 samples with 24 normally distributed values determined experimentally.

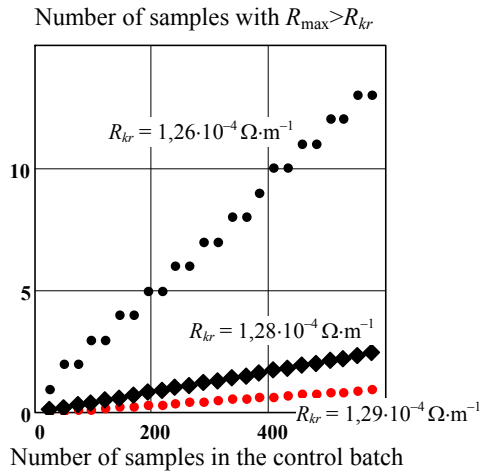

Fig. 5. An illustration of the possible practical application of different upper bounds for technological monitoring of the distribution function of R_{max} in 24 samples at 24 normally distributed samples of SSAP with a cross section of 240 mm^2

According to Fig. 5 within the array of a control batch, from several tens to several hundreds, the monitoring sensitivity provides the use of the upper limit for $R_{max} < R_{kr} = 1.26 \cdot 10^{-4}$ Ω·m^{-1} in sampling for 24 samples. In this case, for batches with a sample size of 50 and larger, the relative number of samples with $R_{max} > R_{kr}$ is stable and remains at 2.5 % if there are no obvious changes in the technological process.

It is important that the limit $R_{kr} = 1.26 \cdot 10^{-4}$ Ω·m^{-1} is not arbitrarily chosen. This value corresponds to the minimum of the second derivative – an expedient technical characteristic, when the decrease in the density of the distribution is sharply slowing down and practically does not affect the number of violations of the established limit. This gives an opportunity to analytically assess the appropriate level of technical guarantee.

Conclusions.

1. The results of the monitoring over 18 months in the conditions of the production of electrical resistance R of solid aluminum wires made by hot pressing confirmed the starting thesis that hot pressing provides the required electrical conductivity of the metal with the simultaneous exclusion of the cost of annealing.

2. An algorithm for determining the probability of unacceptable values of electrical resistance $R > \check{R}$ (probability of claims) is developed for continuous aluminum wires, made by hot pressing, using the known mathematical apparatus of distributions of maximum values R_{max}. The algorithm includes:

- separation of the control batch into statistical groups in accordance with the known requirement of constancy of frequencies (1);
- determination of the parameters of the initial distribution by standard statistical procedures (in this case, by normal distribution);
- determination of the distribution parameters of the maximum values R_{max} by the least squares method in the linear coordinates of the distribution function of the maximum values;
- determination of the critical value of the electrical resistance R_{kr}, which corresponds to the minimum of the

second derivative – the appropriate technical characteristic, when the decrease in the density of the distribution is sharply slowing down and practically does not affect the number of violations of the established limit (in this case $R_{kr} = 1.26 \cdot 10^{-4}$ Ω·$^{-1}$);

- determination of the level of technical guarantee as the ratio of the number of samples with $R_{\max} > R_{kr}$ to the control batch volume (for example, 5/200 = 0.025 or 2.5 %, see Fig. 5).

3. The developed algorithm, tested in production conditions and in accordance with valid certification documentation during 18 months of 2017 and 2018, makes it possible to technically assess the claim potential of the achieved level of specific technology as a product of the probability of unacceptable values $R_{\max} > R_{kr}$ in the control batch for (3) for the accepted the critical level R_{kr} to the corresponding technological cost of the samples in the control batch.

4. The use of the claim potential of the technological solution as the cost of products, for which $R > \check{R}$ is proposed. The comparison of the claim potential of the technology of hot pressing of solid aluminum wires (0.025×1 = 0.025 USD/km) and the technology of cold drawing (0.025×1.2 = 0.03 USD/km) provided the same level of specific electrical conductivity of the metal is carried out.

REFERENCES

1. Karpushenko V.P., Shchebeniuk L.A., Antonets Yu.O., Naumenko O.A. *Sylovi kabeli nyz'koyi ta seredn'oyi napruhy. Konstruyuvannya, tekhnolohiya, yakist'* [Power cables of low and medium voltage. Designing, technology, quality]. Kharkiv, Region-inform Publ., 2000. 376 p. (Ukr).

2. Zolotaryov V.M., Antonets Yu.P., Antonets S.Yu., Golik O.V., Shchebeniuk L.A. Online technological monitoring of insulation defects in enameled wires. *Electrical engineering & electromechanics*, 2017, no.4, pp. 55-60. **doi: 10.20998/2074-272X.2017.4.09**.

3. Golik O.V. Statistical procedures for two-sided limit of a controlled parameter in the process of production of cable and wire products. *Electrical Engineering & Electromechanics*, 2016, no.5, pp. 47-50. (Rus). **doi: 10.20998/2074-272X.2016.5.07.**

4. Gnedenko B.V., Belyaev Yu.O., Solovjev A.D. *Matematicheskie metody v teorii nadezhnosti* [Mathematical methods in theory of reliability]. Moscow, Nauka Publ., 1965. 524 p. (Rus).

5. Bauser M., Sauer G., Siegert K. *Pressovanie* [Pressing]. Moscow, Alumsil MViT Publ., 2009. 922 p. (Rus).

6. Kuznetsov V.P. *Interval'nye statisticheskie modeli* [Interval statistical models]. Moscow, Radio i sviaz' Publ., 1991. 352 p. (Rus).

7. Tutubalin V.N. *Granitsy primenimosti* [Limits of application]. Moscow, Znanie Publ., 1977. 64 p. (Rus).

8. Shchebeniuk L.A., Golik O.V. *Matematychni osnovy nadiynosti izolyatsiyi elektroobladnannya* [Mathematical foundations of the reliability of electrical insulation]. Kharkiv, NTU «KhPI» Publ., 2003. 102 p. (Ukr).

Received 30.05.2019

Y.A. Antonets[1], *Candidate of Technical Science,*
L.A. Shchebeniuk[2], *Candidate of Technical Science, Professor,*
O.M. Grechko[2], *Candidate of Technical Science, Associate Professor,*
[1] Private Joint-stock company Yuzhcable works,
7, Avtogennaya Str., Kharkiv, 61099, Ukraine,
phone +380 57 7545248,
e-mail: zavod@yuzhcable.com.ua
[2] National Technical University «Kharkiv Polytechnic Institute»,
2, Kyrpychova Str., Kharkiv, 61002, Ukraine,
e-mail: agurin@kpi.kharkov.ua, a.m. grechko@gmail.com

How to cite this article:
Antonets Y.A., Shchebeniuk L.A., Grechko O.M. Technological monitoring of electrical resistance of pressed cable conductors in production conditions. *Electrical engineering & electromechanics*, 2019, no.4, pp. 48-52. **doi: 10.20998/2074-272X.2019.4.07.**

UDC 621.319 **doi: 10.20998/2074-272X.2019.4.08**

G.V. Bezprozvannych, A.G. Kyessayev, I.A. Mirchuk, A.V. Roginskiy

IDENTIFICATION OF TECHNOLOGICAL DEFECTS IN HIGH-VOLTAGE SOLID INSULATION OF ELECTRICAL INSULATION STRUCTURES ON THE CHARACTERISTICS OF PARTIAL DISCHARGES

Introduction. High-voltage insulation systems always have some background level of the partial discharges, which does not have any significant effect on the life of the electrical insulation design. At the same time, partial discharges destroy high-voltage insulation, leading to a carburization zone around the defect. This is the «hidden» period of development of the defect. The development of a defect zone, sooner or later, leads to an arc breakdown of the entire insulating gap. Purpose. The substantiation of the efficiency of detection of technological defects in high-voltage solid insulation of electrical insulating structures according to the characteristics of partial discharges. Methodology. The conditions for the occurrence of partial discharges in the thickness of the polymer insulation are considered. The possible values of the voltage of the beginning of partial discharges are determined for a model of a cylindrical air gap near the conductor of a power cable. It is shown that with the same applied voltages to high-voltage insulation, in the latter case, air inclusions of smaller thickness are activated in comparison with a flat structure. Practical value. The efficiency of detection of technological defects in solid composite case insulation of the stator winding of turbo- and hydrogenerators is shown. Based on the comparison of the amplitude of the pulses of partial discharges of positive and negative polarity, the estimated location of the* **technological defects in the insulation has been established.** References 19, figures 7, table 1.

Key words: **technological defects, partial discharges, voltage of the start of partial discharges, glass-mica paper tape, amplitude of pulses of partial discharges, location of the defect**.

Визначено можливі значення напруги початку часткових розрядів для моделі циліндричного повітряного зазору поблизу струмопровідної жили силового кабелю. Показано, що при однакових прикладених напругах до високовольтної ізоляції в останньому випадку активізуються повітряні включення меншої товщини в порівнянні з пласкою конструкцією. На підставі результатів проведених випробувань силового кабелю на напругу 3 кВ встановлено, що грубі технологічні дефекти в товщі ізоляції відсутні. Амплітуда розрядів в повітряних включеннях не перевищує 10 пКл при прикладеній випробувальній напрузі 5 кВ частоти 50 Гц. Показана ефективність виявлення технологічних дефектів у твердої композитної корпусної ізоляції обмотки статора турбо- і гідрогенераторів. Встановлено, що в макетах, ізоляція яких виконана стрічками меншої товщини, технологічні дефекти розташовані в товщі ізоляції. Для макета, ізоляція якого виконана стрічками більшої товщини, технологічні дефекти у вигляді розшарування розташовані на кордоні розділу провідник – композитна ізоляція. Бібл. 19, табл. 1, рис. 7.

Ключові слова: **технологічні дефекти, часткові розряди, напруга початку часткових розрядів, склослюдопаперова стрічка, амплітуда імпульсів часткових розрядів, місце розташування дефекту.**

Определены возможные значения напряжения начала частичных разрядов для модели цилиндрического воздушного зазора вблизи токопроводящей жилы силового кабеля. Показано, что при одинаковых приложенных напряжениях к высоковольтной изоляции в последнем случае активизируются воздушные включения меньшей толщины в сравнении с плоской конструкцией. На основании результатов проведенных испытаний силового кабеля на напряжение 3 кВ установлено, что грубые технологические дефекты в толще изоляции отсутствуют. Амплитуда разрядов в воздушных включениях не превышает 10 пКл при приложенном испытательном напряжении 5 кВ частоты 50 Гц. Показана эффективность выявления технологических дефектов в твердой композитной корпусной изоляции статорной обмотки турбо- и гидрогенераторов. Установлено, что в макетах, изоляция которых выполнена лентами меньшей толщины, технологические дефекты расположены в толще изоляции. Для макета, изоляция которого выполнена лентами большей толщины, технологические дефекты в виде расслоения расположены на границе раздела проводник – композитная изоляция. Библ. 19, табл. 1, рис. 7.

Ключевые слова: **технологические дефекты, частичные разряды, напряжение начала частичных разрядов, стеклослюдобумажная лента, амплитуда импульсов частичных разрядов, место расположения дефекта.**

Introduction. The most typical defects in solid high-voltage insulation during the production of electrical insulating structures are air inclusions. The reason for their occurrence in the thickness of the insulation may be manufacturing errors. For example, in power cables – insufficient drying of polymer granules before loading them into the extruder or the insulation cooling rate at the exit from the extruder is too high [1-3].

Internal gas inclusions during the process of vacuum-injection impregnation and baking are inevitably present in thermosetting insulation systems based on mica tapes used in high-voltage electrical machines. As a rule, each electric machine manufacturer uses its own design and manufacturing technology for coil and cabinet high-voltage insulation, which differs from other manufacturers in the types and thickness of materials used, in the number of layers and total insulation thickness, in duration and value of temperature effects during its manufacture [4 -6].

When operating under high voltage of power frequency of high voltage solid insulation, in air

inclusions partial discharges (PDs) occur. High-voltage insulation systems always have some background level of the PD, which does not have any significant effect on the life of the electrical insulation design. At the same time, partial discharges destroy high-voltage insulation, leading to a carburization of the zone around the defect. This is the «hidden» period of development of the defect. The development of a defect zone, sooner or later, leads to an arc breakdown of the entire insulating gap.

The goal of the paper is substantiation of the efficiency of detection of technological defects in high-voltage solid insulation of electrical insulating structures according to the characteristics of partial discharges.

Problem definition. For partial discharges there are no standard normalized values. The existing local norms and recommendations are valid only for small groups of electrical insulating structures [7, 8]. For this reason, in most cases, a quantitative assessment of the state of the insulation of electrical machines using partial discharge parameters can be made only by comparison with the results of previous measurements performed on the same equipment [9, 10].

For power cables with cross-linked polyethylene insulation, measurements of PD characteristics are performed with a smooth rise of the test voltage to twice the operating voltage of the power frequency for 10 seconds, and then slowly decrease to 1.73 from the nominal value [11]. PD level should not exceed 10 pC.

Partial discharges are characterized by the following parameters: voltage of the beginning of the PD; apparent charge amplitude; frequency of pulses of PD. In modern diagnostic systems, the following are used: maximum amplitude of partial discharge pulses of positive and negative polarity, measured in millivolts (mV); level of PD of positive and negative polarity (pC); amplitude-phase diagrams of PD pulses (dependence of the number of discharges with specific values of the apparent charge on the voltage phase of the power frequency – the so-called PD-diagrams) [7-10, 12-19].

The connection of the start of partial discharges with the thickness of the air inclusions. Suppose that in the insulation layer with thickness h there is an air inclusion with thickness x (Fig. 1,*b*). For quality insulation, usually $x << h$ [18].

In Fig. 1 the following is indicated: x – the thickness of air inclusion in the insulation; h – the thickness of the insulation; ε – the dielectric permeability of the dielectric, C_x – the inclusion capacitance; $C_{h\text{-}x}$ – the capacitance of the insulation part opposite the inclusion; C_0 – the capacitance of the rest of the insulation [18].

Let us determine what part U_x of external voltage U falls on inclusion with thickness x (Fig. 1,*b*).

Inclusion capacitance is defined as

$$C_x = \varepsilon_0 S_x / x , \quad (1)$$

where ε_0 is the dielectric constant (ε_0 = 8,85·10^{-12} F/m); S_x is the inclusion area, m^2.

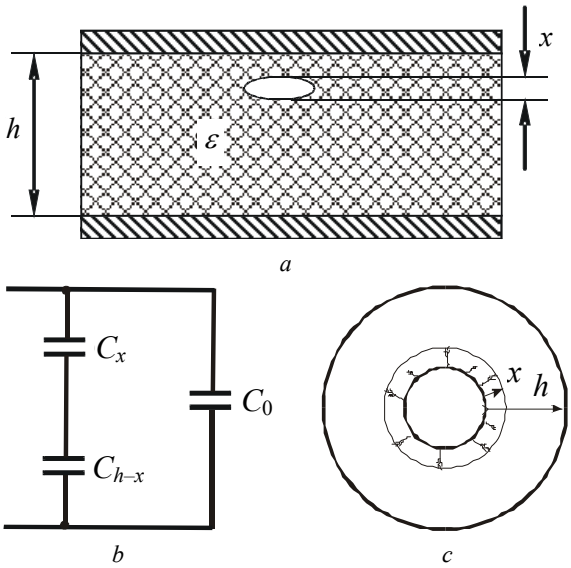

Fig. 1. Flat (*a*) and cylindrical (*c*) models for calculating the voltage of the beginning of the PDs on the basis of a capacitive replacement circuit (*b*) of insulation

Capacitance of a continuous dielectric layer located opposite the inclusion

$$C_{h-x} = \varepsilon\varepsilon_0 S_x / (h - x) . \quad (2)$$

From the capacitive replacement circuit (Fig. 1,*b*) we find U_x

$$U_x = U \frac{1/(\omega C_x)}{1/(\omega C_x) + 1/(\omega C_{h-x})} = U \frac{\varepsilon x}{h + (\varepsilon - 1)x} . \quad (3)$$

At $x \to 0$, the voltage on the inclusion tends to zero $U_x \to 0$ (because its own capacitance increases indefinitely), at $x \to h$ all external voltage falls on the inclusion $U_x \to U$ (because the inclusion takes up the entire insulating gap).

When the voltage on the inclusion reaches the level of the breakdown voltage U_{xbr} the inclusion breaks through

$$U_x \geq U_{xbr} . \quad (4)$$

Since here only part x of the insulating gap h breaks through, the discharge is accordingly called partial. The corresponding voltage on the electrodes, at which the condition (4) begins to be fulfilled, is the voltage of the beginning of the PD [12-18].

The breakdown voltage U_{xbr} of inclusion depends on its thickness x. This experimental relationship (Paschen curve) is shown in Fig. 2, curve 1. As the thickness x decreases, the breakdown voltage decreases and at x = 7 μm it reaches a minimum of U_{xbr} = 320 V ampl. = 226 V eff., and then even increases slightly [18]. In accordance with the empirical Paschen law, the breakdown voltage of the gas gap is a function of the product of pressure p and thickness x: $U_{xbr} = U_{xbr}(px)$.

Consider the conditions of occurrence of PD in the thickness of the insulation. The results of calculations according to (1) – (3) are shown in Fig. 2,*a* (curves 2 – 4) and Fig. 2,*b* (curves 2 – 5).

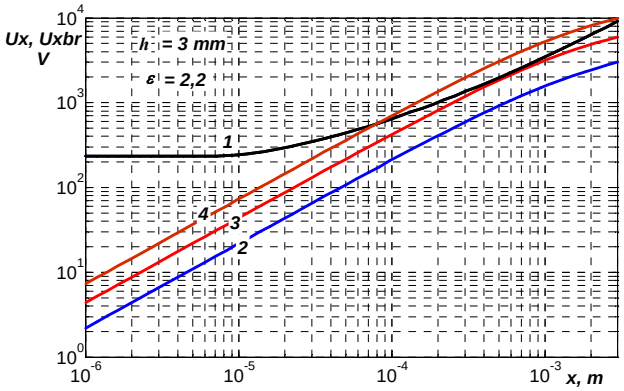

a

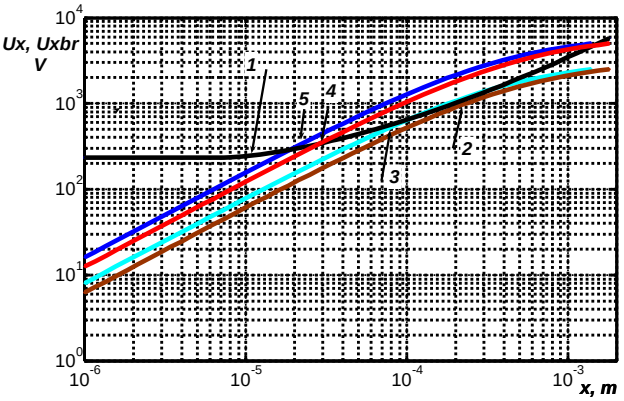

b

Fig. 2. Dependencies on the thickness (x) of the air inclusion of its breakdown voltage U_{xbr} and the calculated voltages U_x on the inclusions

Insulation voltages (Fig. 2,*a*): 2.5 kV (curve 2), 5 kV (curve 3) and 10 kV (curve 4). Insulation thickness h = 3 mm, dielectric permeability ε = 2.2 (polyethylene non-polar insulation of power cables). At voltage of 2.5 kV, the PDs are impossible in insulation (Fig. 2,*a*): curve 2 – $U_x(x)$ lies below curve 1 of the breakdown voltage of air inclusions. At voltage of 5 kV, the PDs in insulation are possible if it contains 0.6 mm thick air inclusions (intersection of curves 3 and 1). At voltage of 10 kV PDs in insulation are possible if it contains air inclusions with a thickness of 0.08 to 3 mm. Note that these are very large inclusions compared with a dielectric thickness of 3 mm. Measurement of the PDs allows to detect the presence of very coarse defects in the insulation.

Insulation voltages (Fig. 2,*b*): 2.5 kV (curve 2), 5 kV (curve 4) for an insulation thickness of 1.8 mm; 2.5 kV (curve 3) and 5 kV (curve 5) for an insulation thickness of 1.4 mm, respectively. The dielectric permeability is ε = 4.5 (characteristic values for composite glass-mica insulation of electrical machines). At voltage of 5 kV PDs in insulation with a thickness of 1.8 mm are possible if it has air inclusions with a thickness of 0.03 mm and more, i.e. from 30 μs (see Fig. 2,*b*, curve 4). For thinner composite insulation (1.4 mm) at applied voltage of 5 kV, air inclusions with a thickness of 20 μm and more are activated (see Fig. 2,*b*, curve 5).

Figure 3 shows the effect of the dielectric permeability of composite insulation with a thickness of 1.8 mm on the calculated voltages U_x on inclusions. Curve 2 corresponds to ε = 4.5; curve 3 – to ε = 4.8 for the same value of the applied voltage, equal to 5 kV. Increasing the dielectric permeability of composite insulation, i.e. the proportion of mica leads to a shift of the $U_x(x)$ curve to the region of smaller values of activated air inclusions (see curve 3 in Fig. 3).

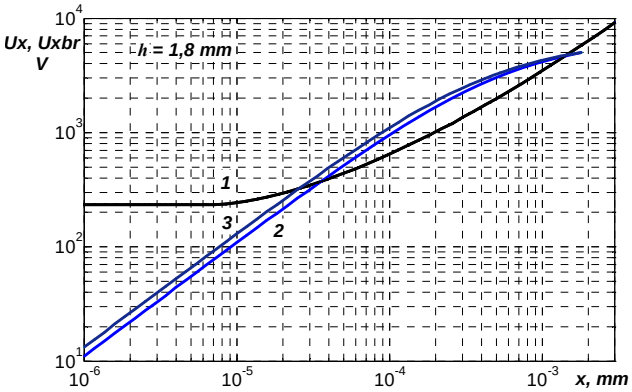

Fig. 3. The effect of the dielectric permeability of composite insulation on the calculated voltages U_x on air inclusions

The influence of the location of the defect on the voltage of the beginning of partial discharges in the power cable. In the process of cooling of extruded polymer insulation on a conductive core, the formation of internal voids in the thickness of the extruded insulation is possible. Here, the probability of formation of bubbles and voids near the core, whose temperature is higher in comparison with the outer layers of insulation, increases significantly [2]. It should be taken into account that the electric field strength near the core is also higher [18]. Let us determine the possible values of the voltage of the beginning of the PDs, using the model of a cylindrical air gap near the core (Fig. 1,*c*).

The results are presented in Fig. 4: the cross section of the conductive core is 25 mm^2, the thickness of the polyethylene insulation is 3 mm, ε = 2.2.

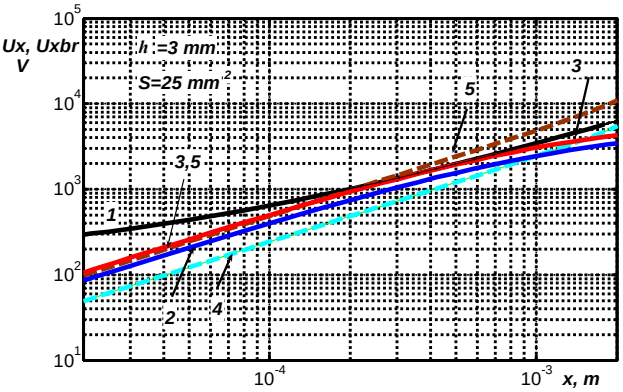

Fig. 4. The influence of the location of technological defect on the voltage of the beginning of the PDs in extruded power cable insulation

Curve 1 – breakdown voltage U_{xbr} of the inclusion; curves 2 and 3 correspond to the case of a technological air defect near the conductive core at 4 and 5 kV on the insulation; curves 4 and 5 – when the air defect is located near the outer surface of the insulation at voltage of 5 and 10 kV on the insulation, respectively. As the results of the calculation show, when applying the test voltage, technological defects located near the conductive core are activated first. When the voltage on the insulation is 5 kV, PDs arise in inclusions with a thickness of 200 μs. At voltage of 10 kV, air inclusions located near the insulation surface are not activated (see Fig. 4, curve 5).

Efficiency of detection of technological defects in solid insulation according to the characteristics of PDs. Figure 5 shows the PDs oscillogram in a sample of a power cable for voltage of 3 kV (cross section of a conductive core 25 mm^2, thickness of polyethylene insulation 3 mm). In the thickness of the insulation there are air inclusions, which are activated at test voltage of 5 kV 50 Hz. The amplitude of the PDs does not exceed 10 pC, which corresponds to the requirements of the Standard [11]. It should be noted that at the operating voltage partial discharges in the cable do not occur.

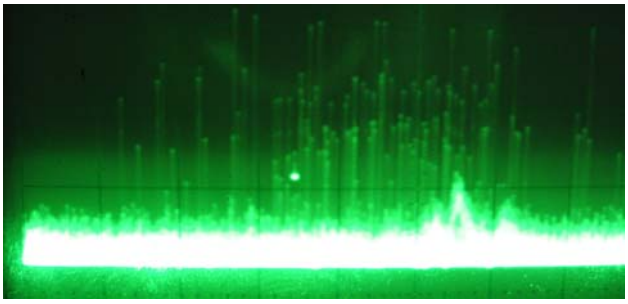

Fig. 5. PDs oscillogram in the thickness of the solid polyethylene insulation of the power cable (the mark in the center of the sweep is a calibration signal of amplitude 2 pC)

Experimental studies on the detection of technological defects in high-voltage composite case insulation of the stator winding of the turbo- and hydrogenerators are carried out on 5 layouts of the same thickness. The insulation of the layouts is made of glass-mica paper tapes of different thickness from different manufacturers (6 samples for each layout).

The PD monitoring method is based, for example, on the use of a portable analyzer with a set of epoxy-mica capacitors with a capacitance of 80 pF as capacitive sensors, which allow measuring PDs in the high frequency range, in which the PD amplitude significantly exceeds the interference amplitude [8-10, 19]. This allows to automatically reliably separate the PDs and interference. The principle of the system operation is based on the detection of voltage pulses of partial discharges arising inside the insulation, using PD sensors, followed by their analog-digital conversion using a PD meter and displaying the PD amplitude of both positive and negative polarity. It should be taken into account that the maximum voltage of the PD pulse in mV is measured (see Fig. 5). The suppliers of relevant measuring equipment indicate the measured value not with a voltage symbol (U), but with a charge symbol (Q), assuming that there is an obvious connection between voltage and charge. The proportionality factor is the electrical capacitance of an insulation system, for example, a stator winding, which can always be measured.

An effective way to determine the state of the insulation system is to compare the results with the database [9. 10] presented in Table 1.

Table 1

Evaluation of insulation by maximum PD pulse amplitude values

PD category	PD pulse amplitude, mV
Minor	0-45
Low	46-98
Typical	99-210
Moderate	211-412

Figure 6 shows the results of measurements of the maximum amplitude of partial discharge pulses of positive and negative polarity in layouts with high-voltage solid composite insulation based on glass-mica paper tapes at voltage of 3.6 kV (Fig. 6,*a*) and 6 kV (Fig. 6,*b*).

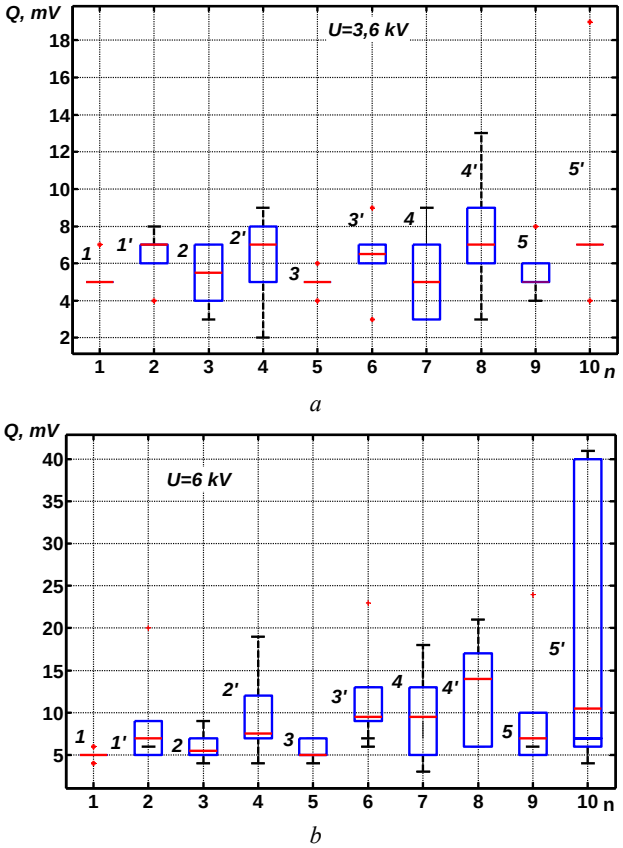

Fig. 6. The results of the statistical distribution of the maximum amplitude of partial discharge pulses depending on the applied voltage of power frequency in composite solid high-voltage insulation

The thickness of the tapes: 1 – h = 0.14 mm, 2 – h = 0.14 mm, 3 – h = 0.15 mm, 4 – h = 0.18 mm, 5 – h = 0.18 mm. The amplitude of the partial discharge pulses of positive polarity is denoted as 1, 2, .., 5; the amplitude of the partial discharge pulses of negative polarity: 1', 2', ..., 5', respectively. PD pulses of negative polarity occur at a positive half-wave of the test voltage of power frequency, positive – at a negative half-wave of voltage.

Comparison of positive and negative PD pulses indicates that the discharges occur exactly inside the insulation for the layouts, the thickness of the tapes of which is less than 0.18 mm (Fig. 7,*a*). The amplitude of the discharges of positive and negative polarity is almost the same (compare 1 and 1', 2 and 2', 3 and 3', 4 and 4', Fig. 6,*b*). These results are consistent with the calculated dependencies (see Fig. 2,*b* and Fig. 3). For samples with glass-mica paper tape 0.18 mm thick, the amplitude of negative polarity pulses is almost 4 times higher than the amplitude of positive polarity pulses (compare 5 and 5', Fig. 6,*b*).

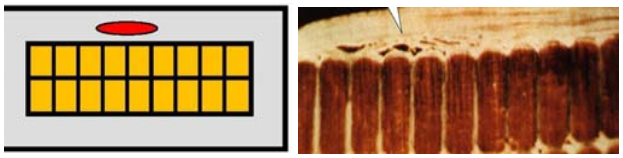

a *b*

Fig. 7. The locations of technological defects in the composite insulation of the windings of electrical machines

Obviously, such a difference is due to the location of the technological defect in the form of a bundle at the interface between the conductor and composite insulation (Fig. 7,*b*). At voltage of 6 kV, the amplitude of the discharge pulses reaches an upper value of 40 mV in the category of the PDs as a minor level (see Table 1).

Conclusions. The dependencies on the thickness of air inclusion of its breakdown voltage and calculated voltages on inclusions for a flat and cylindrical insulation model are obtained. At the same applied voltages to high-voltage insulation, in the latter case, air inclusions of smaller thickness are activated in comparison with the flat structure.

The possible values of the voltage of the beginning of partial discharges and the range of activated technological defects are determined depending on the location of the air inclusion in the structure of the power cable of a coaxial design.

The efficiency of detection of technological defects in solid high-voltage composite case insulation of the stator winding of turbo- and hydrogenerators is shown. Based on the comparison of the amplitude of the pulses of partial discharges of positive and negative polarity, the location of technological defects in the structure is determined.

The results of the studies confirm the efficiency of registration of partial discharges in high-voltage solid insulation for detecting defects at the technological stage of manufacturing of electrical insulating structures, as well as for setting up the technological process itself.

REFERENCES

1. Leonov V.M., Peshkov I.B., Ryazanov I.B., Kholodnyy S.D. *Osnovy kabelnoy tehniki* [Basics of cable technology]. Moscow, Akademiya Publ., 2006. 432 p. (Rus).

2. Bezprozvannych G.V., Mirchuk I.A., Kyessayev A.G. Technological parameters of the cooling mode of polymer insulation of power cables. *Electrical engineering & electromechanics*, 2019, no.3, pp. 44-49. **doi: 10.20998/2074-272X.2019.3.07.**

3. Rao Natti S., Shott Nik R. *Tekhnologicheskie raschety v pererabotke plastmass* [Technological calculations in plastics processing]. Saint Petersburg, Professiya Publ., 2013. 200 p. (Rus).

4. Ogonkov V.G., Serebryannikov S.V. *Elektroizoliatsionnye materialy i sistemy izoliatsii dlia elektricheskikh mashin. V dvukh knigakh. Kn. 2* [Electrical insulation materials and insulation systems for electrical machines. In 2 books. Book 2]. Moscow, Publishing house MEI, 2012. 304 p. (Rus).

5. Pak V.M., Trubachev S.G. *Novye materialy i sistemy izoliatsii vysokovol'tnykh elektricheskikh mashin* [New materials and systems for isolation of high-voltage electrical machines]. Moscow, Energoatomizdat Publ., 2007. 416 p. (Rus).

6. Bezprozvannych G.V., Boyko A.N., Roginskiy A.V. Effect of a dielectric barrier on the electric field distribution in high-voltage composite insulation of electric machines. *Electrical engineering & electromechanics*, 2018, no.6, pp. 63-67. **doi: 10.20998/2074-272X.2018.6.09.**

7. *IEEE Standards 1434. Guide for the measurement of partial discharges in AC electric machinery*. IEEE Park Avenue, New York, USA. 2014. 89 p.

8. CIGRE Working Group A1.01.06 Application. *Of on-line partial discharge tests to rotating machines*. CIGRE. December 2010. 58 p.

9. Iris Power TGA-BTM. *Periodic On-line Partial Discharge Monitoring Using a Portable Instrument for Motors and High Speed Turbine Generators*. Iris Power Ver 5. 08/10. Canada, 2010.

10. *Interpretation of PD results – on-line testing*. Version 3.2 Iris QMS 08/10. Ver. 3.2. 2008.

11. Shidlovsky A.K., Shcherba A.A., Zolotarev V.M., Podoltsev A.D., Kucheryavaya I.N. *Kabeli s polimernoi izoliatsiei na sverkhvysokie napriazheniia* [Polymer insulation cables for ultra-high voltages]. Kyiv, IED of NASU Publ., 2013. 552 p. (Rus).

12. Kuchinsky G.S. *Chastichnye razriady v vysokovol'tnykh konstruktsiiakh* [Partial discharges in high voltage structures]. Leningrad, Energiia Publ., 1979. (Rus).

13. Vdoviko V.P. *Chastichnye razriady v diagnostirovanii vysokovol'tnogo oborudovaniia* [Partial discharges in diagnosing high-voltage equipment]. Novosibirsk, Nauka Publ., 2007. 55 p. (Rus).

14. Naboka B.G., Bezprozvannych G.V., Gladchenko V.Ya. Method of measuring the differential amplitude spectra of partial discharge pulses. *Electricity*, 1990, no.1, pp. 71-74. (Rus).

15. Naboka B.G., Bezprozvannych G.V., Gladchenko V.Ya. Diagnostics of high-voltage insulation using multichannel analyzers. *Electricity*, 1991, no.5, pp. 5-9. (Rus).

16. Bezprozvannych G. V., Kessaev A. G. Analysis of the field structure and justification of the diagnostics voltage for partial insulation discharges of shielded twisted pairs. *Electrical*

engineering & electromechanics, 2014, no.6, pp. 61-65. (Rus). **doi: 10.20998/2074-272X.2014.6.11.**
17. Bezprozvannych A.V. Ways of representation of differential peak spectra of pulses of partial discharges in solid insulation. *Technical electrodynamics*, 2011, no.4, pp. 12-19. (Rus).
18. Bezprozvannych A.V. High electric field and partial discharges in bundled cables. *Technical electrodynamics*, 2010, no.1, pp. 23-29. (Rus).
19. IEC Standard 60270. *High-voltage test techniques – Partial discharge measurements*. IEC, 2000. 55 p.

Received 05.04.2019

G.V. Bezprozvannych[1], *Doctor of Technical Science, Professor,*
A.G. Kyessayev[1], *Candidate of Technical Science,*
I.A. Mirchuk[2], *Postgraduate Student,*
A.V. Roginskiy[3] , *Postgraduate Student,*

[1] National Technical University «Kharkiv Polytechnic Institute», 2, Kyrpychova Str., Kharkiv, 61002, Ukraine,
phone +380 57 7076010,
e-mail: bezprozvannych@kpi.kharkov.ua
[2] Private Joint Stock Company «Ukraine Scientific-Research Institute of Cable Industry»,
2-P, Promychlennaya Str., Berdyansk, Zaporozhye Region, 71101, Ukraine,
phone +380 66 8288554,
e-mail: garik710@ukr.net
[3] SE Plant Electrotyazhmash,
299, Moskovsky Ave., Kharkiv, 61089, Ukraine,
e-mail: roginskiy.av@gmail.com

How to cite this article:
Bezprozvannych G.V., Kyessayev A.G., Mirchuk I.A., Roginskiy A.V. Identification of technological defects in high-voltage solid insulation of electrical insulation structures on the characteristics of partial discharges. *Electrical engineering & electromechanics*, 2019, no.4, pp. 53-58. **doi: 10.20998/2074-272X.2019.4.08.**

UDC 621.317.326 **doi: 10.20998/2074-272X.2019.4.09**

M.I. Boyko, S.O. Syomkin

INVESTIGATION OF AMPLITUDE-TEMPORAL CHARACTERISTICS OF A HIGH-VOLTAGE RESISTIVE VOLTAGE DIVIDER

Purpose. Determination of the possibility of using the developed autonomous voltage divider for measuring high-voltage pulses with sharpened fronts (down to 1 ns). Methodology. We use the technique to determine the division ratio of the divider using a calibrated oscillator and oscilloscope. To determine the rise time of the transition characteristic of the divider, we use an experimental technique based on a high-voltage pulse generator with a steep front and computer simulation using circuit program Micro-Cap. Results. Oscillograms of high-voltage nanosecond pulses with subnanosecond fronts are experimentally obtained using an autonomous resistive voltage divider. A computer simulation of the operation of the created divider in various modes is carried out. Originality. We have shown that an autonomous shielded resistive high-voltage voltage divider can have a rise time less than 1 ns. The values of the parasitic parameters of the divider, which lead to a distortion of the sharpened pulse front with a rise time of ≈0.1 ns, are established. Practical value. The divider can be used to measure the characteristics of high-voltage pulses with a steep front (up to 1 ns as the lower limit). References 7, figures 15.

Key words: **voltage divider, high-voltage pulse generator, computer simulation, electrical circuit, rise time, transient response, pulse front.**

Мета. Визначення можливості використання розробленого автономного дільника напруги для вимірювання високовольтних імпульсів з загостреними фронтами (до 1 нс). Методика. Застосовано методику визначення коефіцієнта ділення дільника за допомогою каліброваного генератора і осцилографа. Для визначення часу наростання перехідної характеристики дільника використовувалась експериментальна методика на основі генератора високовольтних імпульсів з крутим фронтом і комп'ютерне моделювання з використанням програми схемотехнічного моделювання Micro-Cap. Результати. Експериментально отримано осцилограми високовольтних наносекундних імпульсів із субнаносекундними фронтами за допомогою створеного автономного резистивного дільника напруги. Проведено комп'ютерне моделювання роботи створеного дільника в різних режимах. Наукова новизна. Показано, що автономний екранований резистивний дільник високої напруги може мати час наростання менше, ніж 1 нс. Установлені величини паразитних параметрів дільника, що викликають викривлення загостреного фронту імпульсів з часом наростання ≈0,1 нс. Практична значущість. Дільник можна застосовувати для вимірювання характеристик високовольтних імпульсів з крутим фронтом (до 1 нс у якості нижньої границі). Бібл. 7, рис. 15.

Ключові слова: **дільник напруги, генератор високовольтних імпульсів, комп'ютерне моделювання, електрична схема, час наростання, перехідна характеристика, фронт імпульсу.**

Цель. Определение возможности использования разработанного автономного делителя напряжения для измерения высоковольтных импульсов с обостренными фронтами (до 1 нс). Методика. Применена методика определения коэффициента деления делителя при помощи калиброванного генератора и осциллографа. Для определения времени нарастания переходной характеристики делителя использовалась экспериментальная методика на основе генератора высоковольтных импульсов с крутым фронтом и компьютерное моделирование с использованием программы схемотехнического моделирования Micro-Cap. Результаты. Экспериментально получены осциллограммы высоковольтных наносекундных импульсов с субнаносекундными фронтами при помощи созданного автономного резистивного делителя напряжения. Проведено компьютерное моделирование работы созданного делителя в различных режимах. Научная новизна. Показано, что автономный экранированный резистивный делитель высокого напряжения может иметь время нарастания менее 1 нс. Установлены величины паразитных параметров делителя, приводящих к искажению обостренного фронта импульсов с временем нарастания ≈0,1 нс. Практическая значимость. Делитель можно применять для измерения характеристик высоковольтных импульсов с крутым фронтом (до 1 нс как нижней границы). Библ. 7, рис. 15.

Ключевые слова: **делитель напряжения, генератор высоковольтных импульсов, компьютерное моделирование, электрическая схема, время нарастания, переходная характеристика, фронт импульса.**

Introduction. In high-voltage pulse technology, the solution of the problem of measuring nanosecond differences (first of all, fronts) of high-voltage pulses at different loads is relevant [1-5]. In the work, the results of which are presented in [6], a compact autonomous resistive shielded low-resistive voltage divider (ARSLVD) is developed and tested to measure the record amplitude-temporal characteristics of high-voltage pulses from a generator in an apparatus for broadband electromagnetic pulse therapy (ABEMPT). The generator design is described in [6]. If the generator in ABEMPT operated without the use of a sharpening of the pulse front, then the voltage divider transmitted the expected pulse shape, including its front (≈2.5 ns), without distortion. If the mode of operation of the generator with the sharpening of the pulse front was used, then the divider introduced significant distortions at the front of the measured pulses. To register pulses from an ABEMPT generator, a C7-19 analog oscilloscope with a 5 GHz

bandwidth was used. It is known [2] that for a satisfactory measurement of the amplitude-temporal characteristics of pulses, the rise time of the transient characteristic of a voltage divider (VD) should be noticeably shorter than the measured pulse front duration. Since the sharpening of the pulse front using spark gaps – sharpeners leads to a shortening of the front by about 10 times, the required rise time of the transient characteristic of the voltage divider used should be shorter than 0.2 ns for measuring pulses with sharpened fronts without significant distortion.

The definition of a scientific problem and the justification of its relevance with the identification of unsolved problems. In high-voltage pulse technology there is the problem of measuring the amplitude-temporal characteristics of high-voltage pulses with high accuracy [1]. Its relevance is determined by the fact that for different high-voltage electrical technologies, radars, high-voltage tests of various equipment high voltage pulses with a very steep front (units ns or less) are required [1-5].

The goal of the work is the determination of the possibility of using the developed autonomous voltage divider for measuring high-voltage pulses with sharpened fronts (up to 1 ns).

Tasks that need to be solved to achieve the goal:

- to determine the rise time of the transient response of an autonomous compact resistive voltage divider developed;
- to create a computer model of a two-stage resistive voltage divider;
- to determine what caused the appearance of high-frequency oscillations with large amplitude at the front of the measured high-voltage pulses with an extremely steep front (0.1 ns);
- to determine whether a combination of a short transient response (less than 1 ns) of the created autonomous voltage divider with a large division ratio (more than 500) is possible.

The circuit, the design of the divider and the experimental results to determine its division ratio and the rise time of the transient response. The first mention of the divisor considered in this paper is in [6]. The electric circuit of the divider is shown in Fig. 1.

According to measurements made with a multimeter M890G, R_1 = 73.8 Ω, R_2 = 3 Ω, R_3 = 23.9 Ω, R_4 = 1.7 Ω, R_5 = 47.2 Ω taking into account the uncertainty (error) in the readings of the multimeter of 0.4 Ω.

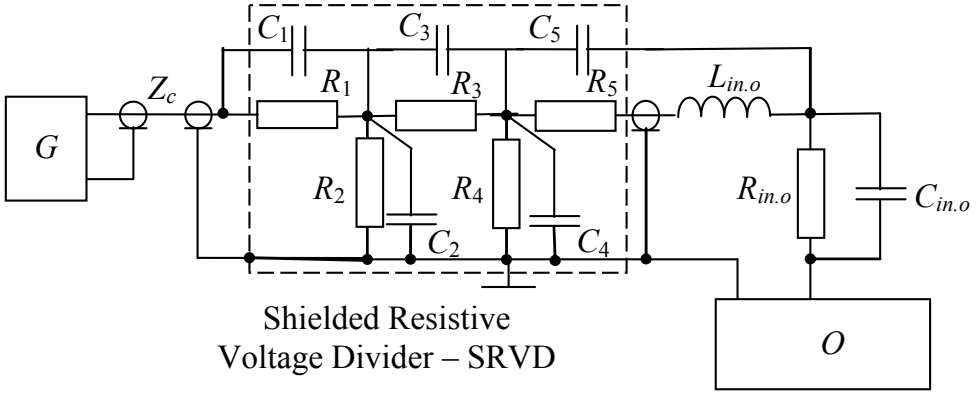

Fig. 1. The electrical circuit of the system of the generator *G* of pulses, resistive divider taking into account the parasitic capacitances and inductance $L_{in.o}$, coaxial broadband connecting cable with a characteristic impedance Z_c = 100 Ω and oscilloscope with input resistance $R_{in.o}$, input capacitance $C_{in.o}$

The divider is designed and manufactured as autonomous, collapsible in an aluminum case. At the input and output of the divider, coaxial connectors-sockets CP-50-165ФВ are applied, the pulsed electrical strength along the insulation surface of which determines the maximum allowable working voltage of the divider. Photo of the divider is presented in Fig. 2. The divider is made on the volume resistors TBO-1, TBO-0,5 and TBO-0,25 and is two-stage. The first stage is formed by the resistances R_1 (high-voltage arm of the first stage of the divider) and R_2 with a chain connected in parallel to it (the low-voltage arm of the first stage of the divider), if generator *G* is connected to the divider as in Fig. 1, i.e. to the 75-Ω input, and has a division ratio $K_{75.1}$.

Fig. 2. Photo of autonomous resistive shielded low-resistive voltage divider (ARSLVD)

The second stage is formed by the resistances R_3 (high voltage arm of the second stage of the divider) and R_4 (low voltage arm of the second stage of the divider) and has a division ratio $K_{75.2}$. Resistance R_5 in

combination with the rest of the resistances of the divider forms a matching resistance equal to the characteristic impedance of 50 Ω of the coaxial cable, if one is connected between the output connector of the divider and the input of the oscilloscope. In this case, the input resistance of the oscilloscope can be either low-resistance (for example, 50 Ω) or high-resistance (for example, 1 MΩ): this does not lead to additional parasitic reflections in the cable as a long line. The total division factor of the divider can have two values: $K_{75high}=K_{75.1}K_{75.2}$, if the input of the oscilloscope is high-resistance, and $K_{75low}\approx 2K_{75.1}K_{75.2}$, if the input is low-resistance, i.e. oscilloscope input impedance $R_{in.o}$=50 Ω. This allows matching the coaxial cable (if used) with a wave resistance of 50 Ω connecting the 50-Ω output of the divider with the input resistance of the oscilloscope $R_{in.o}$=50 Ω from both ends. The body-screen of the divider can be conditionally divided into five component parts: two extreme cylindrical, each connected to its own coaxial connector CP-50-165ФВ, one central cylindrical, separated from the extreme cylindrical parts by two disk parts. In one extreme cylindrical part, the resistance R_1 = 73.8 Ω is located. In the other extreme cylindrical part – resistance R_5 = 47.2 Ω. In the central cylindrical part of the body, the resistance R_3 = 23.9 Ω is located. In the disk parts of the body there are resistors R_2 = 3.0 Ω and R_4 = 1.7 Ω. Resistance R_2 is formed by 7 TBO-0,25 resistors with nominal resistances of 22 Ω each, connected in parallel (see photo in Fig. 2). Resistance R_4 is formed by 4 TBO-0, 5 resistors with nominal resistances of 6.8 Ω each, connected in parallel.

If we do not take into account the influence of parasitic inductances and capacitances, then the division factor K_{75high} of the considered divider when applying a signal from the pulse generator to its 75-Ω input and using an oscilloscope with a high-resistance input can be defined as follows (see circuit in Fig. 1):

$$K_{75.1}=[R_1+R_2(R_3+R_4)/(R_2+R_3+R_4)]/[R_2(R_3+R_4)//(R_2+R_3+R_4)];$$

$$K_{75.2}=(R_3+R_4)/R_4.$$

Then:

$$K_{75high}=[R_1+R_2(R_3+R_4)/(R_2+R_3+R_4)]/[R_2(R_3+R_4)/ /(R_2+R_3+R_4)](R_3+R_4)/R_4 =$$

$$= [73,8+3(23,9+1,7)/(3+23,9+1,7)]/ /[3(23,9+1,7)/(3+23,9+1,7)](23,9+1,7)/1,7\approx$$

$$\approx (76,485/2,685)\cdot 25,6/1,7 \approx 28,5\cdot 15,1=430,35.$$

So,

$$K_{75high}=K_{75.1}K_{75.2}\approx 28,5\cdot 15,1 = 430,35.$$

Here $K_{75low} \approx 2K_{75.1}K_{75.2} \approx 2\cdot 28,5\cdot 15,1 = 860,7$.

The input and output of the divider can be reversed, since the same coaxial connectors CP-50-165ФВ, capable of withstanding pulse voltages up to 6 kV, are installed at the input and output. This changes the division ratio of the divider.

The division ratio K_{50high} of the considered divider when applying a signal from the pulse generator to its 50-Ω input and using an oscilloscope with a high-resistance input $K_{50high}=K_{50.1}K_{50.2}$.

$$K_{50.1}=[R_5+R_4(R_3+R_2)/(R_2+R_3+R_4)]/[R_4(R_3+R_2)/(R_2+R_3+R_4)];$$

$$K_{50.2}=(R_3+R_2)/R_2.$$

$$K_{50high}=[R_5+R_4(R_3+R_2)/(R_2+R_3+R_4)]/[R_4(R_3+R_2)/ /(R_2+R_3+R_4)](R_3+R_2)/R_2=[47,2+1,7\ (23,9+3)/ /(3+23,9+1,7)]/[1,7(23,9+3)/(3+23,9+1,7)]\cdot(23,9+3)/3 \approx$$

$$\approx (48,799/1,599)26,9/3 \approx 30,52\cdot 8,97 \approx 273,76.$$

Then $K_{50low}\approx 2K_{50.1}K_{50.2}\approx 2\cdot 30,52\cdot 8,97 = 547,52$, if the oscilloscope input resistance is $R_{in.o}$=75 Ω.

The input resistances of the divider are selected as low-resistance, since it is the low-resistance resistive voltage dividers that have the shortest rise time of the transient characteristic [2]. Specific values of 75 Ω and 50 Ω of input resistances are chosen based on the fact that the characteristic impedances of the most common coaxial cables in practice are 75 Ω and 50 Ω, and the input resistance of high-speed oscilloscopes with a wide (more than 1 GHz) bandwidth is, usually, 50 Ω.

As a generator in the experimental determination of the division factor of the divider, we used a C1-74 oscilloscope calibrator, which generates sinusoidal signals with known amplitude-frequency characteristics.

The division factor of the divider has been experimentally determined in two stages. At the first stage, we determined the $K_{75.1}$ division factor of the first stage of the divider as the ratio of the voltage amplitude from the calibrator at the 75- Ω input of the divider to the voltage at the low-voltage arm of the first cascade divider. At the second stage, $K_{75.2}$ has been defined as the ratio of the voltage amplitude from the calibrator at the input of the second stage of the divider (at series-connected resistances R_3 and R_4, $R_3+R_4 \approx 25.6$ Ω) to the voltage at the low-voltage arm of the second stage of the divider (on resistance R_4).

At the first stage, the signal from the calibrator has been fed through a coaxial tee to the 75- Ω input of the divider and to the input (1 MΩ, 30 pF) of the C8-13 oscilloscope. At the same time, the 50-Ω input (output) of the divider has not been connected to external devices. Thus, the signal from the calibrator at the input of the divider has been measured. The oscillogram of this signal is presented in (Fig. 3).

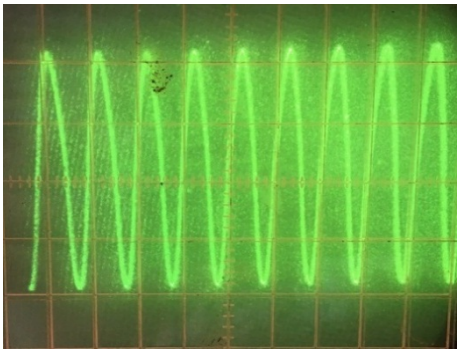

Fig. 3. Oscillogram of the voltage pulse from the calibrator of the C1-74 oscilloscope loaded on the input resistance $R_{in} \approx 75$ Ω of the voltage divider (the scale along the time axis it is 1 μs/div, and along the signal axis is 0.1 V/div)

After that, the signal has been measured – the voltage on R_2 = 3 Ω in the disk part of the divider case with the remainder of the divider connected in parallel to R_2 – the low voltage arm of the first stage of the divider. The middle part of the body was removed from the

voltage divider, the C8-13 oscilloscope input has been connected to R_2 using a coaxial cable, and The 75-Ω divider input has been connected to the calibrator with a separate coaxial cable. The result of measurements in the form of an oscillogram of voltage at R_2 – the output of the first cascade of this two-stage divider is shown in Fig. 4.

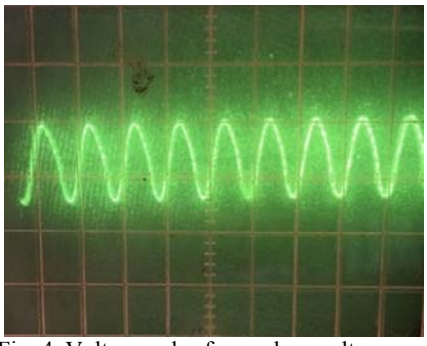

Fig. 4. Voltage pulse from a low-voltage arm the first stage of the voltage divider (the scale along the time axis is 1 μs/div, and along the process axis it is 0.01 V/div)

The ratio of the voltage amplitudes on the oscillograms in Fig. 3, 4 represents the experimentally determined division factor KE75.1 of the first cascade: $K_{E75.1} \approx 27.1$, which, taking into account the uncertainty (error) of measurements using oscillographs ≈ 10 %, is in good agreement with the value $K_{75.1} \approx 28.5$ obtained by calculation by the resistances of the divider elements $R_1 \ldots R_4$.

At the second stage, the voltage (signal) from the calibrator has been fed through a coaxial tee to the input of the second stage of the divider, i.e. for series connection of resistances R_3 and R_4, and to the input (1 MΩ, 30 pF) of the recording oscilloscope C8-13. The 50-Ω input (output) of the divider remained not connected to external devices, and the output of resistance R_3, initially connected to the corresponding pins of R_1 and R_2, has been disconnected from the connection point. This was done to ensure that the very low resistance $R_2 = 3$ Ω does not short the calibrator output. Thus, the signal from the calibrator at the input of the second stage of the divider has been measured. The oscillogram of this signal is presented in Fig. 5. Its amplitude is less than on the oscillogram in Fig. 3, because the calibrator in this case is loaded on the total resistance $R_3+R_4 \approx 25.6$ Ω, significantly less than the input resistance of the divider ≈ 75 Ω, which was the load of the calibrator in the first stage.

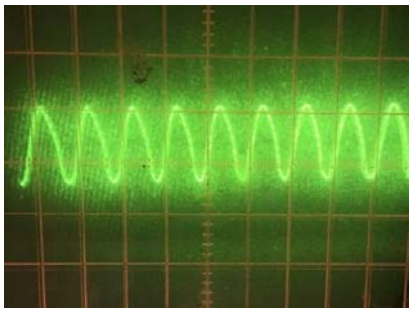

Fig. 5. The voltage pulse from the calibrator of the C1-74 oscilloscope at the input of the second stage of the divider (the scale along the time axis is 1 μs/div, and along the process axis it is 0.1 V/div)

Next, the signal has been measured – voltage on $R_4 = 1.7$ Ω (low-voltage arm of the second stage of the divider) in the disk part of the divider case. The CP-50 connector of the divider, connected by its central output to R_4 through R_5, has not been connected to external devices. The C8-13 oscilloscope input has been connected to R_4 with the help of a coaxial cable, and the input of the second stage of the divider has been connected to the calibrator with a separate coaxial cable. The measurement result in the form of the oscillogram of voltage on R_4 – the output of the second stage of this two-stage divider is shown in (Fig. 6).

Figure 7 shows an oscillogram of voltage from the low-voltage arm of the second stage of the divider for the mode in which in parallel to the high-resistance ($R_{in.o}$=1 MΩ) C8-13 oscilloscope input a 50 Ohm load has been connected.

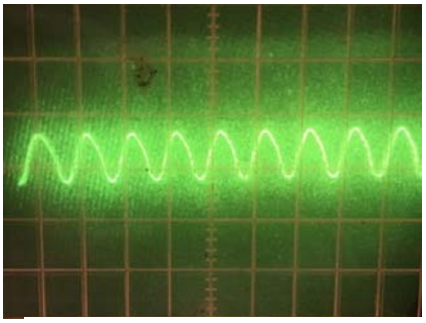

Fig. 6. The voltage pulse from the low voltage arm of the second stage of the voltage divider at the input resistance of the oscilloscope $R_{in.o}$ = 1 MΩ (the scale along the time axis is 1 μs/div, and along the process axis it is 0.01 V/div)

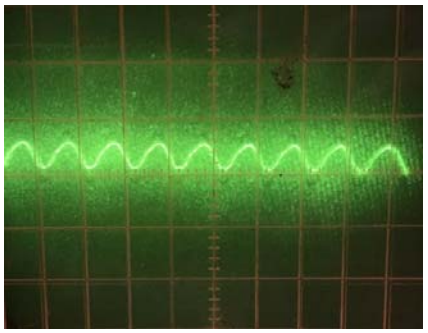

Fig. 7. The voltage pulse from the low-voltage arm of the second stage of the voltage divider when connecting a load of 50 Ω in parallel to the input resistance of the oscilloscope $R_{in.o}$=1 MΩ (the scale along the time axis is 1 μs/div, and along the process axis it is 0.01 V/div)

From Fig. 6, 7 it follows that connecting of a 50 Ω load in parallel to the input resistance of the oscilloscope $R_{in.o}$=1 MΩ reduces the voltage amplitude from the output of the second stage of the divider by about half, i.e. approximately doubles the division ratio of the divider.

The ratio of the voltage amplitudes on the oscillograms in Fig. 5, 6 represents the experimentally determined division factor $K_{E75.2}$ of the second stage: $K_{E75.2} \approx 15.5$, which, taking into account the uncertainty (error) of measurements using oscillographs ≈ 10 %, is in good agreement with the value $K_{E75.2} \approx 15.1$ obtained by calculation using the resistances of the divider elements $R_3 = 23.9$ Ω, $R_4 = 1.7$ Ω.

So,

$$K_{E75high} = K_{E75.1}K_{E75.2} \approx 27{,}1 \cdot 15{,}5 = 420{,}05;$$

$$K_{E75low} \approx 2K_{E75.1}K_{E75.2} \approx 840{,}1;$$

$$K_{75high}/K_{E75high} = K_{75low}/K_{E75low} = 430{,}35/420{,}05 \approx 1{,}0245,$$

i.e. the relative error (uncertainty) between the calculated value and the experimental value of the division factor for this divider does not exceed 2.5 %.

Determination of the rise time of the transition characteristics of the divider in the experiment. There are two main options for determining the rise time in the transmission system [2]. The first option implies as the rise time a period, during which the measured value (for example, voltage) increases from 0.1 to 0.9 of its maximum value. In the second variant, the rise time is the time during which the output signal reaches a certain percentage of the steady-state value when a rectangular pulse or voltage jump $u_1(t)$ of a given amplitude U_0 is input to the system

$$u_1(t) = U_0 1(t),$$

where $1(t)$ is the unit function:

$$1(t) = \begin{cases} 0 & \text{at} \quad t < 0; \\ 1 & \text{at} \quad t \geq 0. \end{cases}$$

If a jump occurs after a time interval τ after the origin, then the unit function is zero at $t<\tau$, equal to 1 at $t\geq\tau$, and is denoted by $1(t-\tau)$ [7].

The voltage $u_1(t)$ causes the voltage $u_2(t)$ – the response to a rectangular pulse in the output of the system (in our case, in the output of the voltage divider connected to the oscilloscope input and matched with it). The dimensionless function of time

$$h(t) = u_2(t)/ U_0 \qquad (1)$$

is called a transition function or temporal characteristic of the system [2, p. 39], as well as the transient response of the circuit [7, p. 116].

In our case, $h(t)$ is represented as oscillograms. Here, the voltage at the output of the divider $u_2(t)$ can be determined using the Duhamel integral as a response to the input signal $u_1(t)$ of any form [2, p. 40]:

$$u_2(t) = u_1(+0)h(t) + \int_{\tau=0}^{\tau=t} u_1'(t-\tau)h(\tau)d\tau \,. \qquad (2)$$

Since in our case the duration of the pulse front from the generator, both when using sharpening and without sharpening, is much less than the half-drop time (drop to half the pulse amplitude) ≈ 50 ns, as far as in the first approximation, the pulse from the generator can be considered as a voltage jump (square pulse). Therefore, the time derivative $u'_1(t-\tau)$ in (2) can be taken equal to zero, since the function u_1 itself has only two values (two constants): 0 for $t<\tau$ and 1 for $t\geq\tau$ (taking into account the limits of integration – at $t = \tau$), and formula (2) is simplified to:

$$u_2(t) = u_1(+0)h(t). \qquad (3)$$

If we take into account that $u_1(+0) = U_0$ in (1), then (2) fully corresponds to (1).

Fig. 8 shows the oscillograms of voltage pulses from the output of the voltage divider under study, connected to the input of C7-19 oscilloscope with 5 GHz bandwidth and an input active resistance of 50 Ω.

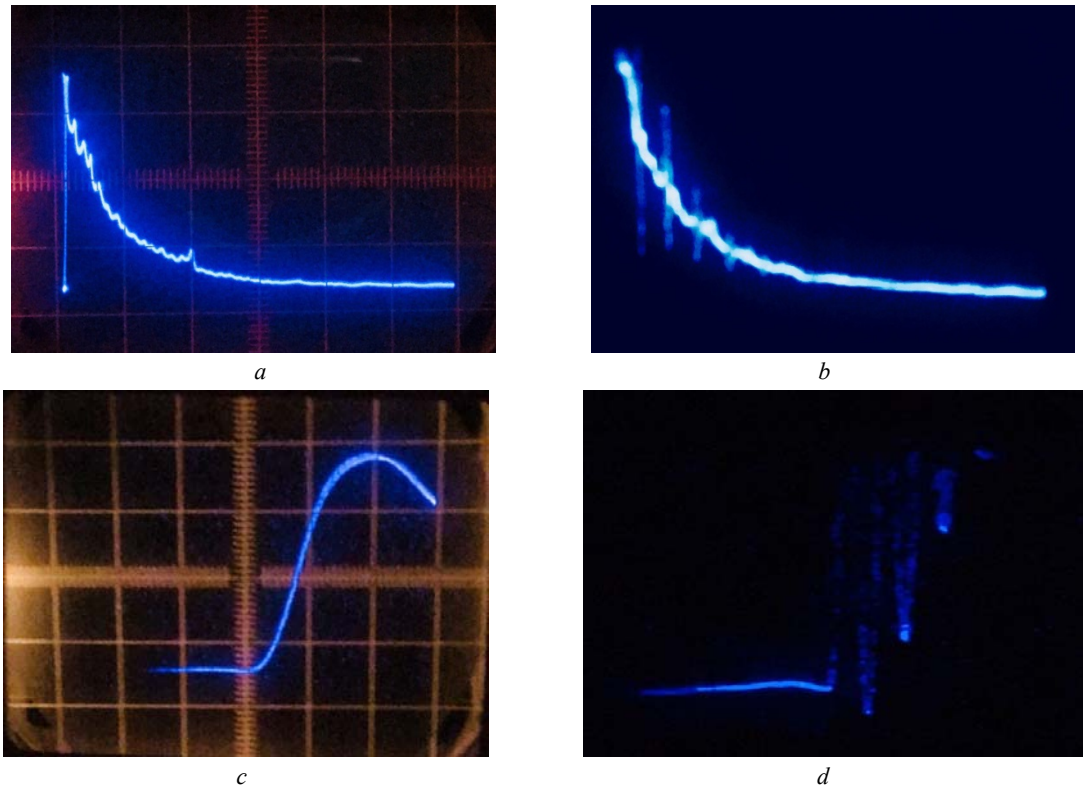

a *b* *c* *d*

Fig. 8. Oscillograms of the pulses as a whole and of the front part of the pulses from the generator, measured by the divider and recorded with the C7-19 oscilloscope: *a*, *c* – without sharpening of the pulse front; *b*, *d* – using the sharpening of the front. On oscillograms *a*, *b* the scale along the time axis is 100 ns/div and 50 ns/div, respectively, on the oscillograms *c*, *d*, the scale along the time axis is 2.5 ns/div. The scale along the process axis is 1.5 V/div on all oscillograms, the division ratio of the divider $K_{75low} \approx 860.7$

The front of the pulses from the high-voltage generator [6] without sharpening is ≈ 2.5 ns. The divider transmits it without distortion (see the oscillogram in Fig. 8,*a*). From oscillograms in Fig. 8,*b*,*d* it can be seen that at sharpening (significant shortening) of the pulse front from the generator, parasitic oscillations occur on it (at the front). These oscillations are excited in this resistive voltage divider containing parasitic capacitances and inductances, by sharpened (subnanosecond) pulse front from the generator. Oscillogram in Fig. 8,*d* shows that the first voltage surge during sharpening of the front of measured and recorded pulses is significantly steeper than in the absence of sharpening, and in the rise time it is ≤0.5 ns.

To validate the experimental results and find out exactly which parasitic capacitances and inductances in the divider to the greatest extent affect its transient characteristic (function), computer simulation of the resistive voltage divider taking into account its parasitic parameters is carried out. The presence of a broadband coaxial cable with an impedance of 100 Ω and electrical length of 5-10 ns between the output of the high-voltage pulse generator and the input of the divider is also taken into account.

Computer simulation of the operation of the divider. The circuit used to model the operation of the divider when applying voltage pulses to the 75 Ω input with different fronts duration from the generator through a coaxial cable with an impedance of 100 Ω and an electrical length of 5 ns, is shown in Fig. 9. The values in the circuit elements varied. From the diagram in Fig. 1 it differs taking into account the parasitic inductances in the divider. In the diagram (Fig. 9), the pulse generator has the following characteristics. The amplitude of the pulses is 5 arbitrary units (for example, 5 kV). The delay before the start of the pulse is 10 ns. The duration (rise time) of the pulse front from the generator is 0.1 ns. The duration of the decay of pulses from the generator is 1000 ns. Pulse width (shelf on top) is 100 ns. The pulse repetition period from the generator is 5000 ns. The recording oscilloscope C7-19 in the diagram is represented by the input active resistance *R*6 = 50 Ω and included in parallel with the *R*6 input capacitance *C*1 = 15 pF. The parasitic inductance *L*3 at the point of connection of the divider output to the oscilloscope input during modeling varied in the range *L*3 = 0.1 ... 10.0 nH, and *L*1 – in the range *L*1 = 0.5 ... 10.0 nH. The values of inductances *L*1 and *L*3 have a significant effect on the shape of the front part of the pulse voltage at the output of the divider connected to the input of the oscilloscope.

The maximum step duration in modeling in Microcap-10 was 0.001 ns, the number of points in time was 100,000.

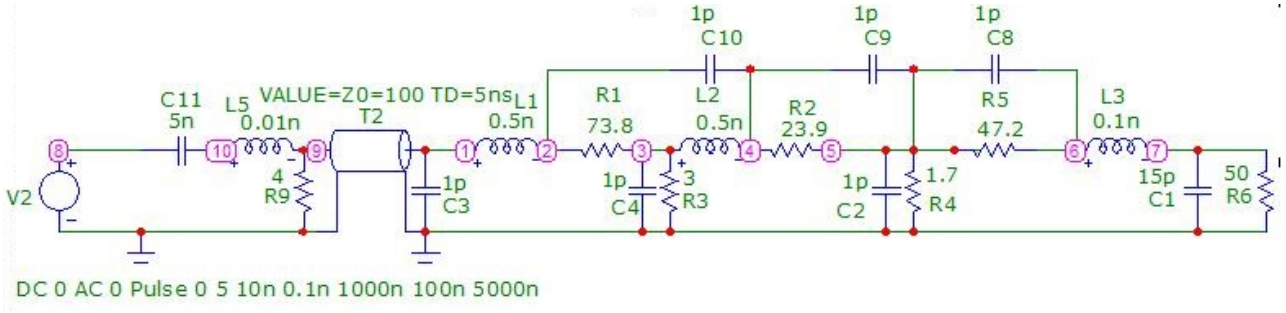

Fig. 9. Circuit for computer simulation of the voltage divider operation

The simulation results for the circuit (Fig. 9) are shown in Fig. 10. In Fig. 10,*a* the amplitude of the voltage *v*(1) and *v*(2) at points 1 and 2 is less than the amplitude *v*(8), *v*(9) and *v*(10), because the characteristic impedance *Z*0=100 Ω of the cable line *T*2 is greater input resistance (≈75 Ω) of the divider. The division coefficient $K_{75.1}$ of the first stage of the divider can be determined from the graphs in Fig. 10,*a*,*b*, as $K_{75.1} \approx v_{max}(1)/v_{max}(3) \approx$ ≈ 4270/150≈28.5 excluding the outlier, which corresponds to the above calculated value of $K_{75.1}$. From the graphs in Fig. 10,*c*,*d*, similarly, we determine $K_{75.2} \approx v_{max}(3)/v_{max}(5) \approx 150/9.95 \approx 15.1$, which also corresponds to the calculated value $K_{75.2}$.

Regular bursts with a repetition period of 10 ns on the graph (Fig. 10,*a*) of the voltage transient at point 2 (at the 75-Ω input of the divider) at the pulse front from the 0.1 ns generator are caused by the longitudinal capacitance in the divider $1/(1/C8+1/C9+1/C10) = 0.33$ (pF). The repetition period is determined by the electric length of 5 ns of the cable *T*2 and is equal to twice the running time of the voltage wave from the generator through the cable to the input of the divider. Similar bursts were observed on oscillograms from the C7-19 oscilloscope. Only the period of these bursts was longer (approximately 20-25 ns) due to the longer cable length. If the longitudinal capacitance in the divider during modeling is reduced by an order of magnitude – to 0.033 pF, then the amplitude of bursts sharply decrease and become hardly noticeable. The bursts also decrease with increasing duration of the pulse front from the generator, which agrees well with the experimental data (see Fig. 8).

The numbers affixed to Fig. 9 are the numbers of the points at which the voltage was measured in the simulation (the voltage between this numbered point of the circuit and the grounded point of the circuit – the body of the divider). Filter *C*11-*L*5-*R*9 provides on the resistance *R*9, to which the input of a coaxial cable with an impedance *Z*0 = 100 Ω and an electrical length of 5 ns, is connected, the pulse shape in the form of a falling exponent with a steep front. If in the diagram in

Fig. 9 take $C1$ = 5 pF instead of 15 pF, the amplitude (range) of oscillations at point 6 at the input to the oscilloscope decreases slightly, and negative surges in oscillations disappear, as shown by the curves in Fig. 10,*d* and Fig. 11.

According to [2, p. 49] $t_f \approx 0.35/B$, where B is the bandwidth determined by attenuation 3 dB, t_f is the rise time for the system under study, in our case for the studied low-resistance resistive voltage divider or for a recording oscilloscope. Therefore, for a C7-19 oscilloscope with a 5 GHz bandwidth, the front t_f of pulses, which it transmits without significant distortion, $t_f \approx 0.35/5$ GHz = 0.07 ns.

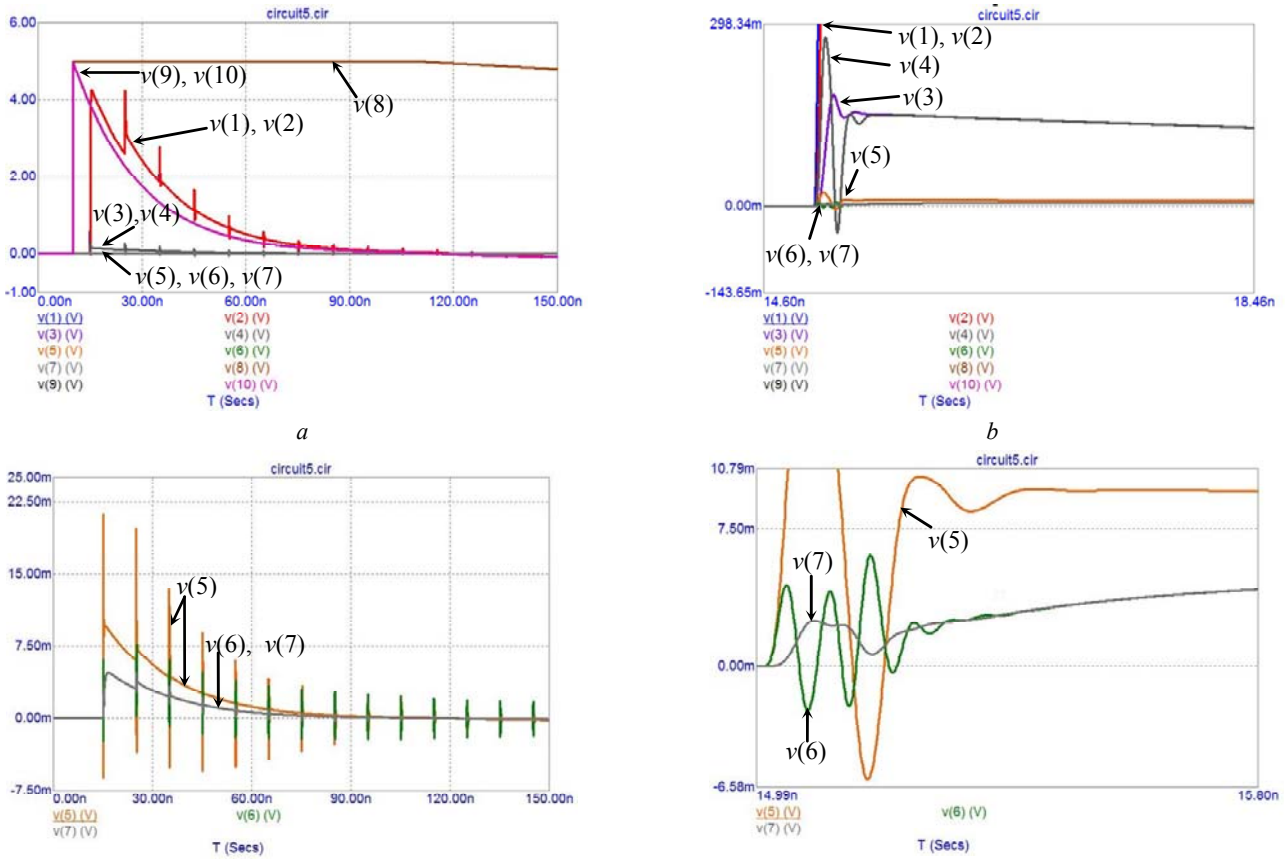

Fig. 10. The results of the simulation of transient in the circuit in Fig. 9

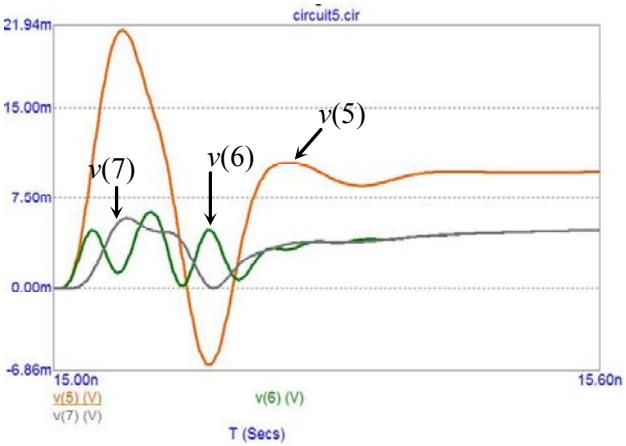

Fig. 11. The voltage at the output of the divider according to the circuit in Fig. 9 at $C1$ = 5 pF

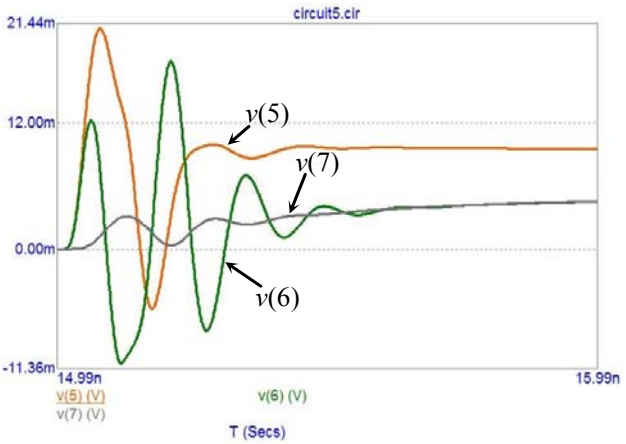

Fig. 12. The oscillations at the output of the divider according to the circuit in Fig. 9 at $L3$ = 0.5 nH

If in the circuit in Fig. 9 to increase $L3$ from 0.1 nH to 0.5 nH, then the amplitude of oscillations at point 6 at the pulse front from the generator increases by about 2.5 times, which illustrates the simulation result in Fig. 12.

Under these simulation conditions, the oscillations at point 6 at the front decay beyond ≈ 0.6 ns, which is less than in the experiment (see Fig. 8,*d*).

If in the simulation circuit in Fig. 9 set the duration of the pulse front from the generator not 0.1 ns, but 2.5 ns,

which corresponds to the operation of a real pulse generator in the mode without sharpening of the front, as a result of the simulation we obtain the dependence of voltage on time at various points of the circuit, shown in Fig. 13.

Small fluctuations in the form of bursts and valleys at a front duration of 2.5 ns are caused by breaks in the initial pulse from the generator: at the beginning of the pulse and when going from the front to the flat top.

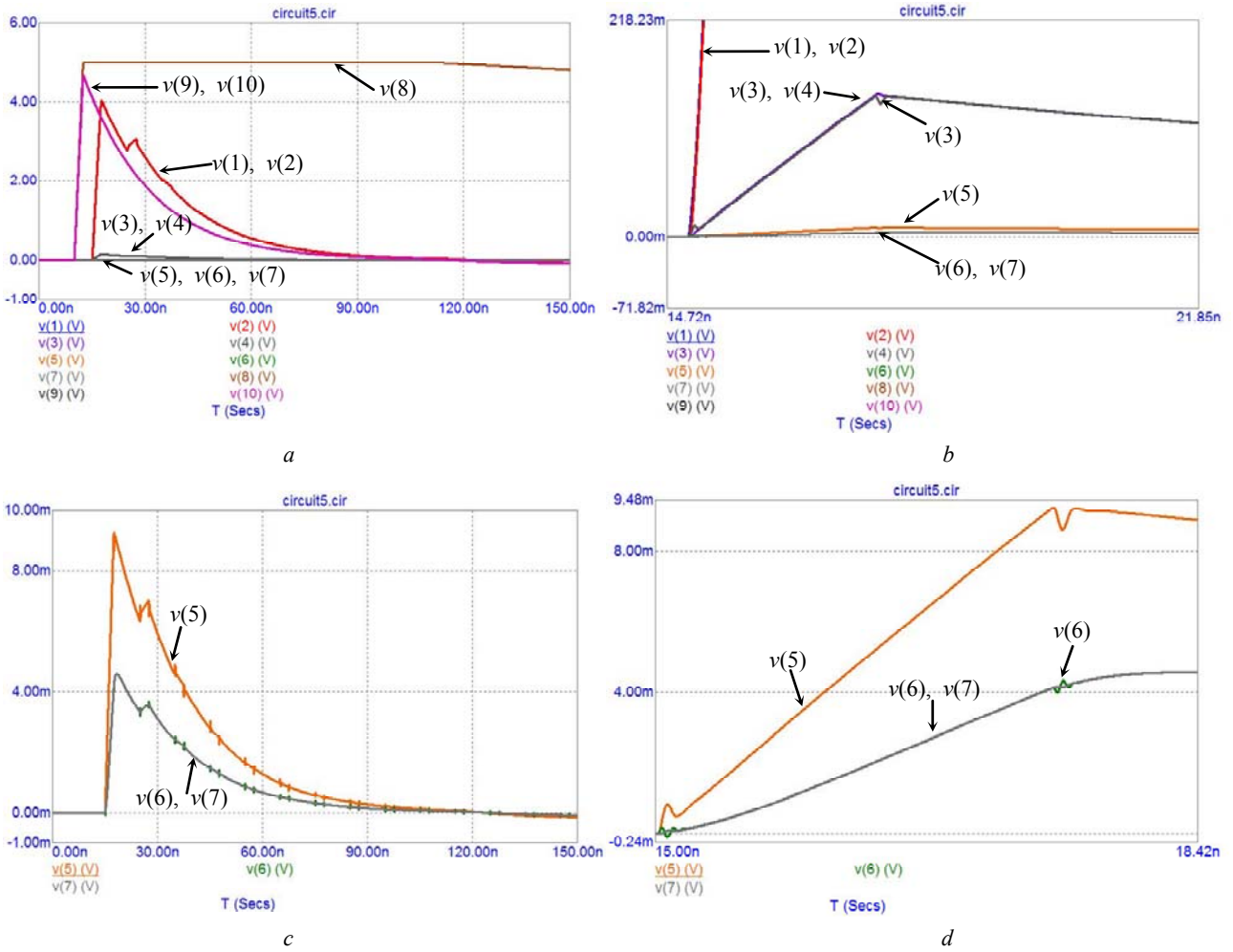

Fig. 13. The results of the simulation of the transient according to the circuit in Fig. 9 at a pulse front duration 2.5 ns from the generator

Modeling at extremely short rise times of the front from the pulse generator, causing the appearance on the front of the oscillograms from the output of the divider of high-frequency oscillations (see Fig. 8,*d*), turned out to be the most difficult at modelling the operation of the divider.

The task is complicated by the fact that the duration of the pulse front from the generator in experiments in the sharpening mode is unknown. It was only clear that the shorter the front from the generator, the greater the amplitude of oscillation on the oscillograms from the output of the divider.

Experiments have shown that the amplitude of these oscillations reaches twice the value compared with the amplitude of the voltage from the output of the divider in the mode without sharpening the front. The selection of the parasitic inductances and divider capacitances in the simulation of oscillations on the front part in the mode of sharpening the front of pulses made it possible to achieve good agreement between the simulation results and the experimental results (see Fig. 8,*d*). The circuit, which allowed to model the oscillations on the front of a sharpened pulse, is shown in Fig. 14, and the simulation results are presented in Fig. 15. The front part of the simulated pulse, close to that in the experiment using the sharpening mode, was obtained with a front duration of 0.1 ns of the original pulse from the generator in the simulation circuit. Hence, in the sharpening mode, the duration of the front from the generator in the experiment was also ≈ 0.1 ns.

The simulation does not take into account the processes in the divider as in a long line, which lead to the emergence of higher types of electromagnetic waves when a long line is excited by pulses with steep fronts whose duration is comparable or less than the electric line length (in our case, of the voltage divider). With a pulse front duration of 0.1 ns, the corresponding path length of an electromagnetic wave in air is 3 cm, and the

divider length is 18 cm. Therefore, the appearance of higher-type waves in it is real. This can explain the somewhat higher intensity of oscillations at the front of a sharpened pulse at the output of the divider in the experiment (as compared with the results of computer simulation).

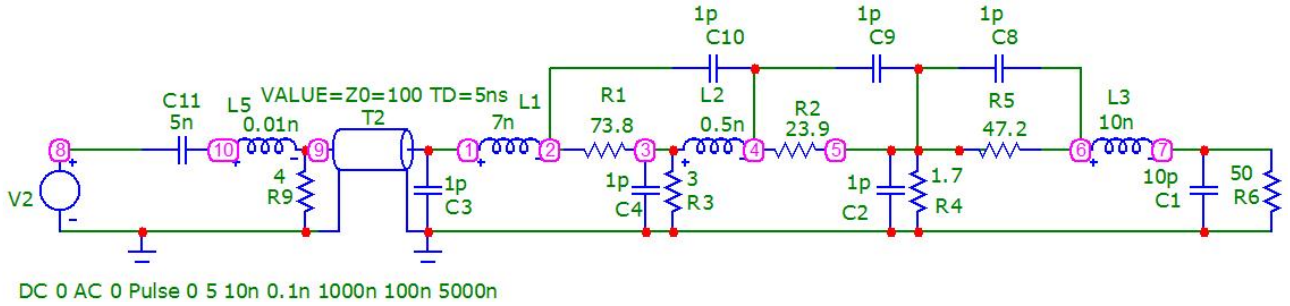

Fig. 14. Circuit with parasitic inductances and divider capacitances, which provided the simulation results of the pulse front at the divider output, closest to the experimental ones

Thus, computer simulation has allowed to clarify the duration of the pulse front from the high-voltage generator used in the experiment in the sharpening mode and to estimate quantitatively the values of the parasitic inductances and capacitances in the considered divider. In particular, the value of the simulated parasitic inductance at the input of the divider was $L1$ = 7 nH, and at the output the divider $L3$ = 10 nH. The rise time of the front of the voltage pulse $v(7)$ at the RC-input of the oscilloscope ($R6$ = 50 Ω, $C1$ = 10 pF in Fig. 14 at point 7) was approximately 0.7 ns (see Fig. 15,*b*), while the rise time of the voltage pulse front $v(7)$ from the generator at point 8 is 0.1 ns. From here it follows that the rise time the transitional characteristics of the divider is ≈ 0.7 ns.

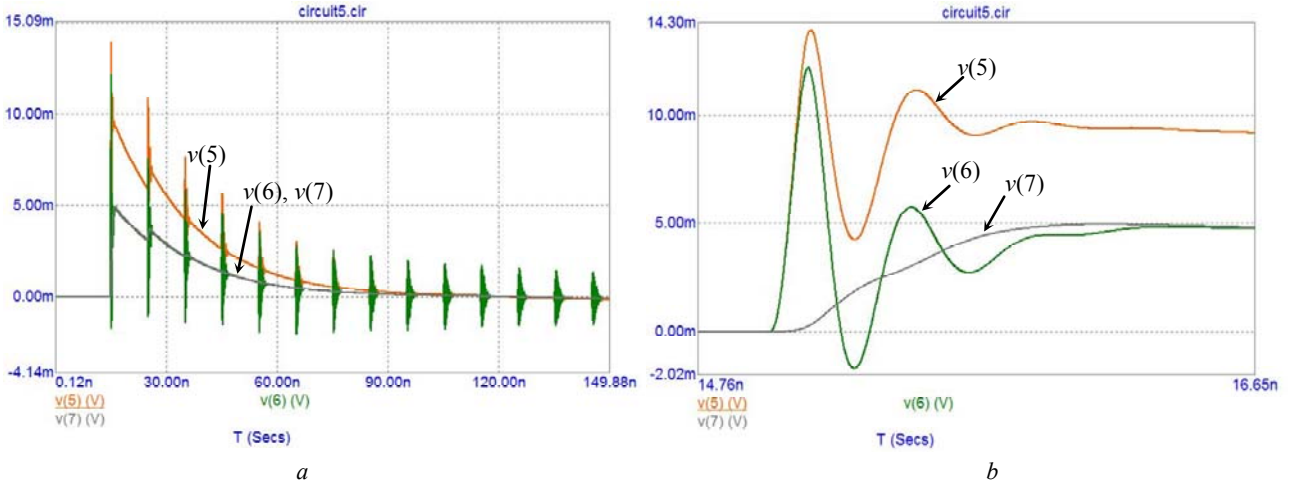

a *b*

Fig. 15. The results of the simulation of the transient at the output of the divider, close to the experimental results; *a* – pulse as a whole, *b* – front part of pulse

Simulation has shown that the influence of parasitic capacitances and inductances in the investigated divider at subnanosecond and even shorter rise times of pulses at the input of the divider should be taken into account.

Conclusions.

1. Theoretically (using computer simulation) it is reasonable and experimentally it is confirmed that the developed voltage divider with the rise time of the transient response ≈ 0.7 ns allows to measure high-voltage pulses with a steep front (up to 1 ns as the lower limit) and provides the division factor K_{75low}≈ 861 when using a 75-Ω divider input and with an oscilloscope input resistance of 50 Ω (K_{50low}≈548 when using 50-Ω divider input and at the input resistance of the oscilloscope, equal to 75 Ω).

2. A computer model of VD is created, with the help of which it was possible to explain the presence in the experiment of oscillations with amplitude twice as large as the amplitude of the pulses according to the division factor of the divider at the front of the pulses from the output of the divider. These oscillations (arising when pulses with a very steep front ≈ 0.1 s are applied to the divider input) are caused by the presence in the divider of a parasitic longitudinal capacitance ≈ 0.3 pF and parasitic inductances, the total value of which is ≈ 17.5 nH).

3. This divider can be recommended for measuring the characteristics of high-voltage pulses with steep (nanosecond) fronts.

REFERENCES

1. Mesiats G.A. *Impul'snaia energetika i elektronika* [Pulsed power and electronics]. Moscow, Nauka Publ., 2004. 704 p. (Rus).

2. Shvab A. *Izmereniia na vysokom napriazhenii. Izmeritel'nye pribory i sposoby izmereniia* [Measurements at high voltage. Measuring instruments and methods of measurement]. Moscow, Energoatomizdat Publ., 1983. 264 p. (Rus).

3. Kuffel E., Zaengl W.S., Kuffel J. *High Voltage Engineering (Fundamentals). Second edition*. Oxford, Butterworth-Heinemann Publ., 2000. 539 p.
4. Parks H. High-Voltage Divider Calibration with the Reference Step Method. *NCSLI Measure*, 2016, vol.11, no.1, pp. 34-36. **doi: 10.1080/19315775.2016.1149008.**
5. Early M.D., Sira M., Andersson B.-O., Christian L.A., Gunnarsson O., Rydler K.-E., Streit J. A Simple Build-Up Method for the DC Voltage Scale of a Source. *IEEE Transactions on Instrumentation and Measurement*, 2013, vol.62, no.6, pp. 1600-1607. **doi: 10.1109/TIM.2012.2230734.**
6. Boyko N.I., Safronov I.A., Tondii L.D. ASHEMIT: A device for wideband electromagnetic pulse therapy. *Instruments and Experimental Techniques*, 2000, vol.43, no.5, pp. 675-682. **doi: 10.1007/bf02759082**.
7. Demirchian K.S., Neiman L.R., Korovkin N.V., Chechurin V.L. *Teoreticheskie osnovy elektrotekhniki: V 3-kh t. Uchebnik dlia vuzov. Tom 2* [Theoretical bases of electrical engineering. In 3 vols. Vol.2.]. St. Petersburg, Piter Publ, 2004. 576 p. (Rus).

Received 27.02.2019

M.I. Boyko[1]*, Doctor of Technical Science, Professor,*
S.O. Syomkin[1]*, Master of Science,*
[1] National Technical University «Kharkiv Polytechnic Institute», 2, Kyrpychova Str., Kharkiv, 61002, Ukraine,
phone +380 57 7076245,
e-mail: qnaboyg@gmail.com

How to cite this article:
Boyko M.I., Syomkin S.O. Investigation of amplitude-temporal characteristics of a high-voltage resistive voltage divider. *Electrical engineering & electromechanics*, 2019, no.4, pp. 59-68. **doi: 10.20998/2074-272X.2019.4.09.**

UDC 621.3 **doi: 10.20998/2074-272X.2019.4.10**

M. Dehghani, Z. Montazeri, O.P. Malik

ENERGY COMMITMENT: A PLANNING OF ENERGY CARRIER BASED ON ENERGY CONSUMPTION

Purpose. Energy consumption is one of the criteria for determining the quality of life in a country. Continued supply of energy and the possibility of long-term access to resources require a comprehensive plan. One of the key issues in the field of energy planning is energy carriers. In this paper, a new theory is introduced to energy network studies for planning of energy carriers called Energy Commitment. In this theory, an appropriate planning is applied for energy carriers based the final energy consumption. Energy carriers are available either naturally or after the energy conversion process. Energy commitment is modeled on an energy network with the presence of electrical energy, gas energy, transportation section, agriculture section, industrial section, residential section, commercial section, and general section. References 25, tables 3.

Key words: **energy, energy commitment, energy carrier, energy consumption, unit commitment.**

Цель. Потребление энергии является одним из критериев определения качества жизни в стране. Непрерывные поставки энергии и возможность долгосрочного доступа к ресурсам требуют комплексного плана. Одним из ключевых вопросов в области энергетического планирования являются энергоносители. В данной статье в исследования энергетических сетей для планирования энергоносителей вводится новая теория под названием Energy Commitment («энергетическое обязательство»). В этой теории для энергоносителей применяется соответствующее планирование на основе конечного потребления энергии. Энергоносители доступны либо естественным путем, либо после процесса преобразования энергии. Energy Commitment моделируется в энергетической сети с учетом электрической энергии, энергии газа, транспортной отрасли народного хозяйства, сельскохозяйственной отрасли, промышленного сектора экономики, жилищно-коммунального хозяйства, реального сектора экономики и прочих видов экономической активности. Библ. 25, табл. 3.

Ключевые слова: **энергия, энергетическое обязательство, энергоноситель, энергопотребление, единичное обязательство.**

Introduction. Energy consumption is one of the criteria for determining the level of development and quality of life in a country [1]. If energy used properly and reasonably, it can in any country make progress in the science, technology and welfare of its people. Otherwise, it will cause irreparable economic losses and a massive economic downturn [2]. The energy consumption trend has been very fast and critical in recent years. Continued supply of energy and the possibility of long-term access to resources require a comprehensive energy planning, which is why energy planning is indisputable economic, national and strategic imperatives. One of the key issues in the field of energy planning is energy resources.

Many studies is done on the power system such as: transformers [3], battery energy storage [4], distributed generation [5], energy [6]. One of the most important studies of electric power network is the issue of Unit Commitment (UC) [7]. UC is to determine the most appropriate electrical power generation pattern at power plants, firstly, to meet technical requirements, and then to be the most economical [8]. UC has been studied using various methods. The priority list method and dynamic programing are the first methods in UC [9]. In the Lagrange method, equal and unequal constraints were added to the objective function [10]. In [11] UC problem is investigated the in presence of FACTS devices and energy storage. In [12] UC problem is studied under cyber-attacks. In addition, evolutionary methods have been used for solving UC in recent years. In [13] a method is proposed based on the classical genetic algorithm. Integer-coded genetic algorithm in [14] is proposed. Researchers have also used other methods to solve the UC problem such as: Particle Swarm Optimization (PSO) [15], Teaching Learning Based Optimization (TLBO) [16], Gravitational Search Algorithm (GSA) [17] , Water Cycle Algorithm (WCA) [18] and Grey Wolf Optimization (GWO) [19], Whale Optimization Algorithm (WOA) [20]. Other algorithms are also suggested for UC solving [21-24].

Energy Commitment (EC) is to determine the most appropriate pattern for using energy resources to meet energy demand, firstly, to meet technical requirements, and secondly, to be the most economical. In other words, energy sources should be used as much as needed, if the energy sources are in line with the demand peak it will cost a lot. Therefore, EC reduces energy supply costs.

This problem can be articulated mathematically, so that a function called F is defined as the objective function, which is equal to the total cost of supplying energy demand. In this case, the problem is to minimize F. Note that losses are discarded and there is no explicit mention of any exploitation restrictions in the issue. So:

$$F = F_1\left(E_{s_1}\right) + F_2\left(E_{s_2}\right) + F_3\left(E_{s_{13}}\right) + \\ + \ldots + F_{N_s}\left(E_{s_{N_s}}\right) = \sum_{i=1}^{N_s} F_i\left(E_{s_i}\right), \quad (1)$$

where F is the objective function, F_i is the cost of i-th source, E_{s_i} is the i-th kind of energy demand and N_s is the number of energy carriers.

The above issue is an optimization problem that can be examined using appropriate methods.

Problem Formulation. Energy grid modelling. The energy network consists of the following sections: transportation, agriculture, industrial, residential, commercial and general.

In the energy grid, energy demand is calculated as a sum of sub networks of the grid:

$$EC_f = EC_1 + EC_2 + \ldots + EC_N = \sum_{i=1}^{N} EC_i, \quad (2)$$

where EC_f is the final energy consumption, N is the number of different sections of energy consumption and EC_i is the energy consumption of i-th section.

Firstly, the final energy consumption matrix based on different sections is determined as

$$E_1 = [EC_1\ EC_2\ ...\ EC_i\ ...\ EC_N]^T, \quad (3)$$

where E_1 is the final energy consumption matrix based on different sections.

Now final energy consumption matrix based on different energy carriers is determined as

$$E_2 = T_{1,2} \times E_1, \quad (4)$$

where E_2 is the final energy consumption matrix based on different energy carriers and $T_{1,2}$ is the transpose matrix of different sections to different energy carriers.

Energy losses is modeled as

$$E_3 = T_{2,3} \times E_2, \quad (5)$$

where E_3 is the final energy consumption based on different energy carriers considering losses and $T_{2,3}$ is the efficiency matrix.

At this stage, electrical energy is converted into energy carriers. The electrical energy of different power plants is determined as

$$E_u = T_u \times E_e, \quad (6)$$

where E_u is the electrical energy of different power plants, T_u is the separation matrix of electricity generation by different power plants and E_e is the total electricity demand.

Input fuel for different power plants is determined as

$$E_{e_1} = T_{u,f} \times E_u, \quad (7)$$

where E_{e_1} is the input fuel for different power plant and Electrical manufacturer carriers is determined as

$$E_{e_2} = T_{f,c} \times E_{e_1}, \quad (8)$$

where E_{e_2} is the electrical manufacturer carriers and $T_{f,c}$ is the conversion matrix of input fuel to energy carriers.

After simulation of electrical energy, final energy consumption is calculated as

$$E_4 = E_3 + E_{e_2} - E_e, \quad (9)$$

where E_4 is the final energy consumption after conversion of electrical energy.

At this stage, the process of refining crude oil is simulated as

$$E_{p_1} = T_p \times E_p, \quad (10)$$

where E_{p_1} is the energy carriers produced by refining, T_p is the separation matrix of produced products from refining crude oil and E_p is the maximum capacity of refineries.

After simulation of process of refining crude oil, final energy consumption is calculated as

$$E_5 = E_4 + E_p - E_{p_1}, \quad (11)$$

where E_5 is the final energy consumption after refining crude oil. Actually E_5 determines energy carriers in order to supply of energy demand.

Test energy grid. EC is applied to energy grid with 10 power units. Electrical network information is adapted from [25].

Simulation. After modeling the energy network, EC is simulated on energy grid.

The simulation results of EC on the energy grid studied are presented in Tables 1-3.

In Table 1, dynamic scheduling results are presented with equal paths to the maximum number of states per hour of the study. The second path, (S2) is identified as an appropriate strategy. The cost of EC in this path is equal by 8,554,182 USD. The need for energy carriers to provide final energy consumption is specified in Table 2. The result of economic distribution of electrical energy is presented in Table 3.

Table 1

The output result of dynamic planning in ten unit energy grids

Strategy						Hour
S6	S5	S 4	S3	S2	S1	
2	2	2	2	2	2	The initial state
3	3	3	3	3	3	1
3	3	3	3	3	3	2
3	3	3	3	3	3	3
3	3	3	3	3	3	4
3	3	3	3	3	3	5
4	4	4	4	4	4	6
4	4	4	4	4	4	7
9	9	9	9	9	9	8
9	9	9	9	9	9	9
9	9	9	9	9	9	10
10	10	10	10	10	10	11
10	10	10	10	10	10	12
10	10	10	10	10	10	13
9	9	9	9	9	9	14
9	9	9	9	9	9	15
9	9	9	9	9	9	16
9	9	9	9	9	9	17
9	9	9	9	9	9	18
9	9	9	9	9	9	19
9	9	9	9	9	9	20
9	9	4	4	4	4	21
9	6	4	4	3	3	22
7	6	4	4	3	3	23
7	6	5	4	3	2	24
8,557,932	8,557,192	8,557,153	8,554,502	8,554,182	8,555,398	Cost (USD)

Table 2

The need of energy carriers in ten unit energy grids

8	7	6	5	4	3	2	1	Hour
3721.1	3721.1	3721.1	3721.1	3721.1	3721.1	3721.1	3721.1	Petroleum
51.78965	44.67028	37.55091	23.31218	16.19281	1.95407	–12.2847	–19.404	Liquid gas
–350.552	–365.265	–354.657	–429.906	–466.355	–539.254	–612.154	–647.68	Fuel oil
–11.7441	–61.1345	–123.351	–210.1	–253.46	–340.182	–426.903	–470.252	Gas oil
17.72885	1.640607	–14.4476	–46.6241	–62.7124	–94.8888	–127.065	–143.154	Kerosene
405.1893	363.9642	322.7392	240.289	199.0639	116.6137	34.16357	–7.06152	Gasoline
53.06305	50.85209	48.64113	44.2192	42.00824	37.58632	33.1644	30.95344	Plane fuel
4380.603	4190.728	3988.239	3615.204	3432.123	3065.959	2699.796	2519.415	Natural gas
26.60254	25.4941	24.38566	22.16878	21.06034	18.84346	16.62658	15.51815	Coke gas
58.79772	56.34781	53.89791	48.9981	46.54819	41.64838	36.74857	34.29867	Coal
16	15	14	13	12	11	10	9	Hour
3721.1	3721.1	3721.1	3721.1	3721.1	3721.1	3721.1	3721.1	Petroleum
30.43155	51.78965	66.02839	80.26713	94.50586	87.3865	80.26713	66.02839	Liquid gas
–459.901	–350.552	–275.868	–198.861	–135.511	–158.969	–198.861	–275.591	Fuel oil
–141.826	–11.7441	74.99814	161.7678	260.843	205.169	161.7678	75.0014	Gas oil
–30.5359	17.72885	49.90533	82.0818	114.2583	98.17004	82.0818	49.90533	Kerosene
281.5141	405.1893	487.6395	570.0897	652.5398	611.3148	570.0897	487.6395	Gasoline
46.43017	53.06305	57.48497	61.90689	66.32881	64.11785	61.90689	57.48497	Plane fuel
3831.358	4380.603	4751.988	5130.168	5531.033	5323.32	5130.168	4752.798	Natural gas
23.27722	26.60254	28.81941	31.03629	33.25317	32.14473	31.03629	28.81941	Coke gas
51.448	58.79772	63.69753	68.59734	73.49714	71.04724	68.59734	63.69753	Coal
24	23	22	21	20	19	18	17	Hour
3721.1	3721.1	3721.1	3721.1	3721.1	3721.1	3721.1	3721.1	Petroleum
–5.1653	9.073439	37.55091	66.02839	80.26713	51.78965	37.55091	23.31218	Liquid gas
–595.486	–548.095	–423.452	–275.868	–198.861	–350.552	–423.452	–496.351	Fuel oil
–370.456	–277.548	–98.4652	74.99813	161.7678	–11.7441	–98.4652	–185.186	Gas oil
–110.977	–78.8006	–14.4476	49.90533	82.0818	17.72885	–14.4476	–46.6241	Kerosene
75.38865	157.8388	322.7392	487.6395	570.0897	405.1893	322.7392	240.289	Gasoline
35.37536	39.79728	48.64113	57.48497	61.90689	53.06305	48.64113	44.2192	Plane fuel
2913.867	3278.051	4014.44	4751.988	5130.168	4380.603	4014.44	3648.277	Natural gas
17.73502	19.9519	24.38566	28.81941	31.03629	26.60254	24.38566	22.16878	Coke gas
39.19848	44.09829	53.89791	63.69753	68.59734	58.79772	53.89791	48.9981	Coal

Table 3

The electrical energy economical distribution within the energy grid

Unit 10	Unit 9	Unit 8	Unit 7	Unit 6	Unit 5	Unit 4	Unit 3	Unit 2	Unit 1	Hour
0	0	0	0	0	0	0	129.9054	150	420.9897	1
0	0	0	0	0	0	0	130	165.9591	455	2
0	0	0	0	0	0	0	130	266.087	455	3
0	0	0	0	0	0	0	130	366.2149	455	4
0	0	0	0	0	0	0	130	416.2788	455	5
0	0	0	0	0	0	61.40668	130	455	455	6
0	0	0	0	0	0	111.4706	130	455	455	7
0	54.94904	10	25	78.91501	25	20	129.9395	403.1555	454.5755	8
0	54.92522	38.19602	25	79.91727	25	40.51524	129.8847	454.393	453.831	9
0	54.99011	46.54565	75.69185	79.97855	25	129.9675	129.966	454.8779	454.8368	10
55	55	55	85	80	51.98213	130	130	455	455	11
55	55	55	85	80	157.1164	130	130	455	455	12
31.11385	55	55	85	80	25.80435	130	130	455	455	13
0	55	46.5999	25.09276	80	25.18803	130	130	455	454.9096	14
0	50.46745	10	25	42.35772	25	20	129.0834	452.7482	446.8778	15
0	54.57776	10	25	75.61226	25	20	129.572	260.4829	451.0978	16
0	54.58248	10	25	75.74856	25	20	129.4813	209.902	451.5645	17
0	55	10.06585	25.04071	80	25.08315	20.12963	130	401.2152	455	18
0	55	46.61355	25.03679	80	25.13997	130	130	455	455	19
0	53.36535	10	25	79.89353	25	70.70835	129.7906	454.3342	453.5704	20
0	0	0	0	0	0	61.40668	130	455	455	21
0	0	0	0	0	0	0	130	316.1509	455	22
0	0	0	0	0	0	0	130	216.023	455	23
0	0	0	0	0	0	0	130	216.023	455	24

Conclusions.

Energy Commitment (EC) was introduced as a planning of energy carrier based on energy consumption. EC is to determine the most appropriate pattern for using energy resources to meet energy demand, firstly, to meet technical requirements, and secondly, to be the most economical.

The energy grid including different sections was modeled in matrix form. EC was simulated on the one energy grid with ten power plants and result was

presented. Different combinations of power plants are available to provide final energy consumption. Due to the different fuel inputs to each power plant, there are different combinations of energy carriers. The proper combination of energy carriers is determined to provide final energy consumption using the dynamic programming method.

REFERENCES

1. Dehghani M., Montazeri Z., Ehsanifar A., Seifi A.R., Ebadi M.J., Grechko O.M. Planning of energy carriers based on final energy consumption using dynamic programming and particle swarm optimization. *Electrical engineering & electromechanics*, 2018, no.5, pp. 62-71. **doi: 10.20998/2074-272X.2018.5.10.**

2. Montazeri Z., Niknam T. Energy carriers management based on energy consumption. *2017 IEEE 4th International Conference on Knowledge-Based Engineering and Innovation (KBEI)*, Dec. 2017. **doi: 10.1109/kbei.2017.8325036**.

3. Ehsanifar A., Dehghani M., Allahbakhshi M. Calculating the leakage inductance for transformer inter-turn fault detection using finite element method. *2017 Iranian Conference on Electrical Engineering (ICEE)*, May 2017. **doi: 10.1109/iraniancee.2017.7985256.**

4. Dehbozorgi S., Ehsanifar A., Montazeri Z., Dehghani M., Seifi A. Line loss reduction and voltage profile improvement in radial distribution networks using battery energy storage system. 2017 *IEEE 4th International Conference on Knowledge-Based Engineering and Innovation (KBEI)*, Dec. 2017. **doi: 10.1109/kbei.2017.8324976**.

5. Dehghani M., Mardaneh M., Montazeri Z., Ehsanifar A., Ebadi M.J., Grechko O.M. Spring search algorithm for simultaneous placement of distributed generation and capacitors. *Electrical engineering & electromechanics*, 2018, no.6, pp. 68-73. **doi: 10.20998/2074-272X.2018.6.10.**

6. Montazeri Z., Niknam T. Optimal utilization of electrical energy from power plants based on final energy consumption using gravitational search algorithm. *Electrical engineering & electromechanics*, 2018, no.4, pp. 70-73. **doi: 10.20998/2074-272X.2018.4.12.**

7. Shi J., Oren S.S. Stochastic Unit Commitment With Topology Control Recourse for Power Systems With Large-Scale Renewable Integration. *IEEE Transactions on Power Systems*, 2018, vol.33, no.3, pp. 3315-3324. **doi: 10.1109/tpwrs.2017.2772168**.

8. Gupta A., Anderson C.L. Statistical Bus Ranking for Flexible Robust Unit Commitment. *IEEE Transactions on Power Systems*, 2019, vol.34, no.1, pp. 236-245. **doi: 10.1109/tpwrs.2018.2864131**.

9. Yamin H.Y. Review on methods of generation scheduling in electric power systems. *Electric Power Systems Research*, 2004, vol.69, no.2-3, pp. 227-248. **doi: 10.1016/j.epsr.2003.10.002**.

10. Geoffrion A.M. Lagrangian *Relaxation for Integer Programming. 50 Years of Integer Programming 1958-2008*. Nov. 2009, pp. 243-281, **doi:10.1007/978-3-540-68279-0_9**.

11. Luburić Z., Pandžić H. FACTS devices and energy storage in unit commitment. *International Journal of Electrical Power & Energy Systems*, 2019, vol.104, pp. 311-325 **doi: 10.1016/j.ijepes.2018.07.013.**

12. Shayan H., Amraee T. Network Constrained Unit Commitment Under Cyber Attacks Driven Overloads. *IEEE Transactions on Smart Grid*, pp. 1–1, 2019. **doi: 10.1109/tsg.2019.2904873.**

13. Swarup K.S., Yamashiro S. Unit commitment solution methodology using genetic algorithm. *IEEE Transactions on Power Systems*, 2002, vol.17, no.1, pp. 87-91. **doi: 10.1109/59.982197.**

14. Damousis I.G., Bakirtzis A.G., Dokopoulos P.S. A Solution to the Unit-Commitment Problem Using Integer-Coded Genetic Algorithm. *IEEE Transactions on Power Systems*, 2004, vol.19, no.2, pp. 1165-1172. **doi: 10.1109/tpwrs.2003.821625.**

15. Anand H., Narang N., Dhillon J.S. Multi-objective combined heat and power unit commitment using particle swarm optimization. *Energy*, 2019, vol.172, pp. 794-807. **doi: 10.1016/j.energy.2019.01.155**.

16. Krishna P.V.R., Sao S. An Improved TLBO Algorithm to Solve Profit Based Unit Commitment Problem under Deregulated Environment. *Procedia Technology*, 2016, vol.25, pp. 652-659. **doi: 10.1016/j.protcy.2016.08.157**.

17. Barani F., Mirhosseini M., Nezamabadi-pour H., Farsangi M.M. Unit commitment by an improved binary quantum GSA. *Applied Soft Computing*, 2017, vol.60, pp. 180-189. **doi: 10.1016/j.asoc.2017.06.051**.

18. El-Azab H.-A.I., Swief R.A.-W., El-Amary N.H., Temraz H.K. Decarbonized Unit Commitment Applying Water Cycle Algorithm Integrating Plug-In Electric Vehicles. *2018 Twentieth International Middle East Power Systems Conference (MEPCON)*, Dec. 2018. pp. 455-462. **doi: 10.1109/mepcon.2018.8635152.**

19. Srikanth K., Panwar L.K., Panigrahi B., Herrera-Viedma E., Sangaiah A.K., Wang G.-G. Meta-heuristic framework: Quantum inspired binary grey wolf optimizer for unit commitment problem. *Computers & Electrical Engineering*, 2018, vol.70, pp. 243-260. **doi: 10.1016/j.compeleceng.2017.07.023**.

20. Kumar V., Kumar D. Binary whale optimization algorithm and its application to unit commitment problem. *Neural Computing and Applications*, Oct. 2018, pp. 1-29, **doi: 10.1007/s00521-018-3796-3**.

21. Dehghani M., Montazeri Z., Dehghani A., Nouri N., Seifi A. BSSA: Binary spring search algorithm. *2017 IEEE 4th International Conference on Knowledge-Based Engineering and Innovation (KBEI)*, Dec. 2017. **doi: 10.1109/kbei.2017.8324977**.

22. Dehghani M., Montazeri Z., Dehghani A., Seifi A. Spring search algorithm: A new meta-heuristic optimization algorithm inspired by Hooke's law. *2017 IEEE 4th International Conference on Knowledge-Based Engineering and Innovation (KBEI)*, Dec. 2017. **doi: 10.1109/kbei.2017.8324975**.

23. Dehghani M., Montazeri Z., Malik O.P., Ehsanifar A., Dehghani A. OSA: Orientation Search Algorithm. *International Journal of Industrial Electronics, Control and Optimization*, 2019, vol.2, pp. 99-112.

24. Dehghani M., Mardaneh M., Malik O. FOA: Following Optimization Algorithm for solving power engineering optimization problems. *Journal of Operation and Automation in Power Engineering,* 2019. (Article in press). **doi: 10.22098/JOAPE.2019.5522.1414.**

25. Ebrahimi J., Hosseinian S.H., Gharehpetian G.B. Unit Commitment Problem Solution Using Shuffled Frog Leaping Algorithm. *IEEE Transactions on Power Systems*, 2011, vol.26, no.2, pp. 573-581. **doi: 10.1109/tpwrs.2010.2052639**.

Received 19.04.2019

M. Dehghani[1], *Candidate of Power Engineering, PhD Student,*
Z. Montazeri[1], *Candidate of Power Engineering, PhD Student,*
O.P. Malik[2], *Doctor of Power Engineering, Professor,*
[1] Department of Electrical and Electronics Engineering,
Shiraz University of Technology, Shiraz, Iran,
e-mail: adanbax@gmail.com, Z.Montazeri@sutech.ac.ir
[2] Department of Electrical Engineering,
University of Calgary, Calgary Alberta Canada
e-mail: maliko@ucalgary.ca

How to cite this article:
Dehghani M., Montazeri Z., Malik O.P. Energy commitment: a planning of energy carrier based on energy consumption. *Electrical engineering & electromechanics*, 2019, no.4, pp. 69-72. **doi: 10.20998/2074-272X.2019.4.10.**

Матеріали приймаються за адресою:
Кафедра "Електричні апарати", НТУ "ХПИ", вул. Кирпичова, 21, м. Харків, 61002, Україна
Електронні варіанти матеріалів по e-mail: a.m.grechko@gmail.com

Довідки за телефонами: +38 050 653 49 82 Клименко Борис Володимирович
+38 067 359 46 96 Гречко Олександр Михайлович

Передплатний індекс: 01216